Studies on sol–gel-derived monolithic porous polyorganosiloxanes

GEN HAYASE

2014

Contents

General Introduction

Aerogel, one of the lightest known solid materials, was first reported in 1931 by Kistler.[1] In his first paper, he reported aerogels composed of various kinds of substance such as silica, alumina, nickel tartarate, stannic oxide, tungstic oxide, gelatin, agar, nitrocellulose, cellulose, and egg albumin. In particular, he took notice of silica aerogels that can easily be obtained with low density (the lowest one is 0.02 g cm^{-3} at that time) and are highly opalescent. At the end of his report, he addressed the new physical properties developed in the materials are of unusual interest.

In fact, many researchers have investigated silica aerogels for various purposes.[2] They have utilized unique properties of aerogels, such as low thermal conductivity (< 15 mW m^{-1} K^{-1}), high transmittance (~90 % with respect to 10 mm thickness) of visible light, and low refractive index, for applications such as thermal insulators and for studies in broad fields including quantum physics[3] and space exploration[4]. As a thermal insulator, silica aerogels have recorded the lowest thermal conductivity among all solid materials known today. The visible-light transmittance of well-prepared aerogel is comparable to that of window glass. If such materials could be applied in our daily life, they would reduce energy consumptions which keep increasing with the development of human activity. However, extremely poor mechanical strength of aerogels associated with its brittleness has been shuttering such dreams.

The brittleness of aerogel derives from their tenuous microstructure supporting their low-density body as a monolith. The highest barrier for silica aerogels to real applications in our daily life is a necessity of a high pressure and high temperature process using supercritical fluid to remove solvent from wet precursor gels. Generally, low-density porous materials are easily cracked and broken to pieces by the capillary force arisen from surface tension of drying solvent at liquid–solid interfaces inside the pores.[2d] Supercritical fluid has no surface tension, by which the samples can be dried while keeping the original size and shape throughout the drying process. Although the most commonly used carbon dioxide has relatively low critical pressure and temperature, they need to

be kept well above 7.38 MPa and 304.1 K, and a pressure-tight autoclave is required to realize this harsh condition.

Formation of homogeneous microstructure in gels, not limited to silica, is not difficult as we can find various wet gels such as food jellies. Inorganic gels can be easily obtained by the sol–gel process, which is utilized in many industry processes today.[5] For instance, transparent silica wet gels can be obtained by only mixing a silica source, such as tetraalkoxysilanes, and an aqueous solution containing hydrolysis–condensation catalysts, such as acid and base. One of the important things to obtain homogeneous gels is to avoid macroscopic phase separation during the formation of polymeric networks.[6]

The microstructure of silica aerogels is composed of beaded small particles (secondary particles) with ~10–20 nm in diameter as confirmed by microscopic techniques.[2a] Density of these particles is ~1.5 g cm^{-3}, which is lower than vitreous silica, according to analysis by helium pycnometry, because these particles include interstices between dense primary particles of ~2–3 nm in diameter as confirmed by scattering techniques. A schematic view of microstructure in silica aerogels is shown in Figure 1.[7] The reason for low thermal conductivity and high visible-light transmittance of silica aerogels lies in this specific microstructure. Silica aerogels have low solid fraction and uniform mesopores with several dozen nanometers. The low solid fraction suppresses thermal conductivity of solid, and small mesopores suppress the gaseous thermal conduction as far as the pore size is shorter than the mean free path of gas molecules confined in the pores.[8] In total, thermal conductivity of aerogels is much lower than those of commercially available thermal insulators such as polyurethane foams and glass wools.[2a-c] As for visible-light transmittance, the size of porous structure and that of secondary particles play an important role in the Mie and Rayleigh scattering modes, respectively.[2b] It is critically important to form the porous structure with its characteristic length sufficiently shorter than the wavelength of visible light and to reduce the fraction and size of the solid skeletons in order to obtain transparent aerogels. From these points of view, a fine and flexible control over microstructure is the key in the study on silica aerogels.

Aiming at practical uses, many researchers have been investigating improvement and reinforcement of the microstructure of silica aerogels for easier drying and handling, and indeed many possibilities have been proposed. The most common method to improve mechanical strength of silica-based materials is to leverage the Ostwald ripening, which contains a process of dissolution of higher positive curvature part and reprecipitation onto higher negative curvature part observed typically in solid–liquid two-phase systems.[9] Due to the increased thickness of the skeletons, mechanical properties such as Young's modulus of the material are highly improved. However, visible-light transmittance tends to decrease by an increasing contribution of the Mie scattering because of the thicker skeletons, which is undesirable for applications such as thermal insulating windows. Another method to improve the mechanical properties of silica aerogels is to laminate skeletons with organic polymers. By this method, Leventis and coworkers have synthesized some mechanically tough aerogels.[10] They used copolymerization systems of tetramethoxysilane and 3-aminopropyltrimethoxysilane as the precursors to obtain monolithic gels, and then allowed them to react with epoxy compounds on the surface of microstructure. While the obtained materials show good flexibility against compression and bending stresses, their properties such as thermal conductivity and visible-light transmittance are deteriorated compared to pure silica aerogels, due to the enlarged microstructure and partial loss of porosity.

In 2007, Kanamori and coworkers reported new organic-inorganic hybrid aerogels which consist of polymethylsilsesquioxane (PMSQ, $CH_3SiO_{1.5}$) derived from methyltrimethoxysilane (MTMS, $CH_3Si(OCH_3)_3$) as a precursor via an acid–base two-step sol–gel reaction.[11] These "silicone" aerogels show visible-light transmittance, low thermal conductivity like silica aerogels, and strength and elasticity enough to recover their original size and shape from 80 % uniaxial compression, which had never been reported previously.[11-12] These new aerogels take advantage of flexibility for improving brittleness of aerogels, while many of the old methods aim at reinforcement by forming rigid structures. To synthesize such silicone aerogels, there had been several problems prior to the report. Polysilsesquioxanes are organic–inorganic hybrid, and contain

hydrophobic organic moieties in the siloxane network. In the case of PMSQ, one methyl group is directly bonded to each silicon atom in the network. Due to the hydrophobicity of the organic moiety, it was difficult to synthesize a homogenous gel via a sol–gel process in aqueous solution, because hydrophobicity becomes higher with increasing degree of polymerization. To solve the problem, Kanamori et al. employed surfactant to suppress the phase separation during the formation of crosslinked networks until gelation is completed. In addition, they used an acid–base two-step reaction to obtain further homogeneous networks and microstructure.[13] In the acid–base two-step reaction, the acid-catalyzed hydrolysis occurs on alkoxysilanes in the first step, followed by the base-catalyzed condensation in the second step to form highly branched 3-dimensional (3-D) networks; whereas cage-like polyhedral oligomeric silsesquioxanes would become a major condensation product in acidic conditions.[6] The new PMSQ gels have added remarkable features to the history of aerogels. Xerogels with comparable properties with those of aerogels can be obtained via ambient pressure drying without any special conditions due to their flexibility. During ambient pressure drying, wet gels start undergoing linear shrinkage by ~50 % and then recover to their original size and shape by the "spring-back" behavior.[14] This phenomenon can be observed owing to the following three features of the PMSQ network; 1) lower crosslinking density compared to silica for flexible deformation of the network, 2) lower silanol density for suppression of irreversible shrinkage, and 3) hydrophobic methyl groups for enhancement of spring-back. In addition, as-prepared PMSQ aerogels/xerogels already show strong hydrophobicity. This is a considerable advantage compared to silica aerogels which need a hydrophobizing treatment by a silylating agent to avoid degradation by atmospheric humidity.[15]

The first half of this thesis describes the detailed synthesis and characterization of PMSQ aerogels via the sol–gel reaction with suppressing and controlling phase separation with surfactant. The contents of the relevant chapters are as follows:

In chapter 1, changes in the structure and properties of PMSQ aerogels are discussed by employing cationic *n*-hexadecyltrimethylammonium chloride

(CTAC) as a surfactant. Exploration of the synthetic parameters such as the starting composition in the system leads to variations of physical properties of resultant aerogels. Optimization of the parameters in the synthesis of aerogels is also presented.

In chapter 2, controls over phase separation by a nonionic surfactant, Pluronic F127, instead of CTAC are discussed. A transition from transparent aerogels to hierarchically porous monoliths has been observed by decreasing the concentration of F127 due to moderate phase separation by spinodal decomposition (Figure 2).[16] At the same time, relationships between thermal conductivity, gas pressure and pore size have been investigated for the practical application of these porous monoliths to thermal insulators. The obtained data on thermal conductivity have been discussed based on the theory of thermal conduction in porous materials. In addition, an aerogel-like xerogel have been prepared, for the first time, to demonstrate the possibility of utilizing it as a high-performance thermal insulating panel.

In chapter 3, improvement of mechanical properties of PMSQ aerogels by forming composites with cellulose nanofibers (CNFs) is reported. By adding only a small amount of CNFs in the starting solution, bending flexibility has been introduced in the obtained low-density aerogels, which had not been observed in any monolithic aerogels including the pristine PMSQ aerogels. A new possibility toward the reinforcement of the PMSQ networks in a simple manner is demonstrated.

The latter half of the thesis describes novel flexible porous materials as an extension of the above-mentioned sol–gel system discussed in chapter 1. In the previous research on the sol–gel-derived materials, there have been only a few reports on the materials with sovereign flexibility. By replacing a part of MTMS with dimethyldimethoxysilane (DMDMS, $(CH_3)_2Si(OCH_3)_2$) in the sol–gel system, “marshmallow-like” macroporous gels have been successfully obtained. Due to the coarsened microstructure as compared to the PMSQ aerogels and decreased crosslinking density, the obtained marshmallow-like gels show outstanding properties such as flexibility and hydrophobicity in the wide temperature range, while transparency is lost.

In chapter 4, fundamental properties of the marshmallow-like gels have been investigated as a function of synthetic parameters. By increasing the ratio of DMDMS to MTMS, the microstructure is coarsened and the Young's modulus of the gels is dramatically decreased. Variations in the porous structures and corresponding mechanical properties evaluated by compression and bending tests are discussed in detail. Easy applicability of the ambient drying to obtain the marshmallow-like gels is also demonstrated.

In chapter 5, detailed properties and possible applications of the marshmallow-like gels are shown. The flexible porous materials show stable structure and properties in the wide temperature range similarly to the typical silicone polymer, polydimethylsiloxane (PDMS). The marshmallow-like gels show flexibility even at the liquid nitrogen temperature. Utilizing their superhydrophobic surfaces, an application to oil–water separation has been examined. Additionally, alteration of the surface property of the marshmallow-like gels is investigated by employing different combinations of alkoxysilanes instead of MTMS and DMDMS.

In chapter 6, surface modification of the marshmallow-like gels is performed. The surface of the marshmallow-like gels derived from a co-precursor system of vinyltrimethoxysilane (VTMS, CH_2=$CHSi(OCH_3)_3$) and vinylmethyldimethoxysilane (VMDMS, CH_2=$CH(CH_3)Si(OCH_3)_2$) has been reacted with perfluoroalkyl thiol by the thiol–ene click reaction. The resultant marshmallow-like gel shows superoleophobicity, which opens the possibility of designing new antifouling flexible monolithic materials.

In the present thesis, the relationships between properties and microstructure of the polyorganosiloxane (silicone) porous materials with varying synthetic parameters such as starting compositions have been discussed. Appropriate controls over sol–gel transition and selection of precursors and additives critically determine the final morphology and the resultant physicochemical properties of the porous monoliths. In particular, phase separation parallel to the sol–gel transition plays the key role in the polyorganosiloxane systems in aqueous solutions due to the hydrophobicity of the networks. In addition, possible applications of these materials are discussed in

each chapter for the purpose of connecting the fundamental research to practically useful technology.

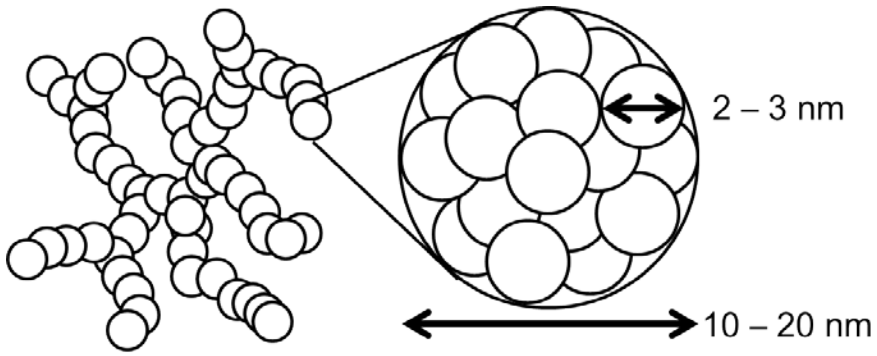

Figure 1 Schematic image of the microstructure of silica aerogels.

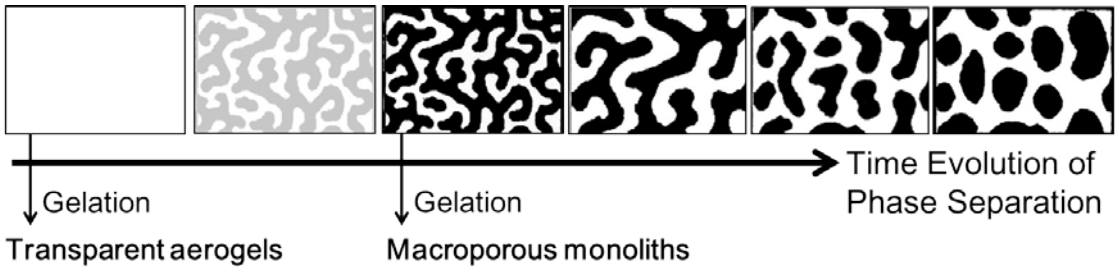

Figure 2 Schematic image of the sol–gel reaction accompanied by spinodal decomposition. The transient structure of spinodal decomposition is irreversibly frozen-in as a PMSQ microstructure by the sol–gel transition.

References

[1] S. S. Kistler, *Nature* **1931**, *127*, 741.

[2] a) N. Hüsing, U. Schubert, *Angew. Chem. Int. Ed.* **1998**, *37*, 23; b) L. W. Hrubesh, *J. Non-Cryst. Solids* **1998**, *225*, 335; c) J. Fricke, T. Tillotson, *Thin Solid Films* **1997**, *297*, 212; d) A. C. Pierre, G. M. Pajonk, *Chem. Rev.* **2002**, *102*, 4243.

[3] M. Tabata, I. Adachi, H. Kawai, T. Sumiyoshi, H. Yokogawa, *Nuclear Instruments & Methods in Physics Research Section A: Accelerators Spectrometers Detectors and Associated Equipment* **2012**, *668*, 64.

[4] J. P. Randall, M. A. B. Meador, S. C. Jana, *ACS Applied Materials & Interfaces* **2011**, *3*, 613.

[5] L. L. Hench, J. K. West, *Chem. Rev.* **1990**, *90*, 33.

[6] D. A. Loy, B. M. Baugher, C. R. Baugher, D. A. Schneider, K. Rahimian, *Chem. Mater.* **2000**, *12*, 3624.

[7] C. J. Brinker and G. W. Scherer, in *Sol-Gel Science: The Physics and Chemistry of Sol-Gel Processing*, Academic Press, San Diego, **1990**, pp. 108-216.

[8] a) X. Lu, M. C. Arduinischuster, J. Kuhn, O. Nilsson, J. Fricke, R. W. Pekala, *Science* **1992**, *255*, 971; b) X. Lu, P. Wang, M. C. Arduinischuster, J. Kuhn, D. Buttner, O. Nilsson, U. Heinemann, J. Fricke, *J. Non-Cryst. Solids* **1992**, *145*, 207; c) X. Lu, R. Caps, J. Fricke, C. T. Alviso, R. W. Pekala, *J. Non-Cryst. Solids* **1995**, *188*, 226; d) M. Reim, W. Korner, J. Manara, S. Korder, M. Arduini-Schuster, H. P. Ebert, J. Fricke, *Solar Energy* **2005**, *79*, 131; e) K. Swimm, G. Reichenauer, S. Vidi, H. P. Ebert, *Int. J. Thermophys.* **2009**, *30*, 1372; f) G. Wei, Y. Liu, X. Zhang, F. Yu, X. Du, *Int. J. Heat Mass Transfer* **2011**, *54*, 2355.

[9] a) C. Wagner, *Zeitschrift Fur Elektrochemie* **1961**, *65*, 581; b) C. J. Brinker, G. W. Scherer, *J. Non-Cryst. Solids* **1985**, *70*, 301.

[10] a) G. Zhang, A. Dass, A.-M. M. Rawashdeh, J. Thomas, J. A. Counsil, C. Sotiriou-Leventis, E. F. Fabrizio, F. Ilhan, P. Vassilaras, D. A. Scheiman, L. McCorkle, A. Palczer, J. C. Johnston, M. A. Meador, N. Leventis, *J. Non-Cryst. Solids* **2004**, *350*, 152; b) M. A. B. Meador, E. F. Fabrizio, F. Ilhan, A. Dass, G. Zhang, P. Vassilaras, J. C. Johnston, N. Leventis, *Chem. Mater.* **2005**, *17*, 1085;

c) U. F. Ilhan, E. F. Fabrizio, L. McCorkle, D. A. Scheiman, A. Dass, A. Palczer, M. B. Meador, J. C. Johnston, N. Leventis, *J. Mater. Chem.* **2006**, *16*, 3046; d) N. Leventis, *Acc. Chem. Res.* **2007**, *40*, 874.

[11] K. Kanamori, M. Aizawa, K. Nakanishi, T. Hanada, *Adv. Mater.* **2007**, *19*, 1589.

[12] a) K. Kanamori, M. Aizawa, K. Nakanishi, T. Hanada, *J. Sol-Gel Sci. Technol.* **2008**, *48*, 172; b) K. Kanamori, *J. Ceram. Soc. Jpn.* **2011**, *119*, 16.

[13] a) D. W. Schaefer, *Science* **1989**, *243*, 1023; b) C. J. Brinker, R. Sehgal, S. L. Hietala, R. Deshpande, D. M. Smith, D. Loy, C. S. Ashley, *Journal of Membrane Science* **1994**, *94*, 85.

[14] S. S. Prakash, C. J. Brinker, A. J. Hurd, S. M. Rao, *Nature* **1995**, *374*, 439.

[15] H. Yokogawa, M. Yokoyama, *J. Non-Cryst. Solids* **1995**, *186*, 23.

[16] a) H. Kaji, K. Nakanishi, N. Soga, *J. Non-Cryst. Solids* **1995**, *181*, 16; b) H. Kaji, K. Nakanishi, N. Soga, *J. Non-Cryst. Solids* **1995**, *185*, 18; c) K. Nakanishi, *J. Porous Mater.* **1997**, *4*, 67.

List of Acronyms

CNF: cellulose nanofiber

CTA: *n*-hexadecyltrimethylammonium

CTAB: *n*-hexadecyltrimethylammonium bromide

CTAC: *n*-hexadecyltrimethylammonium chloride

DMDMS: dimethyldimethoxysilane

MTMS: methyltrimethoxysilane

PDMS: polydimethylsiloxane

VMDMS: vinylmethyldimethoxysilane

VTMS: vinyltrimethoxysilane

Chapter 1

Structure and Properties of Polymethylsilsesquioxane Aerogels Synthesized with Surfactant *n*-Hexadecyltrimethylammonium Chloride

1.1 Introduction

Aerogels are prepared with various chemical compositions ranging from inorganic oxides such as silica and alumina, to organic cross-linked polymers such as resorcinol–formaldehyde (RF) resins.[1] Typical high-quality silica aerogels, which are generally prepared by the sol–gel process, possess high porosity (>90%) and small pore size (~50 nm) with the porous texture consisting of aggregates of silica nanoparticles (~10 nm). Owing to these structural features, a number of excellent properties are attained; high transparency, low refractive index, low thermal conductivity, and low dielectric constant. In particular, applications to (transparent) thermal insulators[2], catalyst supports[3], supercapacitors[4], and low-*k* materials[5] are widely concerned and much effort is made to fabricate aerogels with low-cost and efficient mass production processes. However, aerogels are inherently brittle due to the high porosity and to the weak linkage of the aggregated particles. To keep the delicate pore structure intact during the removal of solvent from the precursor wet gels, supercritical drying instead of simple evaporative drying is required, in which high pressure (and high temperature) is needed. This fatal drawback keeps aerogels away from the extended applications. To improve the mechanical properties, much effort has been paid so far. Some researchers investigated the effect of extended aging in water, monomer solution, and mother solvent[6] to dry wet gels in milder (*i.e.* subcritical) conditions or even under ambient pressure and temperature. During the aging process, small primary particles with high positive curvature preferentially dissolve and re-precipitate onto the “neck” portion with high negative curvature in-between contacting particles. The resultant skeletal structure contains the smoothed linkage of particles, which increases the stiffness

and strength of the original gel. Aging in monomer solution drastically enhances the mechanical properties by incorporating monomers from the aging solution into the as prepared gel networks to increase the cross-linking density. Hybridization with organo-functional silanes or organic polymers is another promising way to increase the mechanical durability of aerogels[7]. Although sacrificing the transparency due to macroscopic phase separation of hydrophobic networks, organic-inorganic hybrid aerogels prepared from MTMS[7d] and MTMS–DMDMS co-precursors[7h] show unusual flexibility, as discussed in chapters 4–6.

Simultaneously, the author has demonstrated that a modified 2-step sol–gel process containing urea and surfactant prevents the occurrence of macroscopic phase separation, and transparent organic-inorganic hybrid aerogels are obtained utilizing MTMS as a single precursor[8]. The resultant ideal gel network is represented as PMSQ. Urea is hydrolyzed into ammonia and carbon dioxide at 60 °C after the hydrolysis of MTMS which is catalyzed by dilute acetic acid, accelerates condensation and promotes homogeneous gelation by raising solution pH. The author used appropriate surfactants which effectively suppress phase separation by making the MTMS-derived condensates hydrophilic. In the case of nonionic surfactant, poly(ethylene oxide)-block-poly(propylene oxide)-block-poly(ethylene oxide) ($EO_{106}PO_{70}EO_{106}$, Pluronic F127)[9], it was deduced that MTMS-derived condensates were made hydrophilic through an attractive interaction between F127 and MTMS condensates. When cationic CTA salt (bromide CTAB or chloride CTAC) is employed, the MTMS condensates are more strongly made hydrophilic by weakly interacting with the hydrophobic chain of CTAB/CTAC. The resultant aerogels showed an unusual spring-back behavior which contains the compression of aerogel without cracking and the following perfect recovery when unloaded. Successful drying of wet gels without utilizing supercritical drying was also reported[8a]. Low-density and transparent xerogels with comparable properties to corresponding aerogels thus obtained are promising for various applications such as to thermal insulators due to their potential for low-cost productions.

In chapter 1, the author shows the control of pore structures and

properties by systematically altering the starting composition. In particular, effects of changing concentrations of surfactant, urea and solvent are investigated. To minimize the effect of drying, all the gels have been processed by supercritical drying. The pore structure of aerogels is observed by field emission electron microscopy (FE-SEM). Properties including bulk density, light transmittance and compressive mechanical properties are also studied. The comprehensive information on relationships between starting compositions and physical properties is highly important to understand and design the pore properties of PMSQ aerogels/xerogels.

1.2 Experimental

1.2.1 Chemicals

Acetic acid, distilled water, urea, methanol, and 2-propanol were purchased from Hayashi Pure Chemical Ind., Ltd. (Japan). Surfactant CTAC was from Tokyo Chemical Ind. Co., Ltd. (Japan). Methyltrimethoxysilane (MTMS) was obtained from Shin-Etsu Chemical Co., Ltd. (Japan). All reagents were used as received.

1.2.2 Synthesis procedures

The sample notations are defined, for example, as C*w*A*x*-*y*U*z*, where *w*, *x*, *y* and *z* are weight of CTAC (in g), concentration of aqueous acetic acid (in mM), volume of aqueous acetic acid (in mL) and weight of urea (in g), respectively. At the typical starting composition C0.4A5-10U3, 10 mL of 5 mM aqueous acetic acid, 0.40 g of surfactant CTAC and 3.0 g of urea were dissolved in a glass sample tube, and then 5 mL of MTMS was added with vigorous stirring. The molar ratio of this typical starting composition is MTMS:water:acetic acid:urea:CTAC = 1.0:1.6 × 10:1.4 × 10^{-3}:1.4:3.6 × 10^{-2}. The mixed solution was continuously stirred for 30 min at room temperature for acid-catalyzed hydrolysis, followed by base-catalyzed gelation and aging at 60 °C in a closed vessel for 4 d. The typical gelation time was about 3 h. The wet gels thus obtained were soaked in water/methanol (volume ratio 1:1) once, then methanol twice and 2-propanol three times each at 8 h duration to remove CTAC and other unreacted reagents. Alcogels obtained in this way were dried from supercritical carbon dioxide at 80 °C, 14.0 MPa for 10 h in a custom-built autoclave (Mitsubishi Materials Corp., Japan) to obtain aerogels.

1.2.3 Measurements

The pore structure was observed with an FE-SEM JSM-6700F (JEOL Ltd., Japan). Bulk density, ρ, was obtained by measuring the volume and weight of a carved gel. Porosity e (%) was then determined as $e = (1 - \rho/\rho_s)\times 100$, where ρ_s represents true density that was fixed to be 1.40 g cm^{-3} determined for a typical

MTMS-derived aerogel by helium pycnometry. For visible-light transmittance measurements, a UV-VIS spectrometer V-670 (JASCO Corp., Japan) equipped with an integrating sphere ISN-723 was employed. Direct-hemispherical transmittance was recorded, and obtained transmittance data at 550 nm were normalized into those of 10 mm-thick samples using the Lambert–Beer equation. The normalized total transmittance is denoted as T. For uniaxial compression tests, specimens carved from large panels (typical length × width × height is 10 × 10 × 6 mm^3) were compressed–decompressed using a load cell of 5 kN with a rate of 0.5 mm min^{-1}. Young's modulus E was calculated using the slope of stress–train curves between 0.1 and 0.2 MPa stress.

1.3 Result and Discussion

1.3.1 Effects of CTAC

In many reaction conditions, MTMS does not form uniform gel networks in polar solvents, due to the high phase separation tendency resulted from the strong hydrophobicity of the polymethylsilsesquioxane networks. To synthesize uniform monolithic aerogels, the author used the method utilizing surfactant in starting compositions to suppress phase separation. In C*w*A5-10U3 system, the author obtained transparent elastic aerogels with $w > 0.10$ g of CTAC (molar ratio [CTAC]/[MTMS] > 0.009), and relationships are presented between w and several properties as T, ρ and Young's modulus in Figure 1.1. Light transmittance at 550 nm showed the maximum at $w = 0.40$ g with $T = 89\%$ (sample shown in Figure 1.2a). Bulk density ρ of this aerogel was 0.138 g cm^{-3} and porosity e was calculated as 90 %. With increasing w, the light transmittance value T gradually decreased due to decreasing network homogeneity. Although monolithic aerogels can be obtained even with > 4.00 g of CTAC ([CTAC]/[MTMS] > 0.36), visible-light transmittance was low. In the cases of other surfactants, for example Pluronic F127, there is the upper limit of the amount of surfactant in the starting composition to obtain a monolithic gel. It is suggested that the interaction between CTAC and the PMSQ condensates is weaker, and interruption of polycondensation hardly occurs. The attractive interaction may be predominantly based on the weak hydrophobic interaction between alkyl chains of CTAC and hydrophobic condensates.

With varying the amount of CTAC, microstructures (Figure 1.3) as well as the physical properties of aerogels were changed. In C*w*A5-10U3 system, these changes can be explained by dividing into 4 regions about the w value. 1) In $w < 0.10$ ([CTAC]/[MTMS] < 0.009), macroscopic phase separation occurred because the amount of CTAC molecules is not enough to suppress the strong hydrophobicity of PMSQ networks. The resultant coarse structure is shown in Figure 1.3a. 2) In $0.10 < w < 0.60$ ($0.009 <$ [CTAC]/[MTMS] < 0.054), the gel network became uniform because the moderate amount of CTAC effectively interacted with the hydrophobic networks and suppressed phase separation. At w

= 0.40 (Figure 1.3b), the aerogel exhibited the highest light transmittance and lowest density, as mentioned above. 3) In 0.60 < *w* < 1.20 (0.054 < [CTAC]/[MTMS] < 0.11), excess CTAC molecules weakly interfere the network formation and gels shrank more during the solvent exchange and supercritical drying, due to the lower crosslinking density and weaker connections between particles composing the gel skeleton. At *w* = 0.80 ([CTAC]/ [MTMS] = 0.072), shrinkage reached a maximum in this system, and the resultant finer structure is exhibited in Figure 1.3c. Bulk density and Young's modulus became larger than those of the aerogels in the region 2) as can be confirmed in Figures 1.1a and c. These factors show a good correlation because both of these factors are strongly influenced by the shrinkage during aging, solvent exchange, and drying; the higher shrinkage leads to the increased bulk density and Young's modulus. 4) With further increasing *w*, the microstructure became coarser (Figure 1.3d), and accordingly the less shrinkage has been observed. The larger particles and their less homogeneous aggregations decreased *T* because of the enhanced Mie scattering as can be confirmed in Figure 1.1b. The mechanism of particles growth and their aggregations may be caused by multiple factors, such as increased stability of condensates covered with CTAC molecules in the solution with an excess of CTAC, which retards the nucleation of colloidal particles.

1.3.2 Effects of Acetic Acid

In acidic conditions, alkoxysilanes including MTMS are efficiently and uniformly hydrolyzed. No hydrolysis occurred without acetic acid in the starting solutions investigated in this study. The author obtained monolithic aerogels when the concentration of acetic acid aqueous solution was in the range of *x* = 1–300 mM. Figure 1.4 shows the relationships between properties of aerogels and *x* (C0.4A*x*-10U3 system). With 1 < *x* < 10, there are no changes in these three properties, but with *x* > 10, *T* gradually decreased. With *x* > 60, ρ became higher but Young's modulus did not clearly change due to the higher shrinkage, which is caused by the enhanced formation of cyclic/polyhedral species (at 1100 cm^{-1}) instead of linear and branched species (at 1025 cm^{-1})[10] as evidenced in the FTIR spectra in Figure 1.5. The cyclic/polyhedral species do

not contribute to the strength of the gel network, and lead to the formation of inhomogeneous gel network due to increasing phase separation tendency (Figure 1.6). These results conclude the optimal concentration range of acetic acid to synthesize transparent aerogel is 1–10 mM. In this range, obtained aerogels possess almost the same properties, though hydrolysis rates are different.

1.3.3 Effects of urea

Although transparent PMSQ aerogel cannot be obtained under the one-step acidic condition due to the enhanced formation of cyclic/polyhedral species, the basic condition promotes polycondensation of MTMS monomers and oligomers into the branched network, which provides the good condition to obtain transparent aerogel monoliths with uniform networks. The author used urea as a base-releasing agent; urea is hydrolyzed into NH_4OH and CO_2 and uniformly raises pH of the aqueous sol. Figure 1.7 shows the pH curve of the solution with the typical starting composition C0.4A5-10U3 (but without MTMS) measured at 60 °C. In C0.4A5-10U3 system, the gelation time was ~3 h, and pH of the solution at the time was ~6.8. After gelation, pH continued to rise and finally reached 9.1 after 4 d.

With varied amount of urea, properties and pore structures of aerogels are clearly changed as shown in Figures 1.8 and 1.9. Monolithic gels could not be obtained with less than 0.50 g of urea. Without urea in the starting composition, the sol was stable even when acetic acid was sufficiently diluted, whereas a small amount of oil was separated after a few days. In C0.4A5-10Uz system, T increased and ρ and Young's modulus decreased with increasing amount of urea, which promoted polycondensation into random networks before an enhanced formation of cyclic/polyhedral species in the acidic condition owing to the higher rate of pH increase and shorter gelation time. The obtained networks also become homogeneous in such condition. In the C0.4A5-10U1 sample, the porous structure is coarser than that of C0.4A5-10U3 (Figure 1.9). Comparing z = 3 and 4 g, the obtained aerogels had almost the same properties because the networks became sufficiently uniform with such high amounts of urea. In z > 4, urea does not completely dissolve in the solution containing CTAC.

1.3.4. Effects of solvent volume

Water acts as the diluting solvent as well as reactant in hydrolysis in the present system. Properties as well as pore structures of aerogels are also affected by the volumetric ratio of 5 mM acetic acid aqueous solution (*y* mL):MTMS volume (5 mL, yielding 2.3 g solid if stoichiometric conversion is assumed) as shown in Figures 1.10 and 1.11. The author synthesized lower density aerogels by increasing the ratio of 5 mM acetic acid aqueous solution while fixing the concentration of urea (i.e. the *y* to *z* ratio is fixed in 10:3). With increasing *y*, ρ drastically decreased from ~0.50 to ~0.050 g cm^{-3} (Figure 1.10a) in all *y* ranges. The Young's modulus naturally decreased accordingly with the decrease of bulk density (*i.e.* the decrease of monomer concentration).

In $y < 20$, no syneresis and shrinkage was observed during gelation and aging processes. This phenomenon is uniquely observed on aerogels synthesized with CTA halide salts, but rarely in the conventional silica aerogels systems. The absence of shrinkage and syneresis during gelation and aging is attributed to the repulsion between the polar head groups on the surface of the network[9]. This fact shows that this starting compositional region is advantageous to form the low-density monoliths by avoiding shrinkage by syneresis. The highest *T* was recorded at $y = 14$ with the value of 91 % (Figures 1.10b and 1.11c). With further increase in *y*, *T* gradually decreased due to the disordering of pore structure by the higher shrinkage, which is caused by the lower mechanical strength of wet gels as shown in Figure 1.10c. In this system, crack-free aerogels are obtained when $y < 100$. At $y = 100$ (C0.4A5-100U30, the microstructure shown in Figure 1.11d), ρ and *e* showed minima with the values 0.045 g cm^{-3} and 97 %, respectively. This gel shrank ~30% of the original size during drying due to the low mechanical strength, and the dried aerogel became translucent (Figure 1.2b). In addition, the outer surface of these samples was easily collapsed on fingers by absorbing oil from the human skin, whereas aerogels can float on water for at least a month. In $100 < y < 150$, monolithic aerogels were obtained, but they had too many and large cracks to characterize physical properties. Gelation occurred even when $y = 1000$, but the alcogels are easily collapsed during solvent exchange so that dried monoliths cannot be

obtained.

With decreasing y from 10, ρ_b steeply increased, which can be predicted from the starting compositions. On the other hand, T was dramatically changed. In $4 < y < 6$, T became lower than 20 %, because viscosity of the sol increased by high concentration of CTAC and the microstructure became coarser due to the inhomogeneous networks formation governed by a slow diffusion. The coarse microstructure and aggregations of PMSQ particles are shown in the FE-SEM image (Figures 1.11a and b). In $y < 4$, aerogels became denser and T became higher than those of in $4 < y < 6$, due to the significant shrinkage and densification during the aging process.

In summary, the range in y = 8–18 mL is the good condition to obtain aerogels with high transparency and the uniform gel networks. Outside this range, features of aerogels such as uniform microstructure and high porosity are lost.

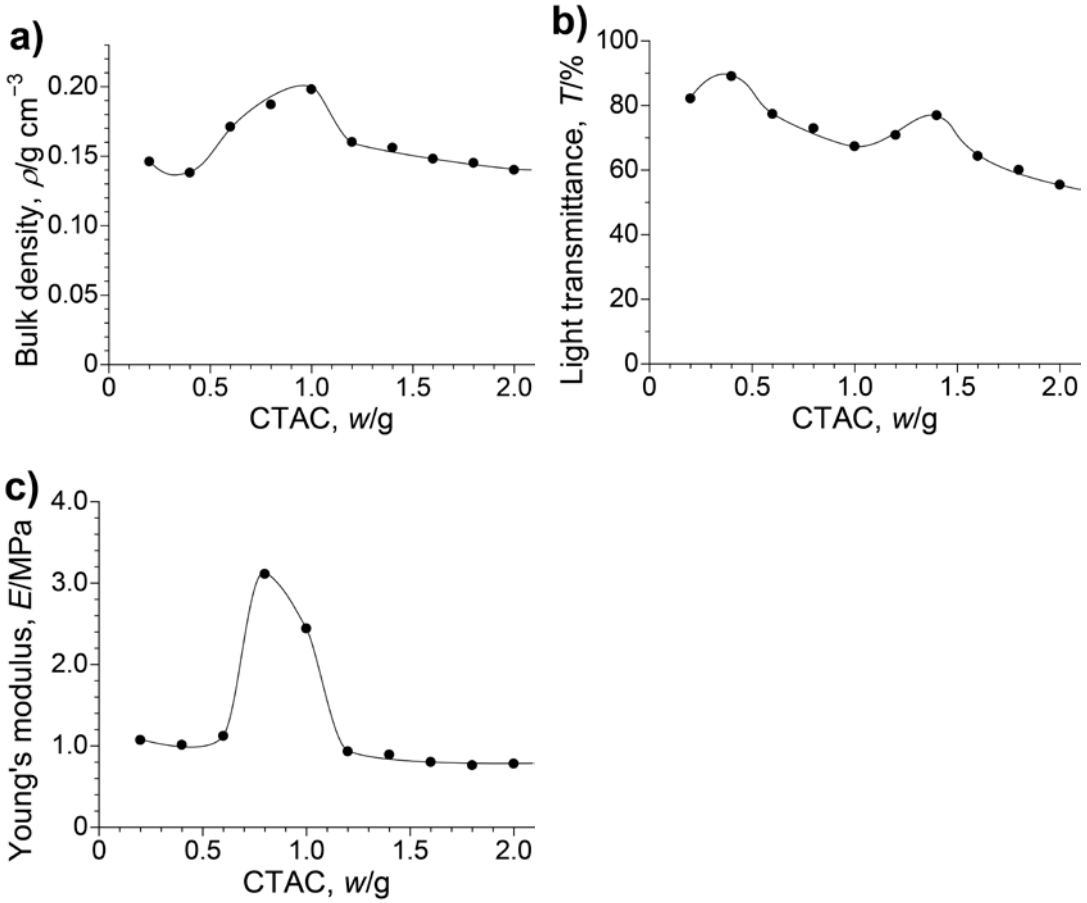

Figure 1.1 Physical properties of aerogels derived with varied amount of CTAC (C*w*A5-10U3 system); a) bulk density, ρ, b) light transmittance at 550 nm, T and c) Young's modulus, E.

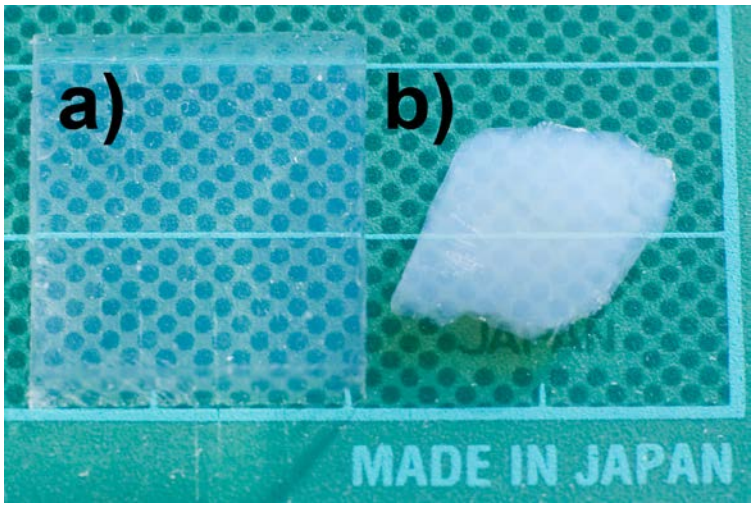

Figure 1.2 Digital camera images of the obtained aerogels; a) C0.4A5-10U3 and b) C0.4A5-100U30.

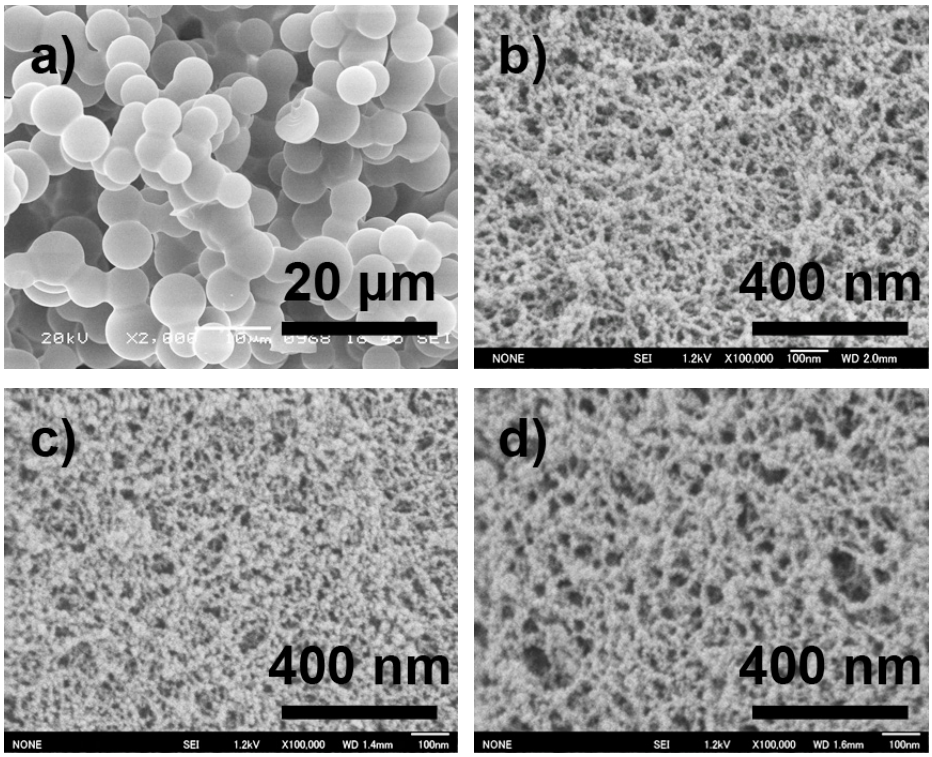

Figure 1.3 SEM images of aerogels derived with varied amount of CTAC (C*w*A5-10U3 system); a) *w* = 0 g, b) 0.4 g, c) 0.8 g and d) 2.0 g.

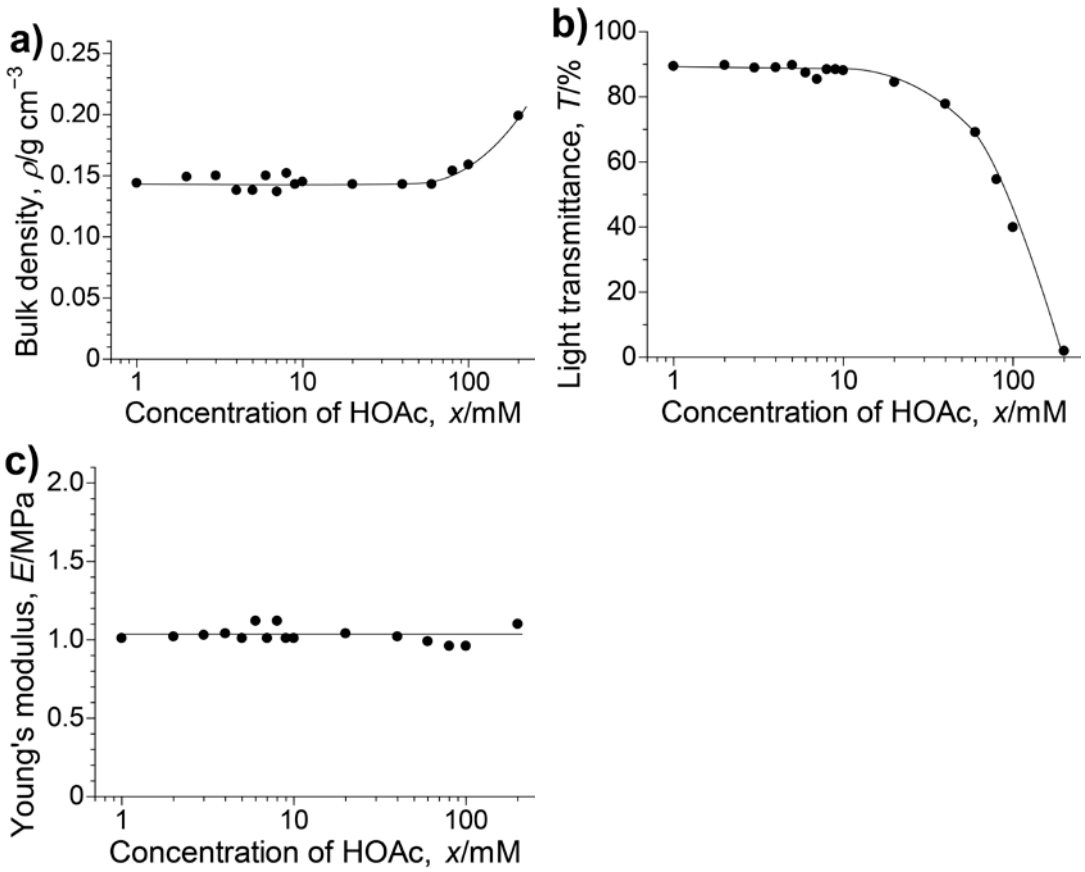

Figure 1.4 Physical properties of aerogels derived with varied concentration of acetic acid aqueous solution (C0.4A*x*-10U3 system); a) bulk density, ρ, b) light transmittance at 550 nm, T and c) Young's modulus, E.

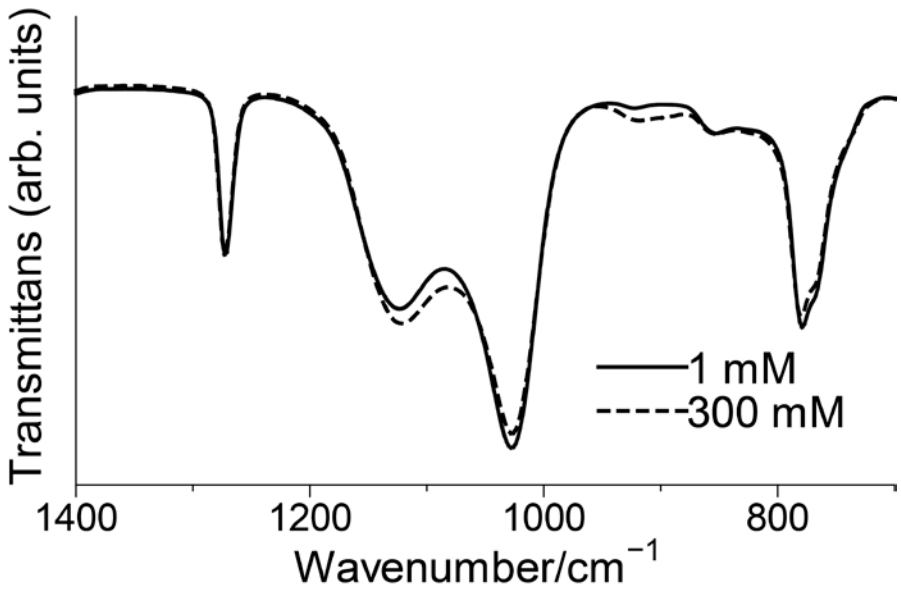

Figure 1.5 FTIR spectra of aerogels derived with varied concentration of acetic acid aqueous solution (C0.4A*x*-10U3 system); 1 mM and 300 mM.

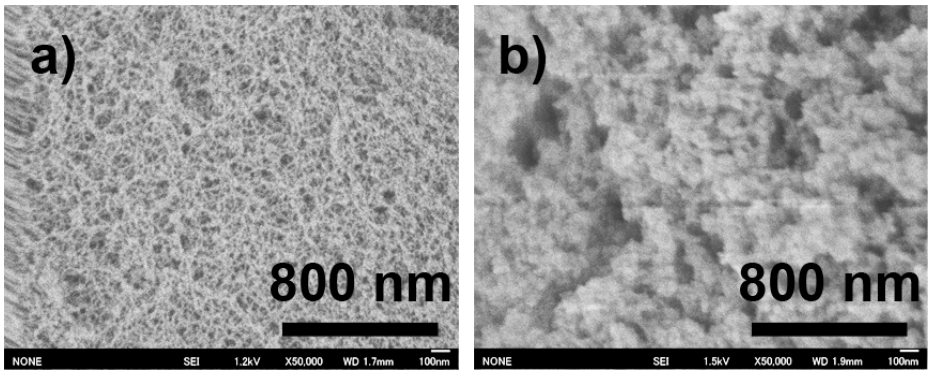

Figure 1.6 SEM images of the aerogels with varied concentration of acetic acid aqueous solution (C0.4A*x*-10U3 system); a) *x* = 5 mM and b) 300 mM.

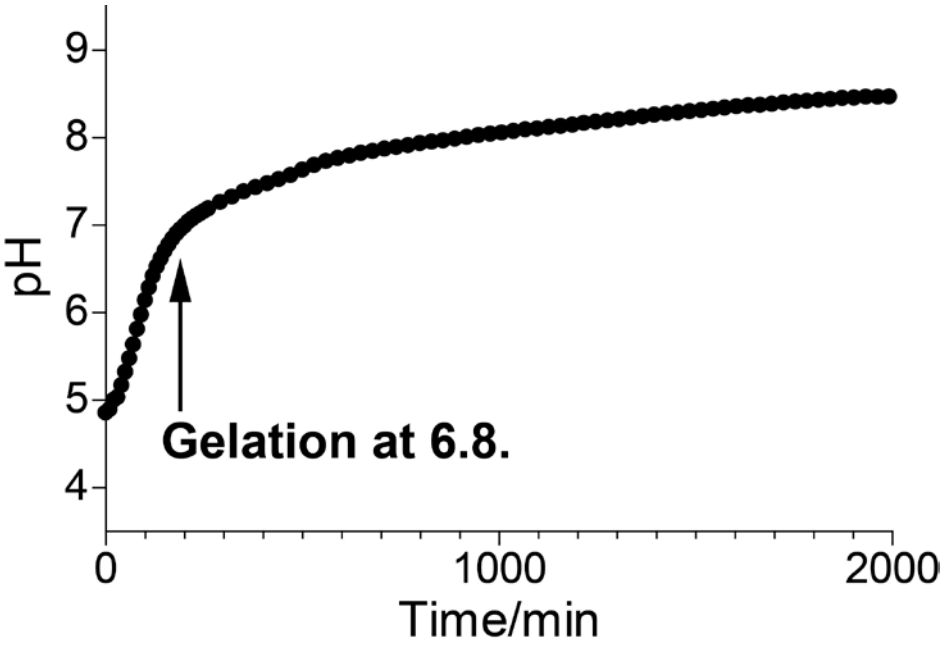

Figure 1.7 Change in pH of the solvent with the typical starting composition C0.4A5-10U3 without MTMS at 60 °C.

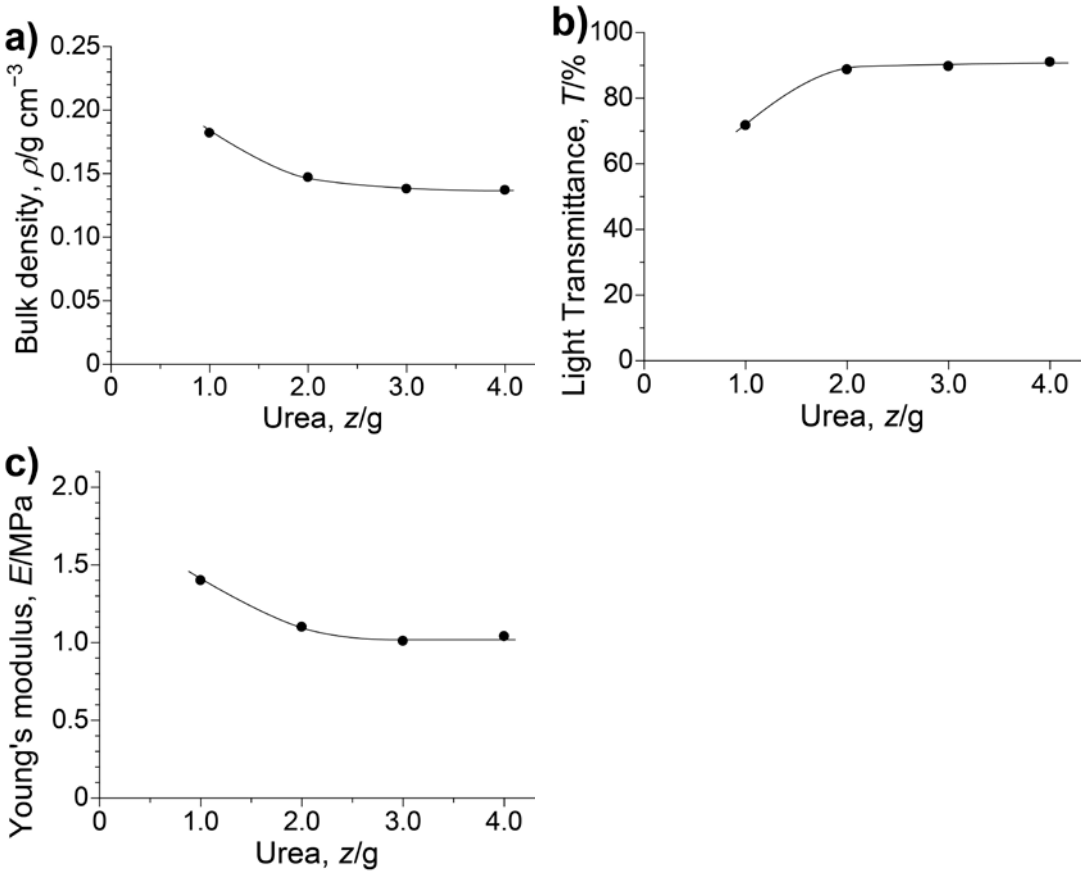

Figure 1.8 Physical properties of aerogels derived with varied amount of urea, *z* (C0.4A5-10U*z* system); a) bulk density ρ, b) light transmittance at 550 nm, *T* and c) Young's modulus *E*.

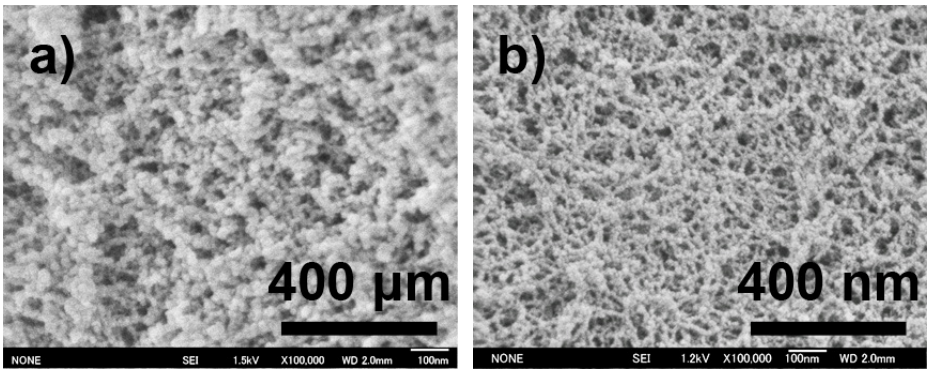

Figure 1.9 SEM images of the aerogels with varied amount of urea *z* (C0.4A5-10U*z* system); a) *z* = 1.0 g and b) 3.0 g.

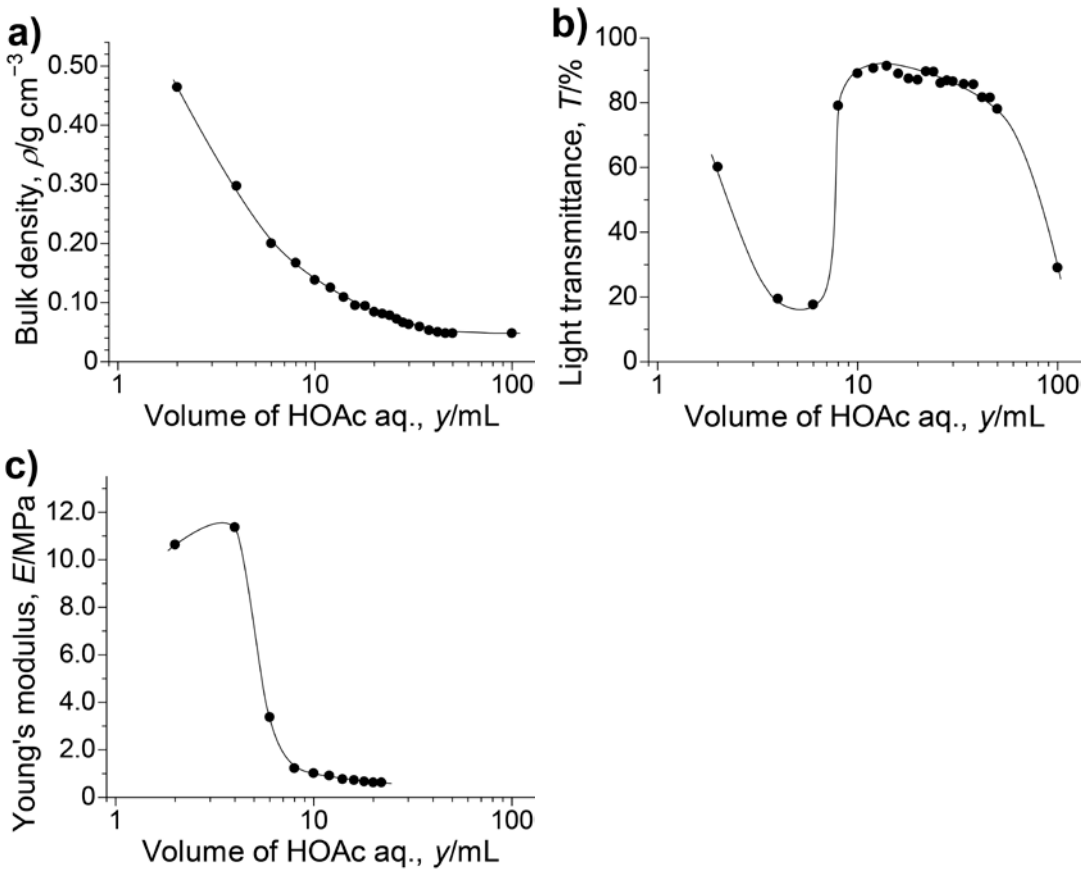

Figure 1.10 Physical properties of aerogels derived with varied volume of solvent (C0.4A5-*y*U*z* system, with keeping *y*:*z* = 10:3); a) bulk density, ρ, b) light transmittance at 550 nm, *T* and c) Young's modulus, *E*.

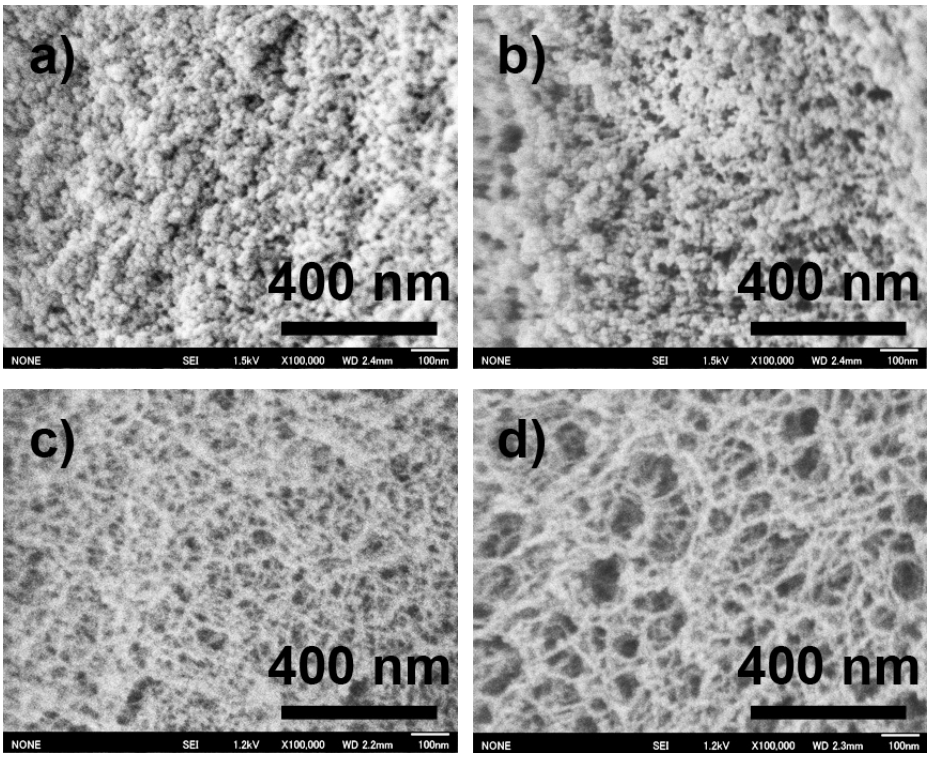

Figure 1.11 SEM images of the aerogels prepared with varied volume of solvent, *y* (C0.4A5-*y*Uz system, with *y*:*z* = 10:3); a) *y* = 2 mL, b) 4 mL, c) 14 mL and d) 100 mL.

1.4 Conclusion

Transparent PMSQ aerogels have been successfully obtained from MTMS under the co-presence of surfactant CTAC in the starting composition to suppress phase separation. As a result of the systematic study in this system, various properties of the aerogels are found to be affected by the starting composition. With the varied amount of CTAC, the porous texture of the gel is changed. To successfully obtain monolithic PMSQ aerogels, at least 0.10 g of CTAC ([CTAC]/[MTMS] = 0.009) should be included in the solution. At 0.40 g of CTAC ([CTAC]/[MTMS] = 0.036), the obtained gel has the highest light transmittance, but it decreases with increasing amount of CTAC. Density and Young's modulus are strongly correlated because both of these properties depend on the structure and strength of the gel networks. Concentrations of acid and base catalysts affect the molecular-level network and porous texture of the gels. With diluted acetic acid and increased amount of urea, the author can obtain aerogels with high light transmittance and low density. With increasing the ratio of solvent volume to MTMS, density becomes lower and higher shrinkage occurs during gelation, solvent exchange and drying. The minimum density of PMSQ aerogels obtained without cracks is 0.045 g cm^{-3}, while light transmittance is partially sacrificed.

References in Chapter 1

[1] a) J. Fricke, T. Tillotson, *Thin Solid Films* **1997**, *297*, 212; b) N. Hüsing, U. Schubert, *Angew. Chem. Int. Ed.* **1998**, *37*, 22; c) A.C. Pierre, G.M. Pajonk, *Chem. Rev.* **2002**, *102*, 4243.

[2] a) K. Duer, S. Svendsen, *Sol. Energy* **1998**, *63*, 259; b) K. I. Jensen, J. M. Schultz, F.H. Kristiansen, *J. Non-Cryst. Solids* **2004**, *350*, 351; c) M. Reim, W. Körner, J. Manara, S. Korder, M. Arduini-Schuster, H.-P. Ebert, J. Fricke, *Sol. Energy* **2005**, *79*, 131.

[3] a) G.M. Pajonk, *Appl. Catal.* **1991**, *72*, 217; b) C. Moreno-Castilla, F.J. Maldonado-Hódar, *Carbon* **2005**, *43*, 455.

[4] a) R. Saliger, U. Fischer, C. Herta, J. Fricke, *J. Non-Cryst. Solids* **1998**, *225*, 81; b) E. Frackowiak, F. Béguin, *Carbon* **2001**, *39*, 937.

[5] W. Volksen, R.D. Miller, G. Dubois, *Chem. Rev.* **2010**, *110*, 56.

[6] a) A. Rigacci, M.-A. Einarsrud, E. Nilsen, R. Pirard, F. Ehrburger-Dolle, B. Chevalier, *J. Non-Cryst. Solids* **2004**, *350*, 196; b) R.A. Strøm, Y. Masmoudi, A. Rigacci, G. Petermann, L. Gullberg, B. Chevalier, M.-A. Einarsrud, *J. Sol–Gel Sci. Technol.* **2007**, *41*, 291.

[7] a) B.M. Novak, D. Auerbach, C. Verrier, *Chem. Mater.* **1994**, *6*, 282; b) N. Hüsing, U. Schubert, *J. Sol–Gel Sci. Technol.* **1997**, *8*, 807; c) H. El Rassy, P. Buisson, B. Bouali, A. Perrard, A.C. Pierre, *Langmuir* **2003**, *19*, 358; d) A. Venkateswara Rao, S.D. Bhagat, H. Hirashima, G.M. Pajonk, *J. Colloid Interface Sci.* **2006**, *300*, 279; e) N. Leventis, *Acc. Chem. Res.* **2007**, *40*, 874; f) A. Fidalgo, J.P.S. Farinha, J.M.G. Martinho, M.E. Rosa, L.M. Ilharco, *Chem. Mater.* **2007**, *19*, 2603; g) T.-Y. Wei, S.-Y. Lu, Y.-C. Chang, *J. Phys. Chem. B* **2008**, *112*, 11881; h) G. Hayase, K. Kanamori, K. Nakanishi, *J. Mater. Chem.* **2011**, *21*, 17077.

[8] a) K. Kanamori, M. Aizawa, K. Nakanishi, T. Hanada, *Adv. Mater.* **2007**, *19*, 1589; b) K. Kanamori, M. Aizawa, K. Nakanishi, T. Hanada, *J. Sol–Gel Sci. Technol.* **2008**, *48*, 172; c) K. Kanamori, K. Nakanishi, T. Hanada, *J. Ceram. Soc. Jpn.* **2009**, *117*, 1333; d) K. Kanamori, K. Nakanishi, *Chem. Soc. Rev.* **2011**, *40*, 754; e) K. Kanamori, *J. Ceram. Soc. Jpn.* **2011**, *119*, 16; f) K.

Kanamori, Y. Kodera, G. Hayase, K. Nakanishi, T. Hanada, *J. Colloid Interface Sci.* **2011**, *357*, 336.

[9] M. Meyer, A. Fischer, H. Hoffmann, *J. Phys. Chem. B* **2002**, *106*, 1528.

[10] H. Dong, J.D. Brennan, *Chem. Mater.* **2006**, *18*, 4176.

Chapter 2

Relationship between Gas Pressure and Thermal Conductivity of Polymethylsilsesquioxane Aerogels/Xerogels with Varied Pore Sizes Controlled by Using Surfactant Pluronic F127

2.1 Introduction

It is no doubt that thermal insulation, which decreases the energy consumption in various processes, is one of the important issues today. Thermal insulating materials with low thermal conductivity are widely used in our life to keep desirable temperature in buildings, to protect from burns, and to reduce energy consumptions in electrical appliances such as refrigerators. In industry, insulating materials are more extensively used for improving the energy balance in plants, preventing equipment from troubles, and storage of liquefied gases. In addition, insulation of engines, batteries, and cargos in transportation is becoming increasingly crucial from the viewpoint of saving energy.

Aerogel is one of the most expected thermal insulating materials, because it shows the lowest thermal conductivity of all solid materials.[1] Typical aerogels specially designed for the thermal insulating purpose show excellent insulation with thermal conductivity < 15 mW m^{-1} K^{-1}, which is appreciably lower compared to those of classical insulating materials, 21–40 mW m^{-1} K^{-1}.[1a,1b,2] Although commercially available vacuum insulation systems outstrip the insulation of aerogels, the vacuum gradually degrades during long-term use by leaks. Vacuum insulation therefore needs robust frameworks and regular maintenance to keep the high insulation. Aerogels, on the other hand, are stable solid as far as being hydrophobized,[3] and can be used at ambient pressure for long duration of time. In addition, aerogel-based thermal insulation has a large advantage in saving space and weight for many applications including space development, because the less amount of insulating materials is required to achieve the comparable insulation to the traditional materials.[1c,2b,3] Especially in typical silica aerogels, aerogel glazings are expected as a transparent window insulating

system,[1c,2b] because silica aerogels have visible-light transmittance and low refractive index.[1b] However, mechanical strength of these low-density materials is so low that they are easily cracked and collapsed even by a slight curvature caused during processing and by the wind while in use. Even worse is the requirement of a supercritical fluid such as carbon dioxide or alcohols as a drying solvent to keep their porous structure throughout the drying process, which needs to be performed under high temperature and pressure. There is a size limitation to available aerogels because of that of an autoclave that can be safely operated from technical and legal aspects. For this reason, there has been limited precedent of large-area monolithic aerogels with, for example, the size of a window glass. Instead, aerogel granules and composites are widely employed for larger-area daylighting and wall insulation systems.[1c,1d]

To improve the mechanical properties of transparent aerogels, many researchers have been trying various strategies. In chapter 1, pore structures and properties are controlled by systematically altering the starting composition with surfactant CTAC. In this system, the obtained aerogels had highly visible-light transmittance, but are difficult to be dried via ambient pressure due to their fine structure. On the other hand, PMSQ aerogels with using nonionic surfactant F127 can be synthesized with continuously controlled pore size from 50 nm to 3 μm.[4] Although these aerogels are designed to possess rather high density (> 0.2 g cm^{-3}) in order to obtain co-continuous structure in the extended length scale, mechanical properties such as Young's modulus are higher compared to the previous PMSQ aerogels, which enables even easier handling. In this chapter, the author discusses the relationships between pore size, mechanical property and thermal conductivity with varied gas pressure. Although several researchers reported the effects of pore size and gas pressure on thermal conductivity using carbon and silica aerogels in these 20 years,[5] this is the first report on the organic-inorganic hybrid aerogels with well-defined morphology and extensively variable pore size. The author also demonstrate the possibility of PMSQ aerogel-like xerogels obtained by a simple drying process in ambient temperature and pressure as a practical insulating material with sufficiently low thermal conductivity of 15 mW m^{-1} K^{-1}.

2.2 Experimental

2.2.1 Chemicals

Acetic acid, methanol, 2-propanol and *n*-heptane were purchased from Kishida Chemical Ltd. (Japan). Distilled water and urea were from Hayashi Pure Chemical Ind., Ltd. (Japan). Surfactant poly(ethylene oxide)-*block*-poly(propylene oxide)-*block*-poly (ethylene oxide) ($EO_{106}PO_{70}EO_{106}$, Pluronic F127, M_w = 12600) was from BASF (Germany). Methyltrimethoxysilane (MTMS) was obtained from Shin-Etsu Chemical Co., Ltd. (Japan). All reagents were used as received.

2.2.2 Synthesis procedures

The starting compositions are listed in Table 2.1. In a typical synthesis, 60 mL of diluted aqueous acetic acid (5 mM), 5 g of urea, and 0–10.0 g of surfactant (Pluronic F127) were mixed in a glass sample bottle, and 50 mL of MTMS was subsequently added under vigorous stirring. Molar ratio of the starting materials is MTMS:water:acetic acid:urea:F127 = 1:9.6:0.00086:0.24:0–0.0023. After the mixed solution was continuously stirred for 30 min at room temperature to allow acid-catalyzed hydrolysis of MTMS, the resultant homogeneous solution was allowed to gel at 60 °C in a closed vessel. At this stage, urea hydrolyzes into ammonia, which promotes the base-catalyzed polycondensation of hydrolyzed MTMS. Gelation time was 6–6.5 h for all samples, and phase separation (if induced) and gelation were almost concurrent. The wet gel was then aged for 4 d to complete the condensation, followed by washing with methanol for three times (more than 8 h at 60 °C for each time) to remove the surfactant, unreacted species, *etc*. The washed sample was subjected to solvent exchange with 2-propanol for three times in the identical way to washing. To dry wet gels, supercritical drying and evaporative drying at ambient pressure and temperature were performed. For supercritical drying, 2-propanol in wet gels was exchanged with supercritical carbon dioxide at 80 °C and 14 MPa in a custom-built autoclave (Mitsubishi Materials Techno Corp., Japan) followed by a slow depressurizing to atmospheric pressure. For

evaporative drying, wet gels were subjected to solvent exchange with *n*-heptane for three times, and heptane was slowly removed by evaporation at room temperature for ~1 d. Obtained xerogels were finally heated with a hot oven at 110 °C in air for 3 h to completely remove heptane and liberate remnant stress and shrinkage of the networks.

2.2.3 Measurements

Bulk density ρ was obtained from the weight/volume ratio of specimens. Porosity Φ was then determined as $\Phi = 1 - \rho/\rho_s$, where ρ_s represents skeletal density of the PMSQ network (1.40 g cm^{-3}) determined by helium pycnometry. A scanning electron microscope (JSM-6700F, JEOL, Japan) was employed to observe the microstructure. Mechanical properties of aerogels were investigated with a material tester (EZGraph, Shimadzu Corp., Japan). For uniaxial compression tests, specimens carved from large panels (typical length × width × height is 15 × 15 × 10 mm^3) were compressed–decompressed using a load cell of 5 kN with a rate of 0.5 mm min^{-1}. For three-point bending tests, carved cuboid specimens were put on a fixture with a 15 mm span and loaded by a wedge-shaped crosshead with 60 ° tip and 0.3 mm diameter with using a load cell of 5 N at a rate of 1 mm min^{-1} to the point of brittle failure. Young's modulus E was calculated using the slope of stress–train curves between 0.1 and 0.2 MPa stress. For light transmittance measurements, a UV–VIS spectrometer V-670 (JASCO Corp., Japan) equipped with an integrating sphere ISN-723 was employed. Direct-hemispherical transmittance was recorded, and obtained transmittance data at 550 nm were normalized into those corresponding to equivalent thickness of 10 mm using the Lambert-Beer equation. The normalized total transmittance is denoted as T. Thermal conductivity was measured under varied pressure on aerogels and under ambient pressure on aerogels/xerogels with a guarded hot plate system GHP 456 Titan and a heat flow meter HFM 436 Lambda (Netzsch GmbH, Germany), respectively.

Table 2.1 Starting compositions and properties of aerogels obtained in the present study.

Materials	MTMS [mL]	HOAc aq. [mL]	Urea [g]	F127 [g]	E [MPa]	T [%]	ρ [g cm^{-3}]	Φ
S3.2	50.0	60.0	5.0	3.20	27	0	0.45	0.68
S3.4	50.0	60.0	5.0	3.40	13	0	0.45	0.68
S3.6	50.0	60.0	5.0	3.60	14	0	0.41	0.70
S4.0	50.0	60.0	5.0	4.00	19	0	0.36	0.75
S6.0	50.0	60.0	5.0	6.00	17	2	0.29	0.80
S10.0	50.0	60.0	5.0	10.0	7	47	0.27	0.81

2.3 Result and Discussion

2.3.1 Structure, mechanical properties and visible-light transmittance of obtained aerogels

Six aerogel panels were prepared via supercritical drying as shown in Table 2.1. The sample name S*x* means an aerogel panel prepared with *x* g of F127 via supercritical drying. With increasing only the amount of surfactant F127 in the starting composition, the pore structures and properties are easily controllable.[4] With change in the microstructure, however, mechanical properties do not show a straightforward variation. This can be explained by the elaborate morphological change in the microstructure (Figure 2.1). Starting from the sample S3.2 prepared with the least amount of F127, the PMSQ aerogel possess macropores derived from the transient structure of spinodal decomposition, the structure of which was "frozen" by the concurrent sol–gel transition.[6] Each skeleton contains only a small amount of mesopores, and Young's modulus is the highest among all the aerogels prepared in this study (Table 2.1). With increasing F127 (*x*), the amount of mesopores inside the macropore skeletons of bicontinuous structure increases. Samples S3.4 and S3.6 have thinner macropore skeletons and the fraction of mesopores is increased, both of which are resulted from the transient structure at an earlier stage of spinodal decomposition. The SEM images of these two samples show the porous structure with diffusive interfaces. The finer and disordered hierarchical pore structures result in the lower Young's modulus and higher fragility. With further increasing *x*, only small macropores are confirmed as interstices of reticular PMSQ networks, which are derived from microphase separation. Young's modulus of the aerogel S4.0 is higher than those of samples with the hierarchical pore structures, and the modulus decreases with a further increase of F127 in the starting composition, due to the finer structures from more effective suppression of phase separation. From these reasons, the S10.0 panel with ~15 nm skeletons shows the lowest Young's modulus among the 6 samples. However, Young's modulus obtained from uniaxial compression and bending strength from 3-point bending are higher in these samples compared to the PMSQ aerogels synthesized with CTAC which the

author discussed in chapter 1, due to the lower porosity and thicker and more continuous skeletons (Figure 2.2), which enables easy handling of large panels.

As for the optical property, S6.0 and S10.0 show some visible-light transmittance (Table 2.1 and Figure 2.3). This is because, when $x > 6.0$, the average size of the pore structure decreases to < 100 nm, where the effect of the Mie scattering becomes small. With increasing amount of F127, since the length scale of the pore structure becomes sufficiently shorter (~50 nm) than the wavelength of visible light, appearance of the aerogel samples turns from opaque to bluish translucent, because the Rayleigh scattering becomes the dominant light scattering mode. These mechanical and optical properties do not degrade by humidity and UV irradiation due to the hydrophobicity (Figure 2.4) and the stability of the silicone polymer network of PMSQ, respectively.

2.3.2 Relationship between gas pressure and thermal conductivity of aerogels

The total thermal conductivity λ_t of a porous material is the sum of three components; thermal conductivities of gas λ_g and solid λ_s, and by radiation λ_r.[5a-d,5f,7]

$$\lambda_t = \lambda_g + \lambda_s + \lambda_r$$

High thermal insulating ability of aerogels is mainly derived from the limited contributions from λ_g and λ_s. The suppression of λ_g can be explained by the relationship between pore size and the mean free path of gas molecules. Typical aerogels possess pore sizes shorter than the mean free path of the molecules in air, which is ~70 nm at ambient pressure. In this small space, thermal conduction by exchange of the kinetic energy of the molecules cannot occur. In other words, the gas molecules cannot transfer the heat, because the mobility of the gas molecules is considerably restricted in the pores. In addition, since the solid fraction is low (~0.1), λ_s is also suppressed. In the conventional insulators such as expanded polymer foams, although λ_s is sufficiently low because of the high porosity, λ_g is much higher than that of aerogels because of the large pore sizes (typically 10–1000 μm).

In detail, thermal conductivity of gas at a given temperature can be

calculated by the theoretical equations developed by Kaganer.[8]

$$\lambda_{\mathrm{g}} = \Phi \frac{\lambda_{\mathrm{g},0}}{1 + 2\beta l p_0/[pD]}$$

where Φ is porosity, p_0 is reference gas pressure, p is gas pressure, $\lambda_{\mathrm{g},0}$ is thermal conductivity of the non-convectional free gas at p_0, β is a constant including the interaction between the gas molecules and the pore walls, l is the mean free pass of the gas molecules at p_0, and D is average pore size of the porous material.

The total thermal conductivity of the present samples with varied pore size was measured under varied nitrogen gas pressure ranging from 10^2 to 10^5 Pa by the guarded hot plate (GHP) method, and the obtained experimental data were fitted with the theoretical curves by setting the parameters of p_0, $\lambda_{\mathrm{g},0}$ and β as 10^5 Pa, 0.026 W m^{-1} K^{-1} and 1.5, respectively (Figure 2.5).[5e,f]

$$\lambda_{\mathrm{t}} = \frac{0.026}{1 + 21/pD}\Phi + \lambda_s + \lambda_r$$

Porosity Φ of each sample is obtained and listed in Table 2.1. However, it is difficult to determine the average pore size D by porosimetry techniques such as mercury intrusion porosimetry and nitrogen adsorption−desorption due to the flexibility of these PMSQ aerogels against compressive stress. Contributions of λ_{s} and λ_{r} also cannot be determined experimentally. Instead, the author obtained D and $\lambda_{\mathrm{s}}+ \lambda_{\mathrm{r}}$ (Table 2.2) from the fitting curves of each aerogel panel, and the obtained D of each sample agree with the SEM images (Figure 2.1). In the cases of S3.2 and S3.4, deviations of experimental curves from the fitting curves are confirmed at the low-pressure region. These deviations are derived from an incomplete contact between the hot plate of the device and the slightly warped aerogel surfaces. Other parts of the data show a good agreement between experimental and theoretical curves. Thermal conductivity of these PMSQ aerogels can therefore be explained and anticipated the theory of thermal conductivity of porous materials.

To design better insulating aerogels, there are two major strategies; decreasing λ_{g} or $\lambda_{\mathrm{s}}+ \lambda_{\mathrm{r}}$. In this system, λ_{g} becomes lower when the amount of F127 in the starting composition, x, is increased predominantly due to the decreased average pore size by enhanced suppression of phase separation during

gelation. At the same time, it is clear from Figure 2.5 that even a rough vacuum like 10^4 Pa can effectively reduce thermal conductivity to 0.015−0.025 W m^{-1} K^{-1} except for the samples with relatively large macropores (S3.2 and S3.4). This is highly advantageous for the design of high-performance insulators, because these samples have higher mechanical strength compared to the conventional aerogels and facility of obtaining crack-free panels by ambient pressure drying. On the other hand, the sum of solid and radiative conductivities, $\lambda_s + \lambda_r$, becomes lower with increasing x in the starting composition, mostly due to lower solid conductivity of the lower-density samples. To further reduce $\lambda_s + \lambda_r$, density of the aerogels should be decreased by changing the starting composition such as by decreasing the concentration of MTMS. By this way, however, pore size cannot be controllable in an extended length scale due to lower gel formation ability and higher phase separation tendency in diluted sols. Overall, in the present system, S10.0 is the best insulator among the 6 samples due to the low λ_g and $\lambda_s + \lambda_r$. In addition, this sample shows the highest visible-light transmittance T as mentioned above. In the next section, a preparation of an S10.0 xerogel insulating panel is demonstrated as a candidate of practical superinsulators.

2.3.3 Obtaining transparent aerogel-like xerogels

Recent years, Kanamori and co-workers have reported on PMSQ xerogels which have almost the same properties as corresponding PMSQ aerogels, without relying on supercritical drying.[9] Although low-density (~0.14 g cm^{-3}) and highly transparent (~90 % at 550 nm) aerogels and xerogels can be obtained with cationic surfactant like CTAC and bromide CTAB, it is still difficult to prepare large area xerogel panels for practical insulating applications. Using F127 as the surfactant, this is the first report on the preparation of large area xerogel panels to test their thermal insulating ability, because aerogels prepared under the co-presence of F127 are mechanically more robust (Figure 2.2) and there is a high possibility to easily obtain crack-free single panels via ambient pressure drying. To successfully obtain PMSQ aerogel-like xerogels, the most important loadstar of the gels is elasticity enough to recover their original size and shape from 50 % uniaxial compression, because wet gels shrink about 50 % in length by the

capillary force in the pores. Among the samples discussed above, S10.0 shows the highest recovery performance from uniaxial strain (Figure 2.6). The author attempted to obtain a large S10.0 xerogel panel by ambient pressure drying.

The author first tested drying of small wet gels with a cylindrical shape of *ca*. 5 mm height and 10 mm diameter. As a result, the author obtained xerogels with almost the same density as S10.0 aerogels; however, all the samples suffered from small cracks. In the case of large wet gel panels, the drying gels started cracking at the early stage of drying, and finally were broken into small pieces. This shows that the aerogel S10.0 is rigid and less bendability against small strains during drying process. To solve this problem, the author prepared gels with lower density by increasing the amount of diluted aqueous acetic acid in the starting composition. By using more than 80 mL (cf. 60 mL in the original composition) of aqueous acetic acid (and proportionally, 6.7 g of urea), the author successfully obtained crack-free xerogel samples by ambient pressure drying. After evaporation of the bulk drying solvent *n*-heptane, the gel starts shrinking by the capillary force exerted on the outer surface of the gel. At the critical point (the leather-hard point), the gel suddenly turns into opaque due to the critical opalescence, and then the gel undergoes spring-back as a relaxation of the capillary force on emptying the pores. The obtained transparent panel synthesized with 80 mL of aqueous acetic acid (named A10.0) shows aerogel-like properties and microstructures (Figure 2.7 and Table 2.3), and shows sufficiently low thermal conductivity as 15.0 mW m^{-1} K^{-1}, which is even lower than that of S10.0 due to the decreased density and $\lambda_s + \lambda_r$. This is the first example of a monolithic aerogel-like xerogel with visible-light transmittance and low thermal conductivity, and would be the first step to bring up the transparent airily materials as a practical insulator used in our daily life by eliminating the size limitation of aerogels.

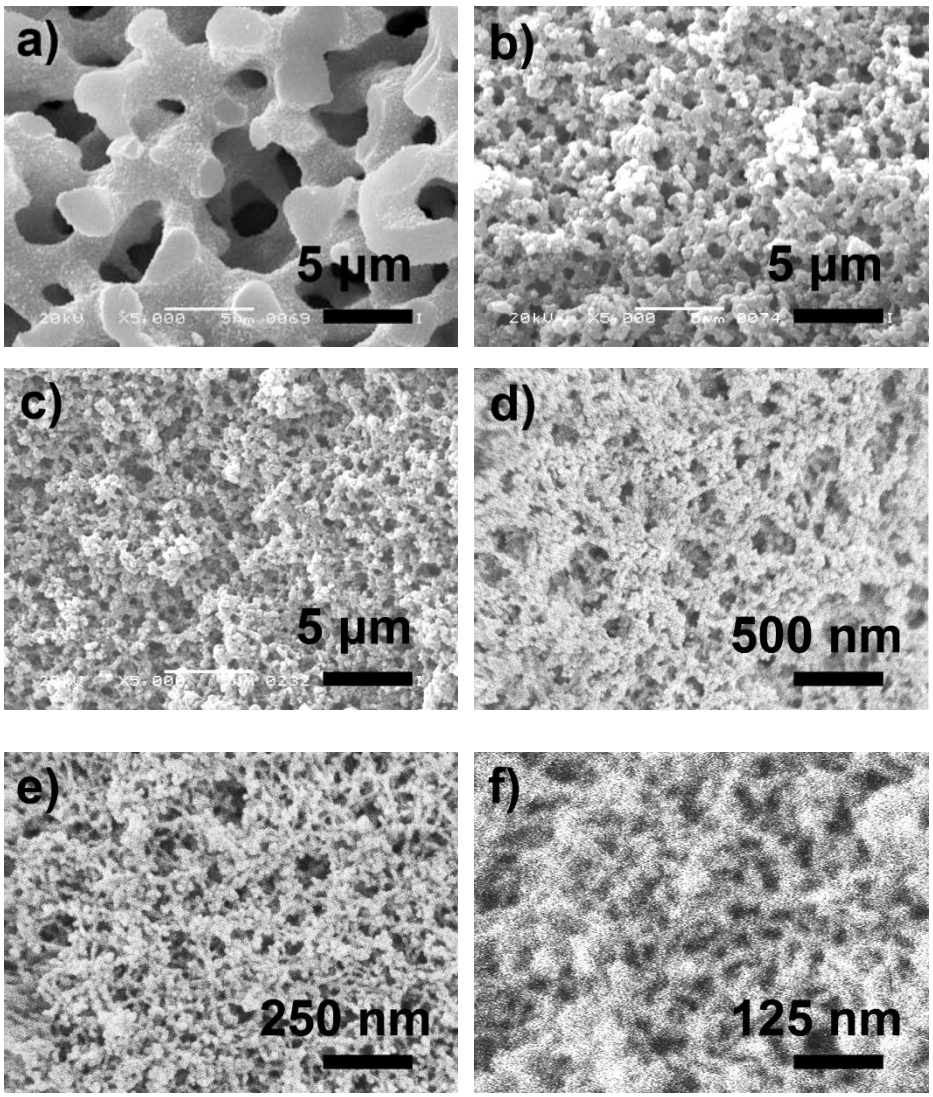

Figure 2.1 SEM images of the aerogel samples. a) S3.2, b) S3.4, c) S3.6, d) S4.0, e) S6.0 and f) S10.0. The pore structure becomes finer from several microns to ~50 nm with increasing amount of F127 in the starting composition.

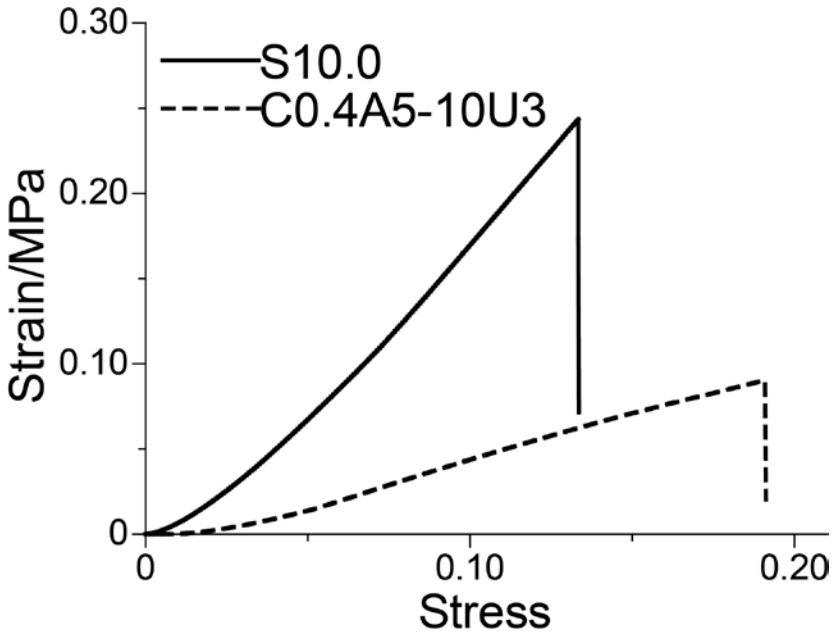

Figure 2.2 Stress−strain curves of aerogel samples synthesized with surfactant F127 (S10.0, with 5.9 mm of thickness and 8.0 mm of width placed on a 15 mm span) and CTAC (C0.4A5-10U3 in chapter 1, with 5.3 mm of thickness and 9.3 mm of width placed on a 15 mm span) obtained by 3-point bending tests.

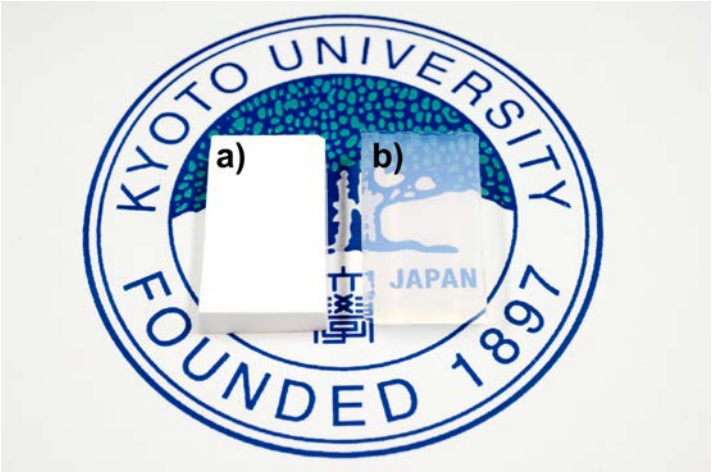

Figure 2.3 Digital camera image of the obtained small aerogel samples; a) S3.2 and b) S10.0.

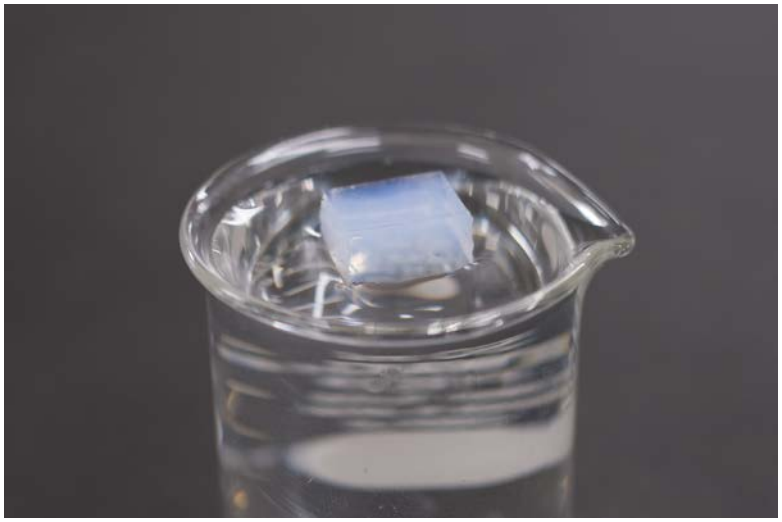

Figure 2.4 The aerogel sample S10.0 shows hydrophobicity enough to float on water at least for 1 month.

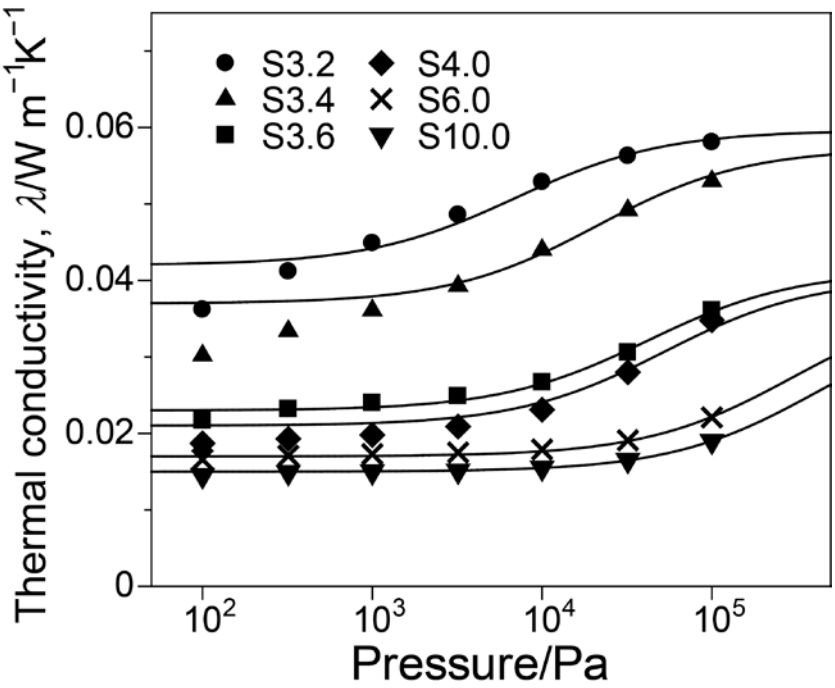

Figure 2.5 Relationship between thermal conductivity and gas pressure on PMSQ aerogel samples with different pore sizes. The solid lines are calculated from the theoretical considerations.

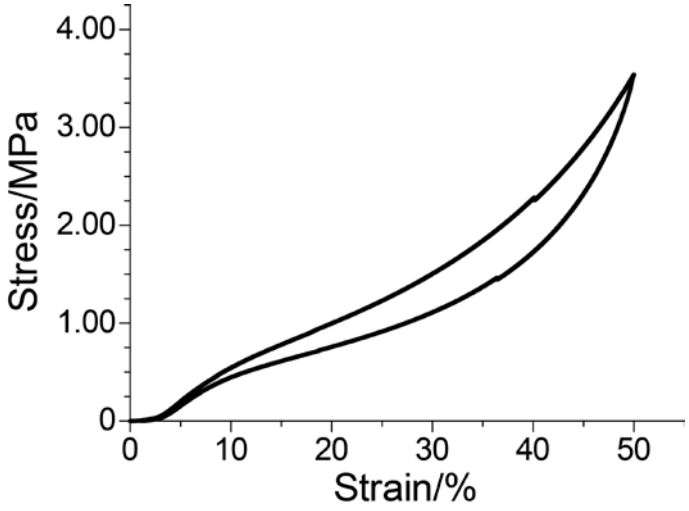

Figure 2.6 Stress−strain curve of S10.0 obtained by uniaxial compression−decompression.

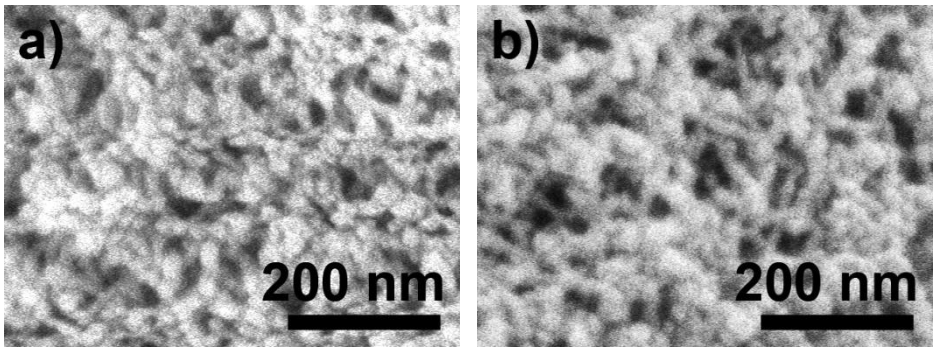

Figure 2.7 SEM images of a) A10.0 obtained via ambient pressure drying and b) via supercritical drying.

Table 2.2 Average pore size D and the sum of solid and radiative thermal conductivities $\lambda_s + \lambda_r$ of the aerogel samples obtained by fitting results.

Materials	D [m]	$\lambda_s + \lambda_r$ [W m^{-1} K^{-1}]
S3.2	3×10^{-6}	0.042
S3.4	1×10^{-6}	0.037
S3.6	5×10^{-7}	0.023
S4.0	4×10^{-7}	0.021
S6.0	7×10^{-8}	0.017
S10.0	5×10^{-8}	0.015

Table 2.3 Properties of the A10.0 xerogel via ambient pressure drying and aerogel via supercritical dring.

Materials	E [MPa]	T [%]	ρ [g cm^{-3}]	Φ
aerogel	13	34	0.21	0.85
xerogel	27	29	0.21	0.85

2.4 Conclusion

Large-area panels of organic-inorganic hybrid PMSQ aerogel with uniform meso- and macropores have been prepared. Pore size has been widely controlled from ~50 nm to 3 μm simply by changing the amount of nonionic surfactant F127 in the starting composition. Thermal conductivity of each aerogel sample varies depending on the gas pressure, and shows a good agreement with the theoretical values. Aerogel panels with larger average pore size trend toward higher thermal conductivity, which can be effectively decreased by lightly reducing the gas pressure; *e.g.* to 10^4 Pa. Aerogel samples with small pores already exhibit low thermal conductivity (0.015−0.020 W m^{-1} K^{-1}) at ambient pressure, which shows these aerogels can be used as a highly insulating material under ambient or lightly reduced pressure. This is advantageous when considering conventional vacuum insulation requires highly conductive robust frameworks and regular maintenance to keep the performance. An aerogel-like xerogel panel with sufficiently low thermal conductivity (0.015 W m^{-1} K^{-1}) and visible-light transmittance (29 % through 10 mm thickness at 550 nm) has also been prepared. Through further improvement of these materials, a new daylighting/transparent thermal insulating system would be developed for practical utilizations in the near future.

References in Chapter 2

[1] a) J. Fricke and T. Tillotson, *Thin Solid Films* **1997**, *297*, 212; b) N. Hüsing, U. Schubert, *Angew. Chem. Int. Ed.* **1998**, *37*, 23; c) M. A. Aegerter, N. Leventis and M. M. Koebel, in *Aerogels Handbook*, Springer, New York, **2011**, pp. 607-633; d) M. Koebel, A. Rigacci, P. Achard, *J. Sol-Gel Sci. Technol.* **2012**, *63*, 315.

[2] a) L. W. Hrubesh, R. W. Pekala, *J. Mater. Res.* **1994**, *9*, 731; b) L. W. Hrubesh, *J. Non-Cryst. Solids* **1998**, *225*, 335.

[3] J. P. Randall, M. A. B. Meador, S. C. Jana, *ACS Appl. Mater. Interfaces* **2011**, *3*, 613.

[4] K. Kanamori, Y. Kodera, G. Hayase, K. Nakanishi, T. Hanada, *J. Colloid Interface Sci.* **2011**, *357*, 336.

[5] a) X. Lu, M. C. Arduinischuster, J. Kuhn, O. Nilsson, J. Fricke, R. W. Pekala, *Science* **1992**, *255*, 971; b) X. Lu, P. Wang, M. C. Arduinischuster, J. Kuhn, D. Buttner, O. Nilsson, U. Heinemann, J. Fricke, *J. Non-Cryst. Solids* **1992**, *145*, 207; c) X. P. Lu, O. Nilsson, J. Fricke and R. W. Pekala, *J. Appl. Phys.* **1993**, *73*, 581; d) X. Lu, R. Caps, J. Fricke, C. T. Alviso, R. W. Pekala, *J. Non-Cryst. Solids* **1995**, *188*, 226; e) K. Swimm, G. Reichenauer, S. Vidi, H. P. Ebert, *Int. J. Thermophys.* **2009**, *30*, 1329; a) R. Baetens, B. P. Jelle, A. Gustavsen, *Energy and Buildings*, **2011**, *43*, 761.

[6] a) K. Kanamori, H. Yonezawa, K. Nakanishi, K. Hirao, H. Jinnai, *J. Sep. Sci.* **2004**, *27*, 874; b) K. Nakanishi, K. Kanamori, *J. Mater. Chem.* **2005**, *15*, 3776; c) H. J. Dong, M. A. Brook, J. D. Brennan, *Chem. Mater.* **2005**, *17*, 2807; d) K. Kanamori, K. Nakanishi, T. Hanada, *J. Sep. Sci.* **2006**, *29*, 2463; e) H. J. Dong, J. D. Brennan, *Chem. Mater.* **2006**, *18*, 541; f) H. Dong, J. D. Brennan, *Chem. Mater.* **2006**, *18*, 4176; g) K. Kanamori, K. Nakanishi, *Chem. Soc. Rev.* **2011**, *40*, 754.

[7] G. Wei, Y. Liu, X. Zhang, F. Yu, X. Du, *Int. J. Heat Mass Transfer* **2011**, *54*, 2355.

[8] M. G. Kaganer, in *Thermal Insulation in Cryogenic Engineering*, IPST Press, Jerusalem, **1969**.

[9] a) K. Kanamori, M. Aizawa, K. Nakanishi, T. Hanada, *Adv. Mater.* **2007**, *19*, 1589; b) K. Kanamori, M. Aizawa, K. Nakanishi, T. Hanada, *J. Sol-Gel Sci. Technol.* **2008**, *48*, 172.

Chapter 3

Polymethylsilsesquioxane–Cellulose Nanofiber Bio-composite Aerogels with High Thermal Insulation, Bendability and Superhydrophobicity

3.1 Introduction

In chapters 1 and 2, properties of PMSQ aerogels with changing starting compositions are discussed and large aerogel-like xerogel panels were obtain to evaluate their thermal conductivity. The thermal conductivity of the aerogel-like xerogel was as low as silica aerogels obtained via a supercritical drying. However, porous PMSQ panels are still fragile against shear and tensile stresses due to fine skeletons composed of a weak linkage of nanoparticles. To obtain low-density bendable materials, the author has also investigated new organopolysiloxane materials obtained from a tri- and difunctional alkoxysilane co-precursor system (discussed in chapters 4–6). It has been succeeded to obtain bendable flexible materials (named as marshmallow-like gels) whose density is as low as aerogels (~0.1 g cm^{-3}) by ambient pressure drying.[1] However, the skeletons and pores in those gels are much larger than PMSQ aerogels, which resulted in increased thermal conductivity (~30–35 mW m^{-1} K^{-1}).

Several researchers are recently studying composite silica aerogels fused with bionanofibers. In particular, cellulose nanofibers (CNFs) are often used because of their abundance in nature and good mechanical properties.[2] Due to the excellent tensile strength of CNFs, which are ~5 times higher ratio of tensile strength and density than steel wires,[3] these composite aerogels are expected to show higher mechanical properties and flexibility even against bending. In addition, CNFs can be obtained from scrap wood, which can reduce the environmental load in industrial productions. Their density and thermal conductivity, however, are far from those of pure silica aerogels and even comparable with conventional thermal insulators such as mineral wools, because of seriously aggregated by condensation between silanol and hydroxyl groups and

heterogeneous pore structures in those composite aerogels.[2e,4] These silica–CNF composite aerogels are highly hydrophilic due to the abundant hydroxyl groups and high surface area, lowers long-term stability even under an ambient condition without an additional process to impart hydrophobicity.[5]

In this chapter, the auther discusses new aerogels composed of the PMSQ networks fused with a small amount of CNFs, to aim at obtaining bendable thermal insulating panels.

3.2 Experimental

3.2.1 Chemicals

Acetic acid, distilled water and urea were purchased from Hayashi Pure Chemical Industry, Ltd. (Japan). Surfactant CTAC was obtained from Tokyo Chemical Industry, Ltd. (Japan). Methytrimethoxysilane (MTMS) was purchased from Shin-Etsu Chemical Co., Ltd. (Japan). All the chemical reagents were used as received.

3.2.2 Synthesis procedures

To obtain cellulose nanofibers, wood powder from Radiata pine (*Pinus radiata D. Don*) sieved under 60 mesh was used. Solvent extraction was first performed in a Soxhlet apparatus with a 2:1 mixture of toluene–ethanol for 6 h. Lignin in the wood was removed using an acidified sodium chlorite solution at 70 °C for 1 h, and the process was repeated until the product became colorless. The sample was then treated in 6 wt % potassium hydroxide over night at RT, and then at the same concentration at 80 °C for 2 h in order to leach hemicelluloses. Finally, a slurry of 1 wt % purified cellulose passed through a grinder (Masuko Corp., Japan) at 1500 rpm.

For preparation of the typical PMSQ–CNF aerogel sample C50, 2.0 g of CTAC, 15.0 g of urea, and 50 mL of 5 mM acetic acid aqueous solution with cellulose nanofibers were firstly mixed in a glass sample tube (see also Table 3.1). Then, 25 mL of MTMS was added under vigorous stirring at RT, and stirring was continued for 30 min for hydrolysis of MTMS. The obtained sol was transferred into a tightly-sealed container, which was then placed in a forced convection oven at 60 °C for 4 d to complete gelation and aging. The obtained gels were washed with methanol several times to remove the residual surfactant and other chemicals, and then solvent-exchanged with 2-propanol. The washed samples were processed with CO_2 supercritical drying at 80 °C and 14 MPa for 10 h.

3.2.3 Measurements

A scanning electron microscope (JSM-6700F, JEOL, Japan) was employed

to observe the microstructure. Mechanical properties of aerogels were investigated by a material tester (EZGraph, Shimadzu Corp., Japan). For uniaxial compression tests, carved gels (typical length × width × height was 10 × 10 × 6 mm^3) were compressed–decompressed using a load cell of 5 kN with a rate of 0.5 mm min^{-1}. For 3-point bending tests, a cylindrical sample with diameter of 8 mm and length of 40 mm were put on a fixture with a 30 mm span and compressed by a wedge-shaped crosshead with 60 ° and 0.3 mm diameter at the point with using a load cell of 5 N at a rate of 5 mm min^{-1}. To assess the molecular-level structure of obtained siloxane networks, ^{29}Si solid-state CP/MAS NMR measurements were performed on an NMR spectrometer Avance III 800 (Bruker Corp., Germany) operated under a static magnetic field of 18.8 T. The contact time for the ^{1}H–^{29}Si cross polarization was fixed at 5.5 ms and the rate of sample spinning was 15 kHz. The ^{29}Si chemical shift was expressed relative to tetramethylsilane (Me_4Si) by using the resonance line at −9.66 ppm for hexamethylcyclotrisiloxane crystals as an external reference. Thermal conductivity was measured with a transient heat flow meter HFM 436 Lambda (Netzsch GmbH, Germany). Contact angle of water was measured with Drop Master DM-561Hi (Kyowa Interface Science Co., Ltd., Japan). Volume of water droplet was fixed at 3.0 μL and the contact angle was determined at 2 s after an attachment to gel surface. Thermogravimetric (TG) analysis was performed with a Thermo plus EVO (Rigaku Corp., Japan) instrument at a rate of 5 °C min^{-1} while continuously supplying air at a rate of 100 mL min^{-1}. Nitrogen sorption measurements were performed to obtain the BET-specific surface area with BELSORP-mini II (BEL Japan, inc., Japan). Before measurement, the sample was outgassed under vacuum at 110 °C for 6 h.

3.3 Result and Discussion

The auther succeeded to obtain PMSQ–CNF aerogels by a quite simple process as shown in Figure 3.1. The PMSQ–CNF composite aerogels were obtained by a one-pot process, similar to the previously-reported pure PMSQ aerogel synthesis, except adding a diluted CNF aqueous solution obtained from wood powder of Radiata pine.[6] These CNFs possess uniform diameter of 15 nm (Figure 3.2), which helps making the uniform networks of composite aerogels, because the diameter is close to the size of the PMSQ nanoparticular networks. To synthesize well-defined PMSQ–CNF composite aerogels, the most important point is to control aggregation of the PMSQ nanoparticles onto the surface of CNFs. To avoid this, the CNF solution was diluted to 0.18 w/w % in water, which is the minimum concentration to homogeneously disperse the CNFs in the sol during gelation by moderate electrostatic repulsion between PMSQ and CNFs. Five composite aerogel panels were prepared with a varied amount of MTMS and one pure PMSQ panel without CNFs as listed in Table 3.1. The BET surface areas obtained by nitrogen adsorption of each aerogel are evaluated to be 550–750 $m^2\ g^{-1}$, and no clear relations in density and specific surface area are found. Thermogravimetric (TG) analysis prove that oxidation of CNFs in the composite aerogel (C50) starts from ~ 250 °C (Figure 3.3), which temperature is higher than degradation temperatures of polymer-based thermal insulators such as polyurethane and polystyrene foams.

From comparison between the pure PMSQ and PMSQ–CNF composite aerogels with the same amount of MTMS (*i.e.* samples P50 and C50), no large difference in the properties is recognized (Table 3.1). This means that CNFs hardly change the morphology of PMSQ networks through the moderate aggregation, while silica–CNF systems suffer from changes in physical properties through strong interaction-induced aggregation as mentioned above. In fact, uniform fibrous networks composed of the PMSQ skeletons and CNFs are observed in SEM images (Figure 3.4); the PMSQ networks and CNFs are discernible due to almost the similar dimensions as mentioned above. It is also shown by ^{29}Si solid-state cross polarization/magic angle spinning (CP/MAS)

NMR and FTIR that the molecular-level structure of PMSQ networks is not affected by the presence of CNFs (Figures 3.5 and 3.6). The T^3/T^2 ratio (here T^n denotes silicon species in $CH_3Si–(OSi)_nX^{3-n}$, where X is OH or OCH_3) is virtually unchanged between P50 and C50, which suggests the PMSQ nanoparticles with less silanol groups compared to silica do not form extensive chemical bonds with CNFs. In FTIR spectra, no obvious change including cyclic/polyhedral (at 1100 cm^{-1}) and linear/branched (at 1025 cm^{-1}) siloxane species[7] was observed between these samples. Nevertheless, the CNFs clearly bring favorable effects on the mechanical properties. Although the lowest density achievable in pure PMSQ aerogels is 0.040 g cm^{-3}, we have obtained a composite aerogel with 0.020 g cm−3 only by adding a small amount of CNFs (C5, Figures 3.1 and 3.4a). Surprisingly, a panel with 100 × 100 × 8.5 mm^3 in dimension is bendable (Figures 3.1 and 3.7) even though the weight ratio of CNF:PMSQ is very low ($1:4.3\times10^2$, assuming all MTMS convert into the PMSQ networks). The bendability cannot be observed in the corresponding pure PMSQ aerogel P5. This bendable composite aerogel panel with low density is established not only by the strength of CNFs, but also by a synergetic effect with PMSQ skeletons.

Thermal conductivity measurements on the PMSQ–CNF composite aerogel panels revealed that C50 shows the lowest value (15.3 mW m^{-1} K^{-1}, Figure 3.8), which is comparable or even lower than other composite aerogels reported elsewhere[2e,8] and conventional thermal insulators such as mineral wools and polymer foams (Figure 3.9). This result can be explained by the absence of morphological changes on compositing with the CNFs. Thermal conductivity of aerogel materials is mainly composed of the gas-phase conduction and the solid-phase one.[9] The gas-phase thermal conductivities in C5, C10 and C25 should be higher than that of C50 due to the larger mesopores in these samples, which are estimated to be longer than the mean free path of the gas molecules in air (~70 nm) (Figure 3.4). On the other hand, the thermal conductivity of solid phase in C75 should be higher than that of C50 because of the higher density (higher fraction of solid phase), resulting in the higher total thermal conductivity in C75.

In addition to the above-mentioned excellent properties, the PMSQ–CNF

composite aerogels are stable against humidity without additional treatments. In the case of silica and silica-based composite aerogels, the aerogel surface is hydrophilic and adsorbs water just as silica gel desiccants, which may collapse the pore structure due to the capillary pressure induced by water adsorption. Cellulose nanofibers also show a hydrophilic property due to their rich hydroxyl groups. Silica and CNFs are therefore an unsuitable combination to use under atmospheric conditions for long without laborious and costly hydrophobic treatments. The PMSQ networks, however, have methyl groups directly bonded to each silicon atom and show strong hydrophobicity. With an additional effect of surface roughness due to the porous morphology, the pure PMSQ (P5 and P50) and the four PMSQ–CNF composite aerogels (C5, C10, C25 and C50) show superhydrophobicity with the water contact angles of > 150 ° (Table 3.1, Figures 3.10a,b). Although the sample C75 did not show superhydrophobicity due to the excessive hydrophilic CNFs and a decreased length scale of roughness (Figure 3.4e), the water contact angle is still high (145.4 °). In fact, all the PMSQ–CNF composite aerogels can float on water at least one month without any changes. Considering that superhydrophobic surfaces show the self-cleaning effect,[10] this is a large advantage for practical uses such as for low-density thermal insulating panels installed outside of buildings. With good formability and scalability as in the case of PMSQ aerogels/xerogels[11], it is highly expected that the present composite materials can also be used for transparent optical panels or films as reported in dense CNF-polymer composite films,[3b,12] because these composite aerogels show acceptable light transmittance that is higher than previously-reported silica–CNF counterparts (Figure 3.10c).[2e] By controlling the dimension and orientation of CNFs in aerogels, there is a possibility to obtain more transparent and flexible panels.

The PMSQ–CNF composite aerogels show elastic properties by uniaxial compression (Figure 3.11), which is similar to the pure PMSQ aerogels reported previously.[11] Although compression set is relatively lower because CNFs do not have enough elasticity to recover the original shape, the PMSQ–CNF panels allow better handling because these panels exhibit both elasticity and bending flexibility. These are not simultaneously observed in the conventional silica,

silica–CNF composites and pure PMSQ aerogels. Further studies are underway for improving the mechanical properties of PMSQ–CNF materials to obtain aerogel-like xerogels by ambient pressure drying.

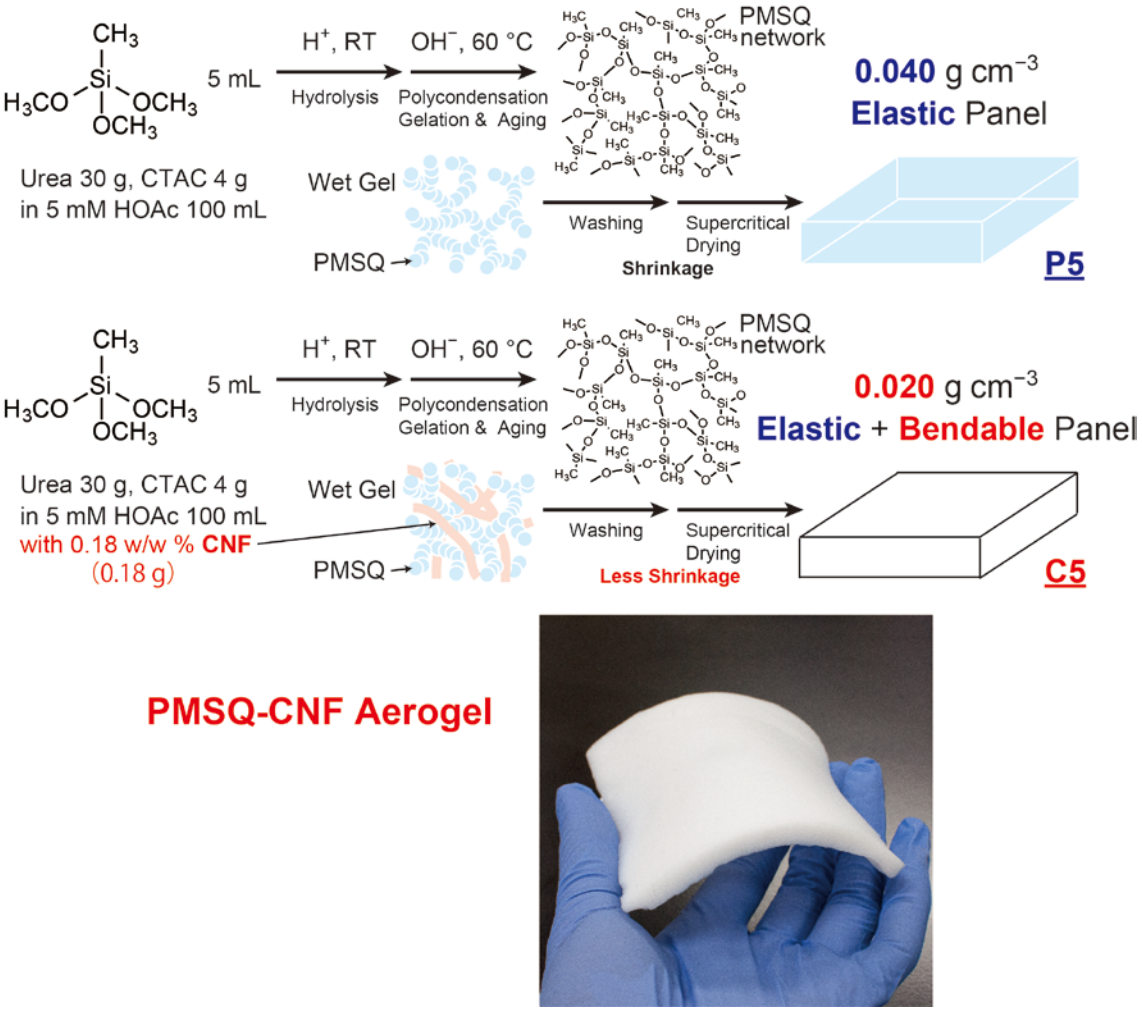

Figure 3.1 Preparation schemes of low-density PMSQ aerogels with and without CNFs (samples P5 and C5, see Table 3.1).

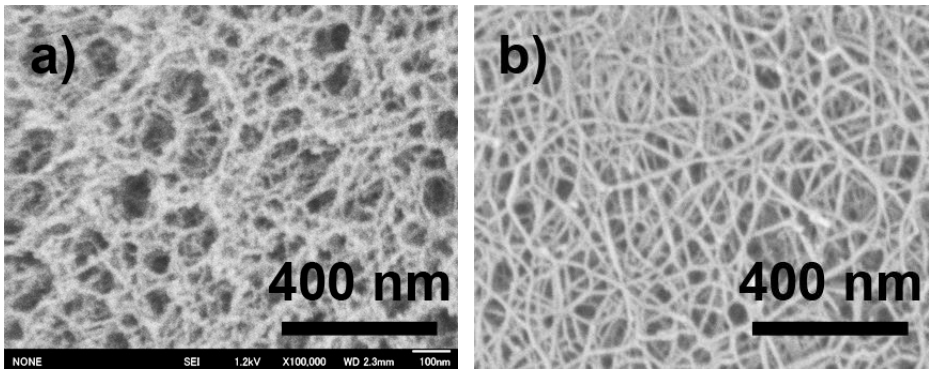

Figure 3.2 SEM images of a) a low-density pure PMSQ aerogel (P5) and b) cellulose nanofibers from wood powder of Radiata pine.

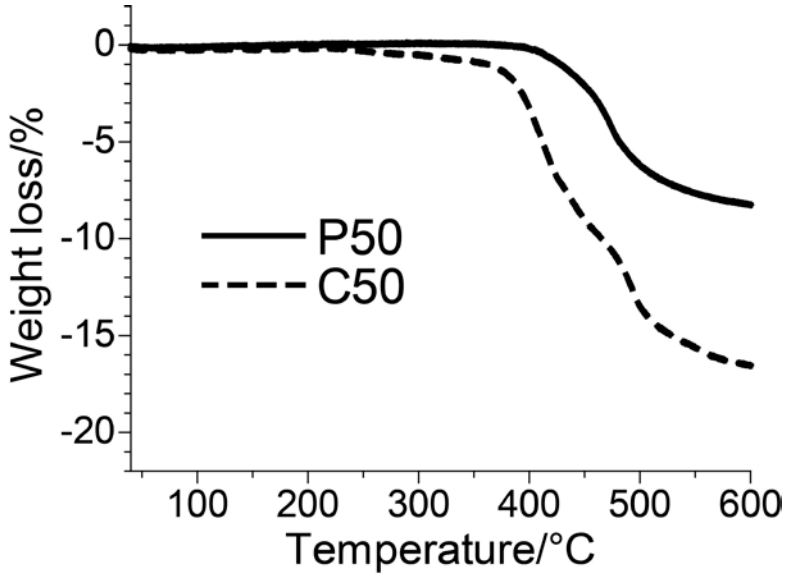

Figure 3.3 Thermogravimetry results on the PMSQ–CNF composite aerogel (C50) and the pure PMSQ aerogel (P50). Oxidation of CNFs and PMSQ starts at ~250 and ~350 °C, respectively.

Table 3.1 Starting compositions and properties of typical aerogels obtained in the present study.

Materials	MTMS [mL]	HOAc aq. [mL]	Urea [g]	CTAC [g]	CNFs in HOAc aq. [wt %]	λ^a	$\rho_b{}^b$	$S_{BET}{}^c$	W.C.^{d}
C5	5	100	30	0.40	0.18	24.3	0.020	657	152.7
C10	10	100	30	0.80	0.18	21.7	0.039	550	152.4
C25	25	100	30	2.00	0.18	18.8	0.097	732	154.3
C50	50	100	30	4.00	0.18	15.3	0.142	525	152.7
C75	75	100	30	6.00	0.18	16.2	0.186	560	145.4
P5	5	100	30	0.40	0	22.5	0.040	601	152.5
P50	50	100	30	4.00	0	14.9	0.135	631	150.6

[a]Thermal conductivity at an ambient condition [mW m^{-1} K^{-1}], [b]Bulk density [g cm^{-3}], [c]BET specific surface area obtained from nitrogen sorption measurements [m^2 g^{-1}], [d]Contact angle of water[º].

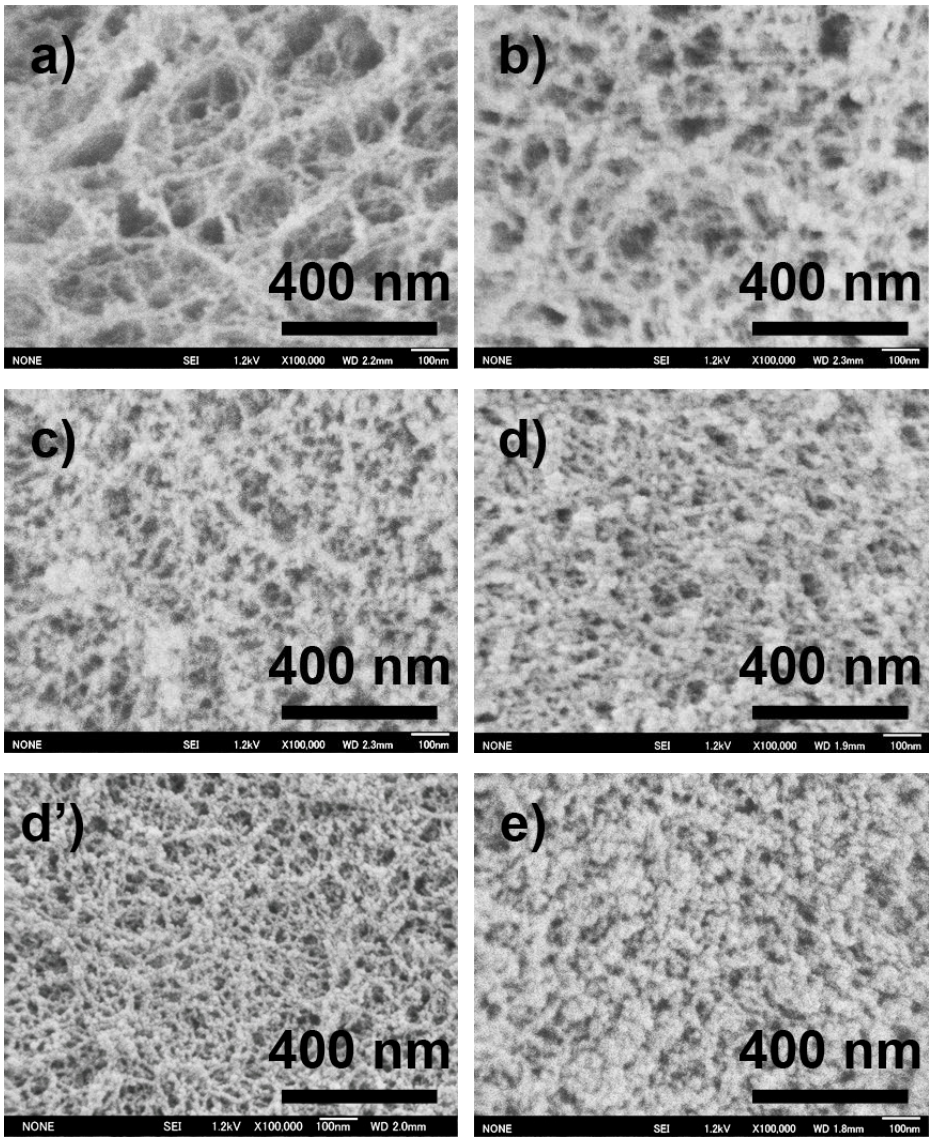

Figure 3.4 SEM images of PMSQ–CNF composite aerogels and a pure PMSQ aerogel without CNFs. a) C5, b) C10, c) C25, d) C50, e) C75 and d') P50.

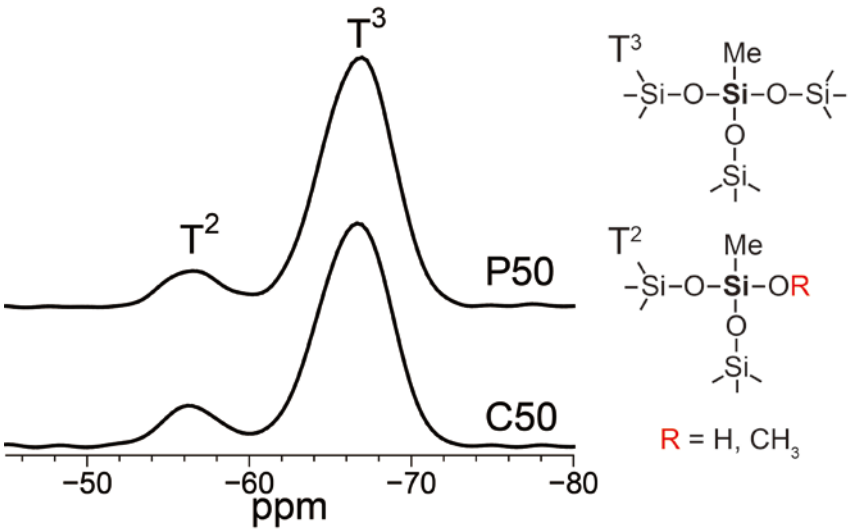

Figure 3.5 ^{29}Si CP/MAS NMR spectra of the pure PMSQ aerogel (P50) and the PMSQ–CNF composite aerogel (C50). No obvious difference was observed between the existence of CNFs.

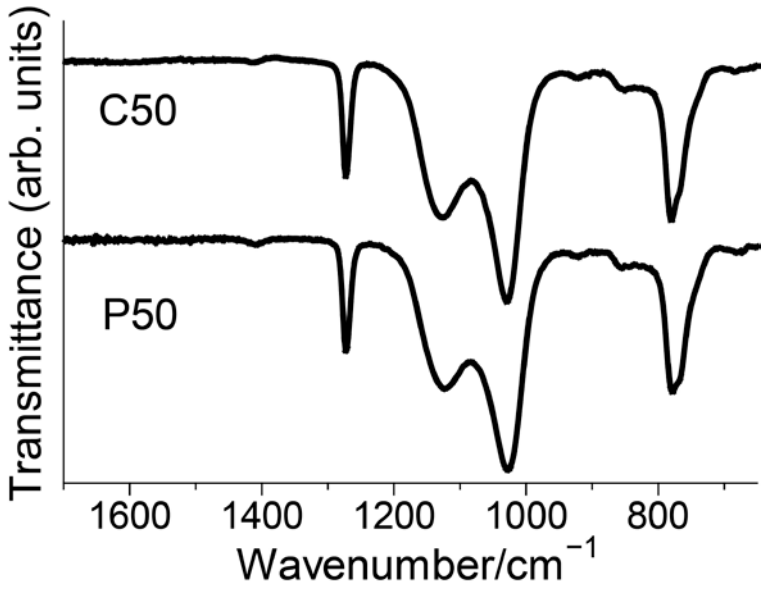

Figure 3.6 FTIR spectra of the PMSQ–CNF composite aerogel (C50) and the pure PMSQ aerogel (P50). There is no obvious change in siloxane peaks at 1100 and 1025 cm^{-1}.

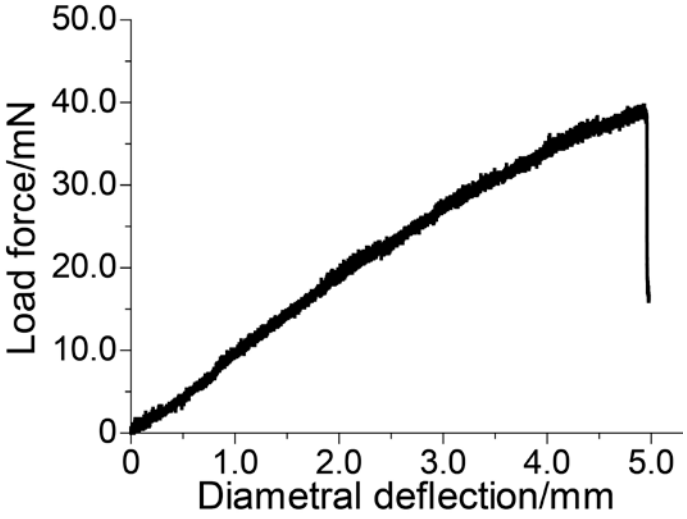

Figure 3.7 Result of 3-point bending test on the PMSQ–CNF composite aerogel (C5).

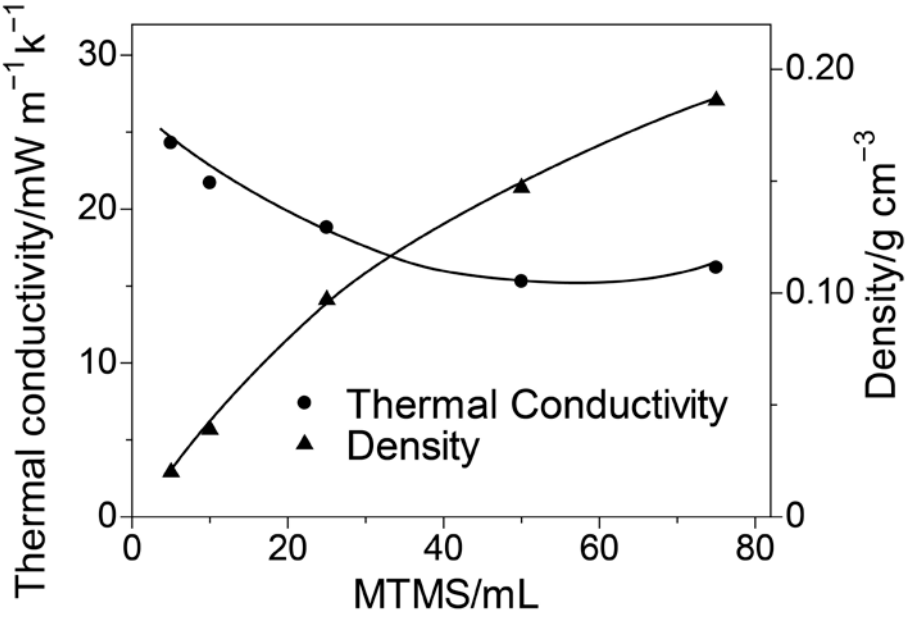

Figure 3.8 Relationship between the volume of MTMS in starting solutions, thermal conductivity and density of the obtained PMSQ–CNF composite aerogels.

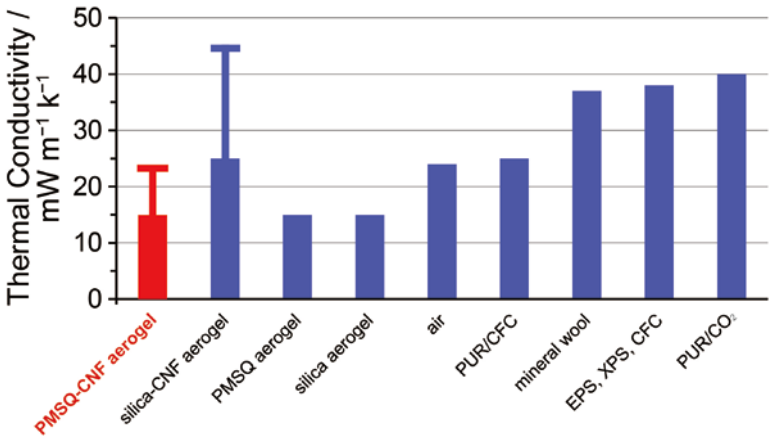

Figure 3.9 Comparison of the thermal insulation properties of aerogels and some commercially available insulating materials. The thin bars on the top of PMSQ–CNF aerogel and silica–CNF aerogel show the reported value ranges. PUR: polyurethane foam, CFC: chlorofluorohydrocarbons; EPS, XPS: expanded and extruded polystyrene.[2e,4]

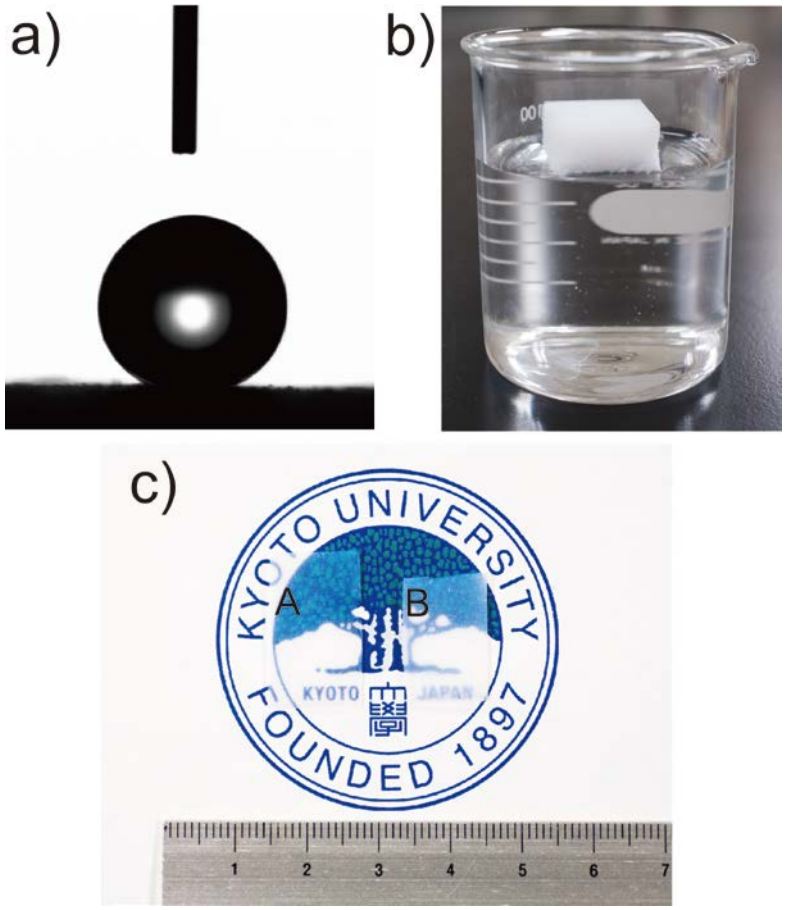

Figure 3.10 a) Water drop on the PMSQ–CNF composite aerogel (C5) panel, showing superhydrophobicity. b) Digital camera image of C50 floating on water. The PMSQ–CNF composite aerogels float on water at least for 1 month. c) PMSQ–CNF composite aerogel sheets of A) C10 and B) C5, showing acceptable visible light transmittance (see also Table 3.2).

Table 3.2 Polymethylsilsesquioxane-cellulose nanofiber composite aerogel sheets show visible light transmittance (see also Figure 3.10c).

Materials	Thickness [mm]	Transmittance at 800 nm [%]	Transmittance at 550 nm [%]
a) C10	1.35	89	84
b) C5	1.65	75	54

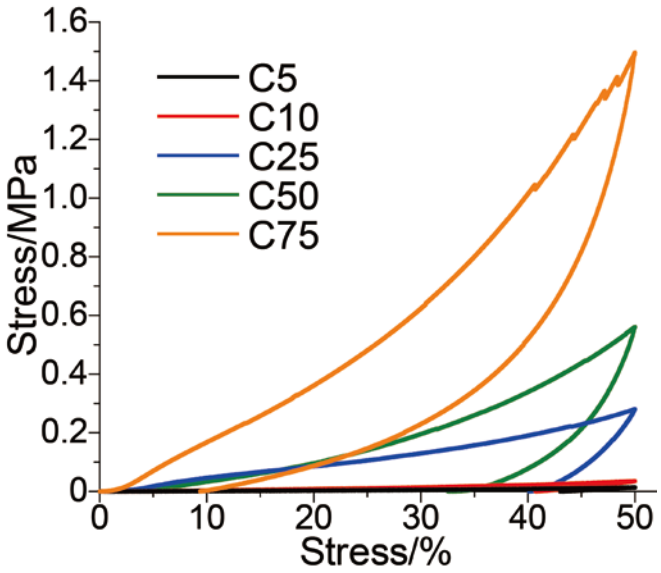

Figure 3.11 Stress–strain curves of PMSQ–CNF composite aerogels.

3.4 Conclusion

New organic-inorganic hybrid aerogels by fusing PMSQ and CNFs have been prepared. Obtained PMSQ–CNF composite aerogels show thermal conductivity as low as pure silica aerogels and high surface area. The composite aerogel panel with the lowest density of 0.020 g cm^{-3} shows bending flexibility, which helps easy handling. The facile one-pot synthesis process for these materials is almost the same with that for pure PMSQ aerogels except adding diluted CNFs aqueous solution, and mechanical properties are considerably improved while maintaining other pore properties. These composites show superhydrophobicity and float on water at least for one month without any hydrophobizing treatments. The robustness of the composites allows applications even in outdoor environments without any change of their properties by dirt, humidity and rain, and of course silicone-based PMSQ networks and CNFs are stable against UV in the solar light. The present study will open up a way for practical utilization of excellent thermal insulation ability of aerogels.

References in Chapter 3

[1] a) G. Hayase, K. Kanamori, K. Nakanishi, *J. Mater. Chem.* **2011**, *21*, 17077; b) G. Hayase, K. Kanamori, M. Fukuchi, H. Kaji, K. Nakanishi, *Angew. Chem. Int. Ed.* **2013**, *52*, 1986; c) G. Hayase, K. Kanamori, G. Hasegawa, A. Maeno, H. Kaji, K. Nakanishi, *Angew. Chem. Int. Ed.* **2013**, *52*, 10788.

[2] a) M. Pääkkö, J. Vapaavuori, R. Silvennoinen, H. Kosonen, M. Ankerfors, T. Lindström, L. A. Berglund, O. Ikkala, *Soft Matter* **2008**, *4*, 2492; b) I. Siro, D. Plackett, *Cellulose* **2010**, *17*, 459; c) C. Aulin, J. Netrval, L. Wågberg, T. Lindström, *Soft Matter* **2010**, *6*, 3298; d) M. Litschauer, M. A. Neouze, E. Haimer, U. Henniges, A. Potthast, T. Rosenau, F. Liebner, *Cellulose* **2011**, *18*, 143; e) J. Cai, S. Liu, J. Feng, S. Kimura, M. Wada, S. Kuga and L. Zhang, *Angew. Chem. Int. Ed.*, 2012, **51**, 2076.

[3] a) A. N. Nakagaito, H. Yano, *Appl. Phys. A-Mater. Sci. Process.* **2005**, *80*, 155; b) M. Nogi, H. Yano, *Adv. Mater.* **2008**, *20*, 1849.

[4] N. Hüsing, U. Schubert, *Angew. Chem. Int. Ed.* **1998**, *37*, 23.

[5] a) H. Yokogawa, M. Yokoyama, *J. Non-Cryst. Solids* **1995**, *186*, 23; b) J. T. Korhonen, M. Kettunen, R. H. A. Ras and O. Ikkala, *ACS Appl. Mater. Interfaces*, **2011**, *3*, 1813.

[6] K. Abe, S. Iwamoto and H. Yano, *Biomacromolecules* **2007**, *8*, 3276.

[7] a) H. J. Dong, J. D. Brennan, *Chem. Mater.* **2006**, *18*, 541; b) G. Hayase, K. Kanamori, K. Nakanishi, *Microporous Mesoporous Mater.* **2012**, *158*, 247.

[8] M. A. B. Meador, E. F. Fabrizio, F. Ilhan, A. Dass, G. Zhang, P. Vassilaras, J. C. Johnston, N. Leventis, *Chem. Mater.* **2005**, *17*, 1085.

[9] a) X. Lu, M. C. Arduinischuster, J. Kuhn, O. Nilsson, J. Fricke, R. W. Pekala, *Science* **1992**, *255*, 971; b) K. Swimm, G. Reichenauer, S. Vidi, H. P. Ebert, *Int. J. Thermophys.* **2009**, *30*, 1329.

[10] R. Blossey, *Nat. Mater.* **2003**, *2*, 301.

[11] a) K. Kanamori, M. Aizawa, K. Nakanishi, T. Hanada, *Adv. Mater.* **2007**, *19*, 1589; b) K. Kanamori, M. Aizawa, K. Nakanishi, T. Hanada, *J. Sol-Gel Sci. Technol.* **2008**, *48*, 172; c) K. Kanamori, K. Nakanishi, T. Hanada, *J. Ceram.*

Soc. Jpn. **2009**, *117*, 1333; d) K. Kanamori, *J. Ceram. Soc. Jpn.*, **2011**, *119*, 16.

[12] a) H. Yano, J. Sugiyama, A. N. Nakagaito, M. Nogi, T. Matsuura, M. Hikita, K. Handa, *Adv. Mater.* **2005**, *17*, 153; b) M. Nogi, S. Iwamoto, A. N. Nakagaito, H. Yano, *Adv. Mater.* **2009**, *21*, 1595.

Chapter 4

New Flexible Aerogels/Xerogels Derived from Methyltrimethoxysilane–Dimethyldimethoxysilane Co-precursors

4.1 Introduction

Since 1931,[1] aerogels have been synthesized with various chemical compositions, such as inorganic oxides (*e.g.* silica, alumina and titania),[2] organic crosslinked polymers (*e.g.* resorcinol–formaldehyde (RF))[3] and biopolymers (*e.g.* cellulose and chitosan).[4] However, all of their mechanical strength of such low-density materials are generally too low even against a small applied stress, the porous structure is easily collapsed and a drying gel body will exhibit shrinkage and cracks. In previous chapters, the author demonstrated the synthesis and characterization of PMSQ aerogels/xerogels and optimized their starting composition to obtain improved aerogels with handling. In result, the author succeeded to obtain a highly thermal insulating aerogel-like xerogel and bendable low-density aerogels. Although this is a substantial progress from classical silica aerogels, there is still a significant hurdle for practical uses in our daily life.

Some bendable aerogels had been also reported before the work in chapter 3, by using organoalkoxysilanes as (co-)precursors. Rao et al. have reported bendable PMSQ aerogels by using an acid/base two-step reaction in a water/methanol mixed solvent,[4] and Guo et al. reported highly flexible aerogels derived from bis[3-(triethoxysilyl)propyl]disulfide, tetramethoxysilane and VTMS, in which the disulphide bridges enhance elastic recovery after compression.[5] There are also reports on the polymer crosslinked aerogels, but the process needs multiple and laborious steps and porosity is partially lost, though mechanical properties are highly improved.[6] In response to the results of these reports and the works in previous chapters, the author tried to synthesis more flexible gels by using a MTMS–DMDMS co-precursor system. Because the flexibility of PMSQ aerogels is from low cross-linking density, DMDMS can

be expected to form more flexible network as far as controlling phase separation successfully. In this chapter, the author discusses new aerogels and aerogel-like xerogels with “marshmallow-like” flexibilities.

4.2 Experimental

4.2.1 Chemicals

Acetic acid, distilled water, urea, methanol, and 2-propanol were purchased from Hayashi Pure Chemical Ind., Ltd. (Japan). Surfactant CTAC was from Tokyo Chemical Ind. Co., Ltd. (Japan). MTMS and DMDMS were obtained from Shin-Etsu Chemical Co., Ltd. (Japan). All reagents were used as received.

4.2.2 Synthesis procedures

In the typical synthesis, 15 mL of 5 mM aqueous acetic acid, 0.80 g of surfactant CTAC and 5.0 g of urea were mixed in a glass sample tube, and then 3.0 mL of MTMS and 2.0mL of DMDMS were added and stirred for 30 min for hydrolysis of these alkoxysilanes. The molar ratio of this typical starting composition is (MTMS + DMDMS):water:acetic acid:urea:CTAC = 1.0:2.4 × 10:2.1 × 10^{-3}:2.4:7.1 × 10^{-2} with MTMS:DMDMS = 5.9:4.1. After the complete mixing, the sol was transferred to a closed vessel and kept at 80 °C for gelation and aging for 2 d in the base-catalyzed condition brought about by hydrolysis of urea. The typical gelation time was about 3 h. The wet gels thus obtained were soaked in water/2-propanol (volume ratio 1:1) once and then 2-propanol twice each at 8 h intervals to wash out CTAC and other unreacted reagents. Then half of the gel was dried from supercritical carbon dioxide at 80 °C and 14 MPa for 10 h. The remaining half of the gel was slowly dried at 40 °C under ambient pressure for 1 d. In this chapter, the author denotes the former gel as “aerogel” and the latter one as “xerogel”, respectively.

4.2.3 Measurements

The microstructure was observed with an SEM JSM-6060S (JEOL Ltd., Japan). Bulk density, ρ, was obtained by measuring the volume and weight of a carved gel. Porosity e (%) was then determined as $e = (1 - \rho/\rho_s)\times 100$, where ρ_s represents true density that was fixed to be 1.47 g cm^{-3} determined by helium pycnometry. Mechanical properties of aerogels were measured by a material tester (EZGraph, Shimadzu Corp., Japan). For uniaxial compression tests, a

carved gel (typical length × width × height was 15 × 15 × 7 mm^3) was to 80 % of its original size at a rate of 0.5 mm min^{-1}, and then the stress was unloaded at the same rate. Thermogravimetric analysis (TG) was performed with a Thermo plus TG 8120 (Rigaku Corp., Japan) instrument at a heating rate of 5 °C min^{-1} while continuously supplying air at a rate of 100 mL min^{-1}.

4.3 Result and Discussion

There have been a number of reports on aerogels with using tetra- and trifunctional alkoxysilanes[7] and with tetrafunctional alkoxysilane and polydimethylsiloxane,[8] but few with tri- and dialkoxysilane because of their too-high phase separation tendency arising from high hydrophobicity of the network. To synthesize the organopolysiloxane materials, the author employed surfactant CTAC to control phase separation, and used the acid–base two-step sol–gel reaction utilizing acetic acid and urea as catalysts, being similar to the case of PMSQ aerogels and xerogels. The synthesis process is a quite simple one-pot reaction. The digital camera image of the obtained flexible xerogel is shown in Figure 4.1.

The morphology of the aerogel frameworks are significantly affected by the starting composition. Figure 4.2 shows the SEM images with varied ratios of MTMS:DMDMS. The total volume of MTMS ($5.0 - X$ mL) and DMDMS (X mL) was fixed to 5.0 mL, and note that molar ratio is about the same as the volume ratio. With no DMDMS ($X = 0$) in the starting composition, the aerogel was transparent and the diameter of the spherical structural unit in the gel networks was about 10 nm, which is essentially the same material discussed in chapter 1. As the fraction of DMDMS was increased, the aerogel became opaque and its microstructure dramatically changed predominantly due to the increase in hydrophobicity of the condensates. Where $1.6 < X < 2.4$, the diameter of the framework slightly grew in size with the increasing amount of CTAC. No monolithic gelation occurred in $X > 2.5$, because the hydrophobicity of MTMS–DMDMS oligomers becomes too high and only hydrophobic precipitates were obtained. The change in the intermolecular structures in the networks with varied X was detected by FTIR (Figure 4.3). The absorbance by the Si–O–Si asymmetric stretching mode of linear and branched siloxanes at 1030 cm^{-1} and of polycyclic oligomers $(CH_3SiO_{1.5})_n$ (where n = 8, 10, and 12) at 1100 cm^{-1} show that DMDMS is incorporated into the siloxane network successfully.[9] The inclusion of DMDMS also can be confirmed by the result of TG measurements. The larger mass decrease by the decomposition of methyl groups is observed at

~400 °C in the sample richer in DMDMS (Figure 4.4). The amount of urea (U g) also affected the microstructures. Where U = 1.0, the gel consisted of the aggregate of spherical particles. With a greater amount of urea, the co-continuous structure with smoother interfaces formed and became finer in proportion to U (Figure 4.5). The amount of CTAC (C g) did not clearly affect the microstructures. However, where C < 0.2, gelation did not occur and precipitation was observed due to the high hydrophobicity of MTMS–DMDMS oligomers in the polar solvent.

The mechanical property was also evaluated by uniaxial compression tests. With increasing X, Young's modulus drastically decreased. Where 1.6 < X < 2.4, the aerogels recovered their original shape and size almost completely after unloading the stress, and the stress of 80 % compression of the sample X = 2.4 was about 1 % of the PMSQ aerogels (X = 0) (Figure 4.6). Although the size of the frameworks becomes larger and the connectivity better, the aerogels become more flexible and extremely soft as X increased, because of the enhanced incorporation of DMDMS. With varying amounts of urea, the flexibility also changed. With increasing U, the aerogels became further flexible and soft (Figure 4.7), because the microstructure became finer as mentioned above. The urea concentration only changes their porous structure and no clear difference in the molecular structure between the samples U = 1.0 and 5.0 was detected by FTIR spectra. This means that the porous structure is determined only by the progress of phase separation and the transient structure of phase separation is frozen by gelation, which is promoted by the base catalyst (urea hydrolysate, NH_4OH). On the other hand, CTAC affected the molecular structure (Figure 4.8). With increasing C, Young's modulus became lower (Figure 4.9). Because there is no difference in microstructures, this difference should be caused by the change of the siloxane networks, but further investigation is necessary for details. From these results, it is confirmed that the flexibility of MTMS–DMDMS aerogels can be extensively controlled by the starting composition. The author also attempted the three-point bending test on this material, but these "marshmallow-like" aerogels were bent even by their own weight and the measurements were found to be difficult.

The flexibility of MTMS–DMDMS gels makes it possible to dry the wet gels by simple solvent evaporation under ambient pressure (the sample shown in Figure 4.1 is a xerogel). In the range of the following three requirements, $1.6 < X < 2.4$, $U > 2.0$ and $C > 0.2$, xerogels can be successfully obtained without any change of the shape and size from the wet gels. The author compared the xerogel with the aerogel from the same starting composition ($X = 2.0$, $U = 5.0$ and $C = 0.8$). Bulk densities of both gels ρ are almost the same at about 0.11 g cm^{-3} and the porosity can be estimated as 93% by ρ_s. Figure 4.10 and b show the stress–strain curves of each gel and there is no visible difference. From SEM observations (Figure 4.10c and d), each gel is confirmed to have identical features. In fact, we can obtain the xerogels with the identical properties even after repetitive re-wetting and re-drying. In addition, since the MTMS–DMDMS xerogels show strong hydrophobicity due to the methyl groups, the gels can float on water for at least a few months.

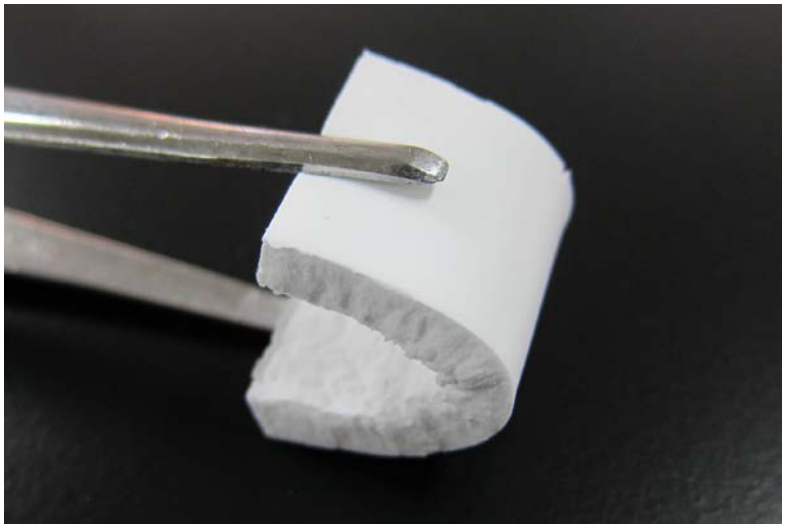

Figure 4.1 Digital camera image of the flexible xerogel derived from the MTMS and DMDMS co-precursor system.

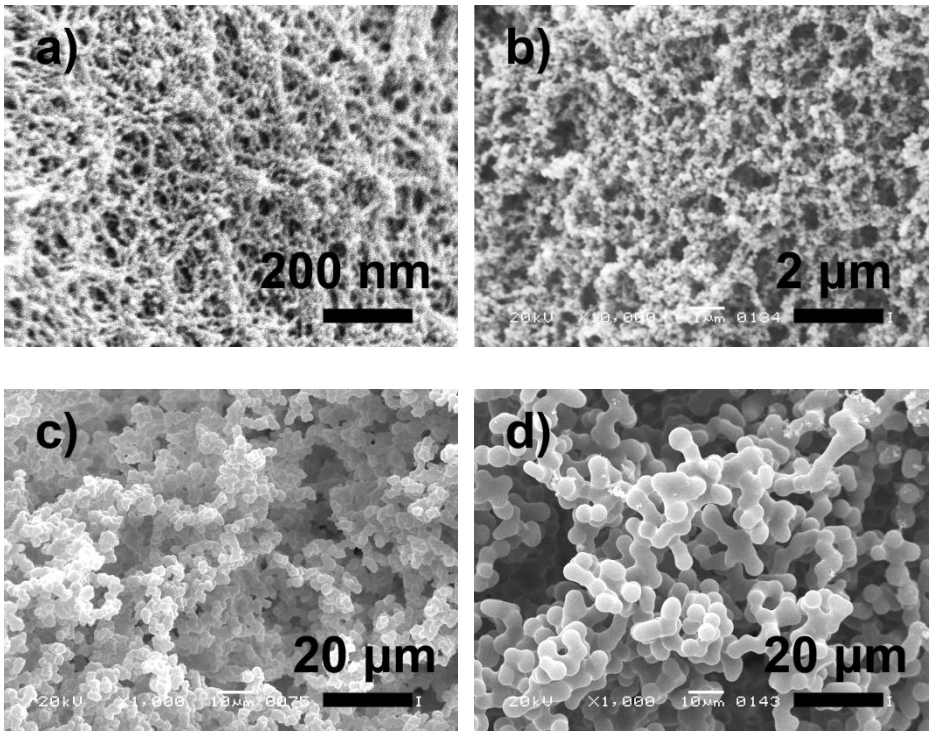

Figure 4.2 SEM images of the samples prepared with varied amounts of MTMS–DMDMS: a) 5.0 mL–0 mL (X = 0), b) 3.8 mL–1.2 mL (X = 1.2), c) 3.4 mL–1.6 mL (X = 1.6), d) 2.6 mL–2.4 mL (X = 2.4).

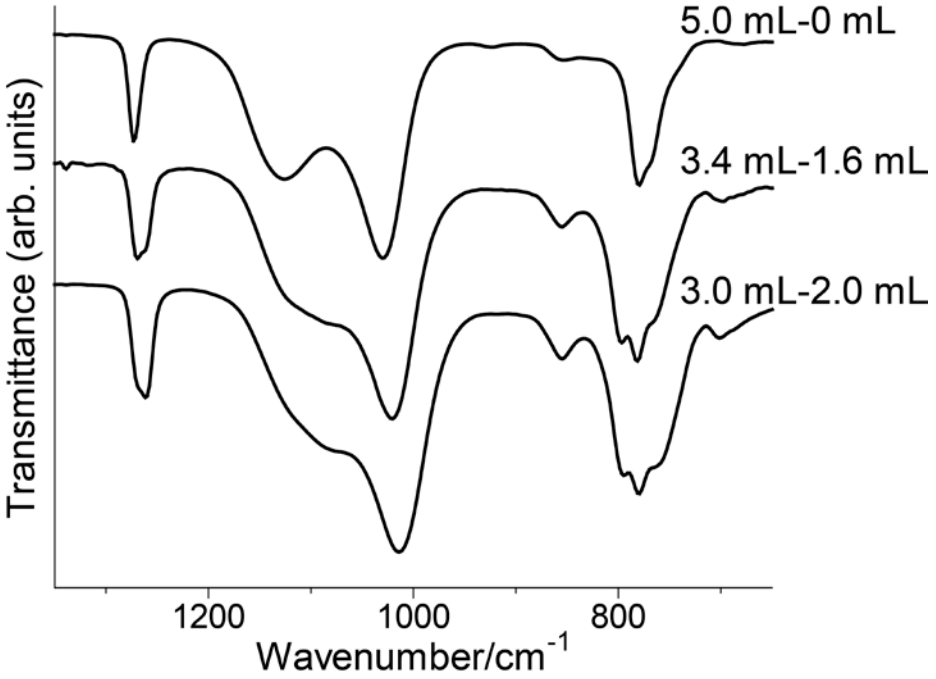

Figure 4.3 FTIR spectra of the aerogels prepared with different ratios of MTMS:DMDMS.

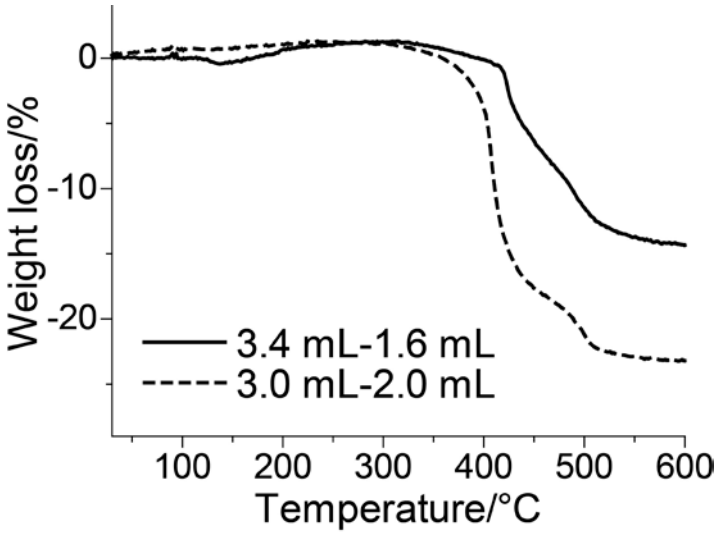

Figure 4.4 TG curves of the aerogels prepared with varied ratios of MTMS:DMDMS.

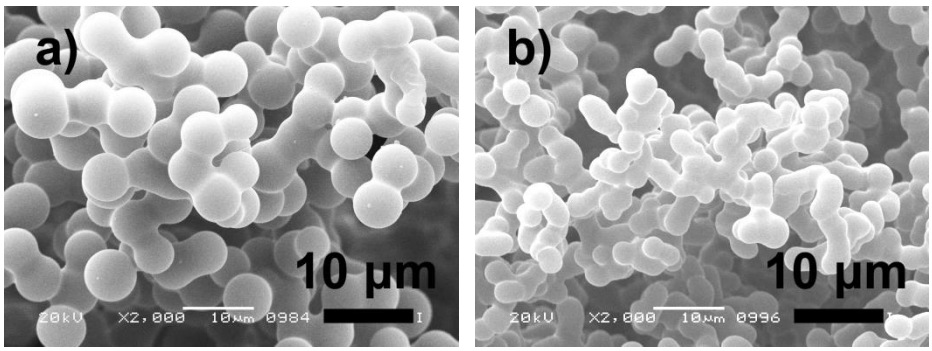

Figure 4.5 SEM images of the aerogels prepared with different amounts of urea: a) 1.0 g (U = 1.0) and b) 5.0 g (U = 5.0).

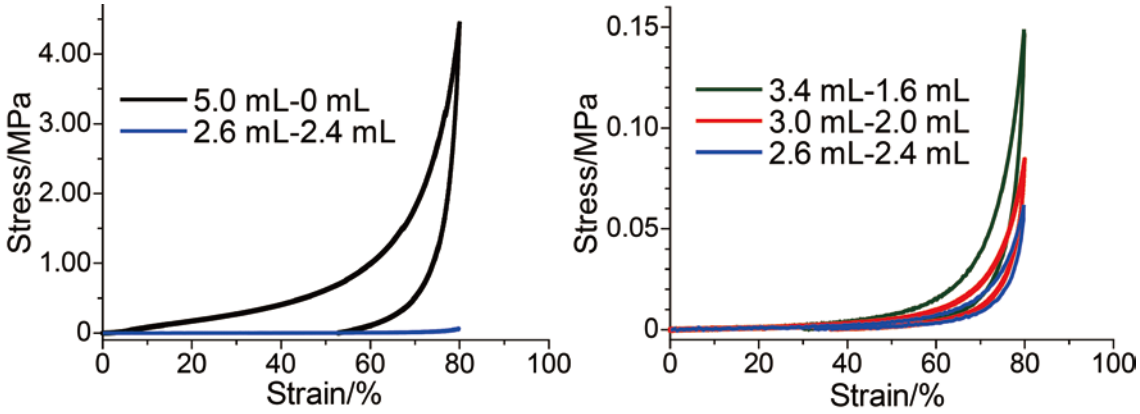

Figure 4.6 Stress–strain curves obtained by the uniaxial compression tests on the flexible aerogels prepared with various amounts of MTMS–DMDMS.

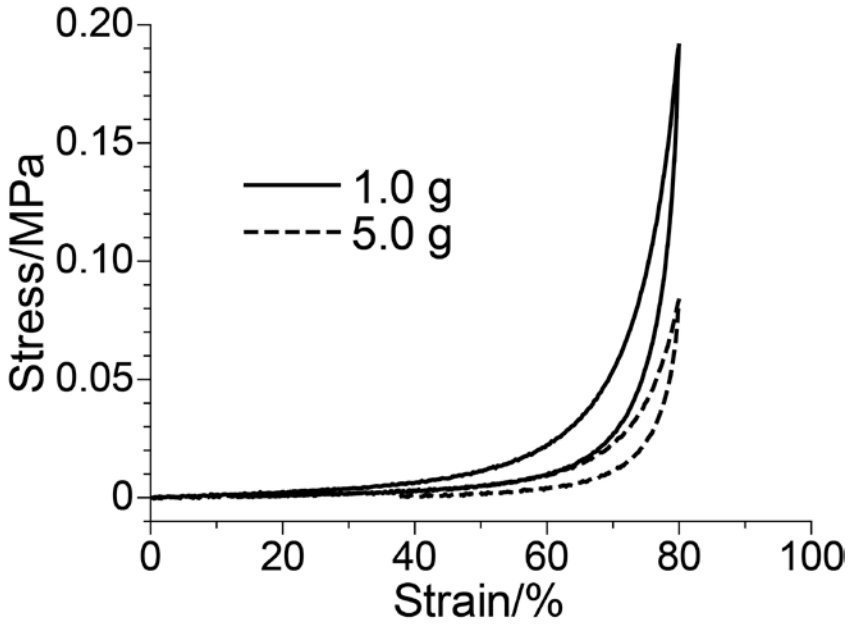

Figure 4.7 Stress–strain curves of the aerogels prepared with varied amounts of urea.

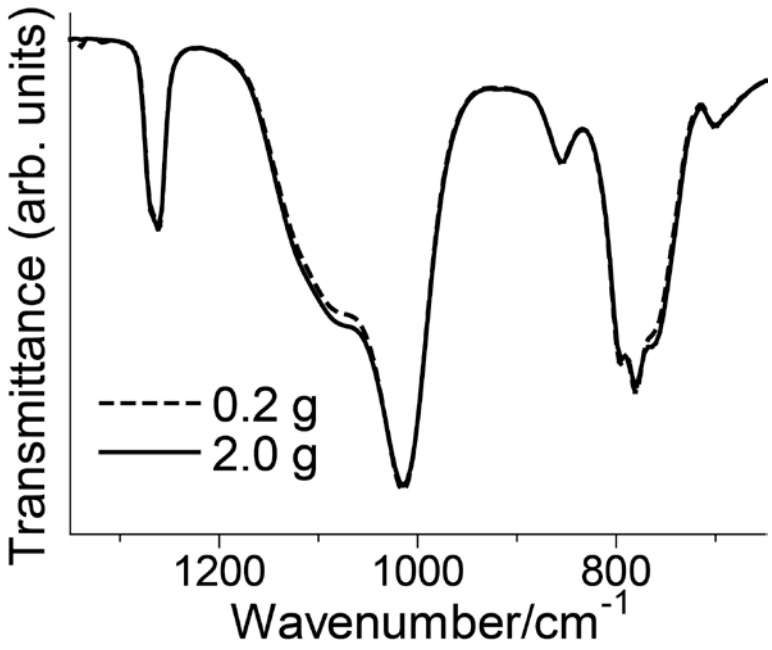

Figure 4.8 FTIR spectra of the aerogels prepared with varied amounts of CTAC.

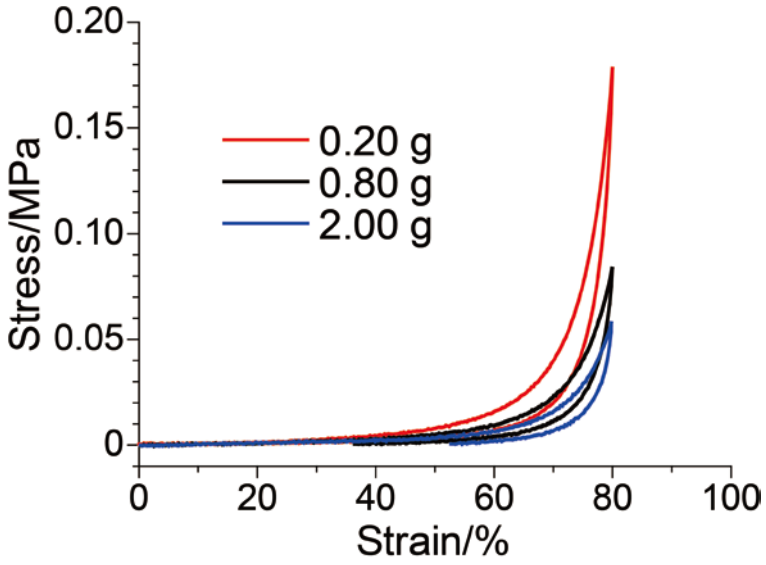

Figure 4.9 Stress–strain curves of the aerogels prepared with varied amounts of CTAC.

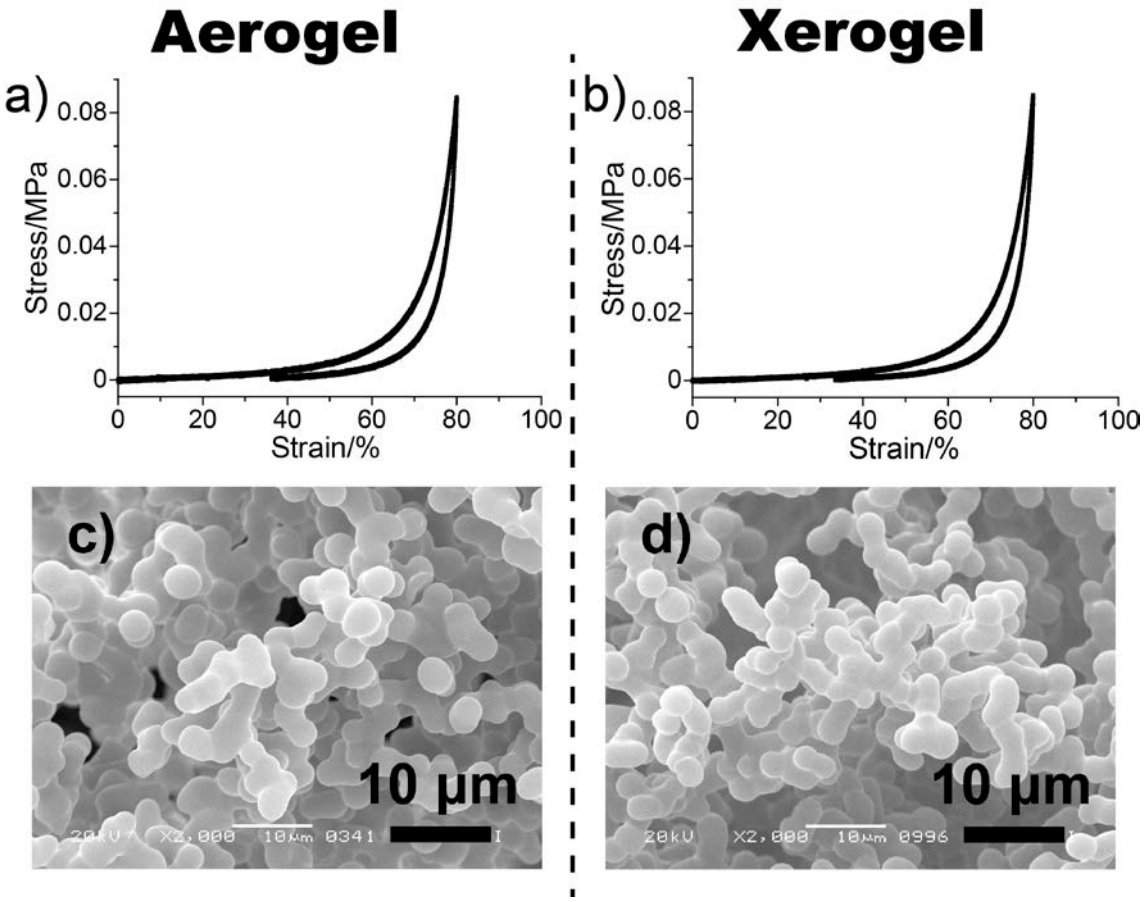

Figure 4.10 Properties of the aerogel/xerogel synthesized from the same starting composition (X = 2.0, U = 5.0, C = 0.8): a) and b) Stress–strain curves obtained by the uniaxial compression tests, and c) and d) SEM images.

4.4 Conclusion

The highly flexible aerogels have been prepared from mixtures of MTMS and DMDMS in the two-step sol–gel process containing surfactant CTAC. Around the ratio of MTMS:DMDMS = 1.5, xerogels by evaporative drying under ambient conditions can be obtained with no difference from the corresponding aerogels. These aerogels and xerogels show the perfect spring-back behavior with small stress (~0.10 MPa). The microstructure and the mechanical properties can be easily changed by varying the ratio of MTMS and DMDMS, the amount of CTAC and urea in the starting composition. Owing to the soft and elastic porous structures, these xerogels can be applied to high performance sound insulators, which we will report on in the near future in detail (Figure 4.11).

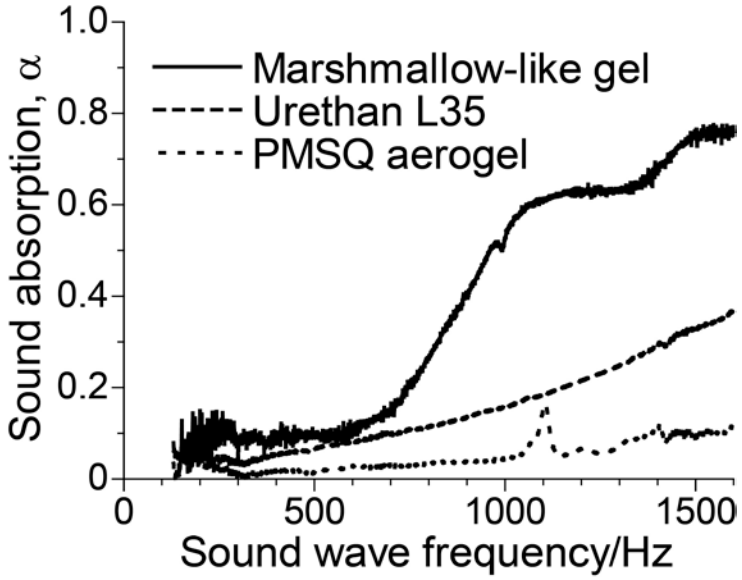

Figure 4.11 Normal incidence sound absorption coefficients of the MTMS–DMDMS xerogel, the PMSQ aerogel and the urethane form (a conventional acoustic absorbent). Absorbance in the MTMS–DMDMS xerogel is the highest among these three.

References in Chapter 4

[1] S. S. Kistler, *Nature* **1931**, *127*, 741.

[2] a) N. Hüsing, U. Schubert, *Angew. Chem. Int. Ed.* **1998**, *37*, 23; b) D. R. Rolison, B. Dunn, *J. Mater. Chem.* **2001**, *11*, 963; c) A. C. Pierre, G. Pajonk, *Chem. Rev.* **2002**, *102*, 4243.

[3] a) R. W. Pekala, C. T. Alviso, F. M. Kong, S. S. Hulsey, *J. Non-Cryst. Solids* **1992**, *145*, 90; b) S. A. Al-Muhtaseb, J. A. Ritter, *Adv. Mater.* **2003**, *15*, 101.

[4] A. V. Rao, S. D. Bhagat, H. Hirashima, G. M. Pajonk, *J. Colloid Interface Sci.* **2006**, *300*, 279.

[5] H. Guo, B. N. Nguyen, L. S. McCorkle, B. Shonkwilerb, M. A. B. Meador, *J. Mater. Chem.* **2009**, *19*, 9054.

[6] a) G. Zhang, A. Dass, A.-M. M. Rawashdeh, J. Thomas, J. A. Counsil, C. Sotiriou-Leventis, E. F. Fabrizio, F. Ilhan, P. Vassilaras, D. A. Scheiman, L. McCorkle, A. Palczer, J. C. Johnston, M. A. Meador, N. Leventis, *J. Non-Cryst. Solids* **2004**, *350*, 152; b) M. A. B. Meador, E. F. Fabrizio, F. Ilhan, A. Dass, G. Zhang, P. Vassilaras, J. C. Johnston, N. Leventis, *Chem. Mater.* **2005**, *17*, 1085.

[7] a) A. V. Rao, D. Haranath, *Microporous Mesoporous Mater.* **1999**, *30*, 267; b) H. E. Rassy, A. C. Pierre, *J. Non-Cryst. Solids* **2005**, *351*, 1603.

[8] a) S. J. Kramer, F. Rubio-Alonso, J. D. Mackenzie, *MRS Online Proc. LIbr.* **1996**, *435*, 295; b) J. D. Mackenzie, E. P. Bescher, in *Handbook of Sol-Gel Science and Technology: Processing Characterization and Applications*, ed. S. Sakka (Volume ed. R. M. Almeida), Kluwer Academic Publishers, Dordrecht, **2004**, vol. II, ch. 16, pp. 313–326.

[9] H. Dong, J. D. Brennan, *Chem. Mater.* **2006**, 18, 4176.

Chapter 5

Facile Synthesis of Marshmallow-like Macroporous Gels Usable under Harsh Conditions for the Separation of Oil and Water

5.1 Introduction

The separation of oil and water is an important pursuit for saving endangered environments. In 2010, the Gulf of Mexico oil spill widely and seriously damaged the ocean and coast near the oilfield. The number of similar accidents is increasing with the development of industry, and materials that can reduce environmental pollution are in high demanded. At the same time, in the area of analytical chemistry, the efficient separation of molecules is a key technique, which determines the efficiency and accuracy of chemical analysis and detection. For these purposes, hydrophobic porous materials are in common use, because hydrophobic surfaces effectively adsorb/absorb oily target compounds that are mixed with an aqueous phase. Therefore, many researchers have been studying hydrophobic porous materials and their application as oil–water separation media.[1] Various chemical compositions have been investigated, such as carbon-based materials,[2] metal oxide nanowires (such as manganese[3]), biomass nanofibers (such as cellulose[4]), organic polymers (such as polyester,[5] polydivinylbenzene, and polythiophene[6]) and hydrophobic macroporous aerogels.[7] Other materials based on polydimethylsiloxane (PDMS) or fluorocarbon-coated materials,[3b,5,7b,8] and the design of a biomimetic rough surface, through the use of etching techniques, to enhance hydrophobicity[4a,9] are also widely reported. However, these methods have problems such as complicated and lengthy processes and high costs for reagents and devices, which prevents the use of these materials in practical and commercial applications.

The author has investigated hydrophobic porous PMSQ materials derived from MTMS, consisting of transparent aerogels and xerogels with mesoporous to macroporous monoliths that are created by controlling phase separation in the sol–gel process (chapters 1–3). Polymethylsilsesquioxane (PMSQ) gels have a

superhydrophobic surface owing to methyl groups that are directly bonded to silicon atoms; this flexible network structure allows the material to spring-back after compression, and the preparation of aerogel-like xerogels by ambient pressure drying. In chapter 4, marshmallow-like gels derived from a co-precursor system of MTMS and DMDMS are also discussed. Marshmallow-like gels show not only compression/re-expansion properties similar to that of PMSQ gels, but also very soft and bendable mechanical features. A high sound absorption property is also shown, owing to the soft networks. The flexibility and intrinsic hydrophobicity indicate that these materials can be used like a sponge as an adsorption/absorption media for the quick removal of unwanted organic liquids. In this chapter, the shows the outstanding capability of these materials for absorbing organic liquids over a wide temperature range, and discuss the possibility for their application as separation media.

5.2 Experimental

5.2.1 Chemicals

Acetic acid, distilled water, and urea were purchased from Hayashi Pure Chemical Industry, Ltd. (Japan). Surfactant CTAC was obtained from Tokyo Chemical Industry, Ltd. (Japan). Precursors VMDMS and bis(methyldiethoxysilyl)ethane were purchased from Tokyo Chemical Industry, Ltd. (Japan) and Gelest, Inc. (USA) respectively, and all other alkoxysilanes from Shin-Etsu Chemical Co., Ltd. (Japan). All of the chemical reagents were used as received.

5.2.2 Synthesis procedures

First, 0.80 g of CTAC, 5.0 g of urea, and 15 mL of 5 mM aqueous acetic acid were mixed in a glass sample tube. Then 0.021 mol of trifunctional and 0.014 mol of difunctional alkoxysilanes were added at the same time under vigorous stirring at ambient temperature, and stirring was continued for 60 min until the solution was homogeneous. In the case of a bis(methyldiethoxysilyl)ethane–DMDMS gel, 0.006 mol of bis(methyldiethoxysilyl)ethane was used instead of the trifunctional alkoxysilane. The obtained sol was transferred into a tightly-sealed container, which was placed in a forced convection oven at 80 °C for 9 h to complete gelation and aging. The obtained gels were washed with methanol by soaking/squeezing by hand for several times to remove the residual surfactant and other chemicals. The washed samples were dried under ambient condition to obtain xerogels.

5.2.3 Measurements

A scanning electron microscope (JSM-6060S, JEOL, Japan) and a laser scanning confocal microscope (LSCM, Carl Zeiss LSM 5 Pascal, Germany) were employed to observe the microstructure. The specific surface area was estimated by 3-D image analysis with a custom-made software.[10] Mechanical properties of aerogels were measured by a material tester (EZGraph, Shimadzu Corp., Japan). For uniaxial compression tests, carved gels (typical length × width × height was

15 × 15 × 10 mm3) were compressed–decompressed using a load cell of 5 kN with a rate of 0.5 mm min^{-1}. For three-point bending tests, a cylindrical sample with 8 mm diameter and 35 mm length were put on a fixture with a 30 mm span and compressed–decompressed for 100 times by a wedge-shaped crosshead with 60 ° and 0.3 mm diameter at the point with using a load cell of 5 N at a rate of 5 mm min^{-1}. To assess molecular-level structure of obtained siloxane networks, FTIR and ^{29}Si solid-state cross polarization/magic angle spinning (CP/MAS) NMR measurements were performed. The FTIR spectra were recorded with IRAffinity-1 (Shimadzu Corp., Japan) using an attenuated total reflection (ATR) attachment. A total of 100 scans were recorded with a resolution of 4 cm^{-1} on the samples dried in vacuum at 80 °C for 1 d in advance. An NMR spectrometer Bruker Avance III 800 (Germany) has been operated under a static magnetic field of 18.8 T. The contact time for the cross polarization was fixed at 5.5 ms and the rate of sample spinning was set to 15 kHz. The ^{29}Si chemical shifts were expressed as values relative to tetramethylsilane (Me_4Si) by using the resonance line at −9.66 ppm for hexamethylcyclotrisiloxane crystals as an external reference. Contact angles were measured with Drop Master DM-561Hi (Kyowa Interface Science Co., Ltd., Japan). Volume of water droplet was fixed at 3.0 μL and a contact angle was determined at 2 s after the attachment to gel surface. Thermogravimetric–differential thermal analysis (TG–DTA) was performed with a Thermo plus TG 8120 (Rigaku Corp., Japan) instrument at a heating rate of 5 °C min^{-1} while continuously supplying air at a rate of 100 mL min^{-1}.

5.3 Result and Discussion

The author succeeded in the preparation of various kinds of marshmallow-like gels derived from tri- and difunctional alkoxysilanes as co-precursors through a facile one-pot reaction. The combinations of alkoxysilanes and the standard synthesis are shown in Figure 5.1a. Regardless of the combinations chosen, the synthetic procedure and conditions remain the same, which means that we can design flexible porous gels with different functional groups (for FTIR spectra, Figure 5.2)[11] without the need for any complicated processes such as chemical vapor deposition, dip coating with PDMS, or additional polymerization of organic groups, all of which are necessary in the above-mentioned reports. To obtain gels, only four simple routine steps are needed: 1) mixing alkoxysilanes, urea, and the surfactant CTAC in a dilute aqueous acetic acid solution, and stirring for 60 min at RT to promote hydrolysis; 2) transferring the solution to an oven for gelation at 80 °C over several hours; 3) washing with alcohol; and 4) evaporative drying under ambient conditions. Alkoxysilanes with higher hydrophobic organic groups such as 3,3,3-trifluoropropyl lead to macroporous skeletons that are more spherical, but each particle is tightly bound together at the neck, the diameter of which is several micrometers (Figure 5.3). The bulk body is elastic and bendable without any failure in the structure (Figure 5.4).

In the case of MTMS–DMDMS copolymers (these precursors are inexpensive and readily commercially available), the synthesis can be completed within a day, even on a multi-liter scale (Figure 5.1b); the resulting gels can be formed in any shape desired. Before obtaining the final product, the author needs to wash out the surfactant and unreacted compounds; the sponge-like flexible nature of the material helps in this process, reducing the work to soaking and squeezing by hand (Figure 5.1c). The ^{29}Si solid-state CP/MAS NMR spectrum shows that residual hydroxy groups are virtually negligible in the structure, which indicates that the network formation is complete in a few hours (Figure 5.1d).[12] This is a great advantage for an emergency, such as an oil-spill accident, because the gels can be immediately synthesized, even on site.

In addition to the simple synthesis process, MTMS–DMDMS gels have a low density (ca. 0.12 g cm^{-3}, which corresponds to a porosity of >92%) and superhydrophobicity (contact angle is ca. 153 °; see Figure 5.5a). The hydrophobicity is caused both by the geometrical rough surface, which is derived from a macroporous structure presumably formed by spinodal decomposition,[13] and by the many methyl groups and relatively few hydroxyl groups exposed on the surface. To evaluate the material as an oil–water separation media, the author tested its absorption–drying behavior using *n*-hexane as a model organic compound (Figure 5.5b). Over ten repetitions, the gel showed stable performance: the gel absorbs ca. 6.2 times its dry weight in *n*-hexane, and no damage is observed. The author also performed an *n*-hexane removal test using this material as a sponge (Figure 5.5c). All of the *n*-hexane was successfully separated from water easily and quickly, even though there was larger quantity of liquid than could be absorbed at once. Also, the gels can absorb other organic liquids and still be dried by squeezing-out, even in the case of high-density oils (such as chloroform) and viscous oils (such as mineral oil with a comparable kinetic viscosity (ca. 44.6 mm s^{-1} at 40 °C) to medium crude oil[14]) in the same way as *n*-hexane. The organics are stored in the abundant pores of this material (Figure 5.1b), and the weight ratio of absorbed solvent/dried gel depends on the density of the organic compounds (Figure 5.5d). Absorbing media specific to the chemical and physical nature of a desired organic compound can be designed both by changing the substituent groups in the precursors and by controlling flexibility and macropore/skeleton diameters of this material, which is accomplished by changing the starting composition, such as the precursor ratio and the amounts of urea and CTAC (discussed in chapter 4).

Because of the PDMS-like network, MTMS–DMDMS gels show high flexibility over a wider temperature range than conventional organic polymers such as polyurethane and polyethylene. MTMS–DMDMS gels can recover their original shape from 80 % uniaxial compression and a 3-point bending test at RT (Figure 5.6). To evaluate their thermal stability, the author conducted thermogravimetry–differential thermal analysis (TG–DTA). The result shows that these materials are stable up to ca. 320 °C, whereas the methyl groups in the

network are oxidized at higher temperatures (Figure 5.7). In fact, there was no change in the FTIR spectra, mechanical properties, or contact angle of water after heat treatment at 315 °C for 24 h. This thermal stability is higher than oil–water separation media based on organic polymers. Moreover, even at low temperatures, the gels show high flexibility. From differential scanning calorimetry (DSC), no obvious glass transition is observed from RT to −130 °C. The author could absorb and squeeze out a dry ice–ethanol mixture at ca. −70 °C. The flexibility of the swollen gel was not lost and they completely recovered their original shape after squeezing out the liquid (Figure 5.8a, strain was completely recovered after measurement). Furthermore, the gel even shows high flexibility in liquid nitrogen (LN_2), although the gel was somewhat hardened (Figure 5.9). The author could use the gel to absorb and squeeze out LN_2 as if it were water in a sponge (Figure 5.8b). Thus, MTMS–DMDMS gels can be also used as oil absorbing media in a very low temperature region, such as the polar zone. In fact, kerosene was successfully absorbed and squeezed out at 0 °C in exactly the same way as RT. No other materials have been reported to show high flexibility at such low temperatures except for entangled carbon nanotubes obtained by the "super-growth" method.[15]

The functional groups on the marshmallow-like gels can be used for specific adsorption/absorption purposes. For example, in the case of (3-mercaptopropyl)trimethoxysilane–(3-mercaptopropyl)methyldimethoxysilane copolymerized gels, gold ions are adsorbed on the surface by simply soaking in an aqueous tetrachloroauric acid solution (Figure 5.10). By positioning organic groups other than methyl (such as phenyl and 3,3,3-trifluoropropyl) on the surface, hydrophobicity can be further increased. Owing to the soft and elastic porous structure it would also be possible to create new separation media for solid-phase extraction.[16] The author has also succeeded in the synthesis of marshmallow-like materials derived from bridged and di-functional alkoxysilanes as co-precursors (bis(methyldiethoxysilyl)ethane–DMDMS) with the same process (Figure 5.11).

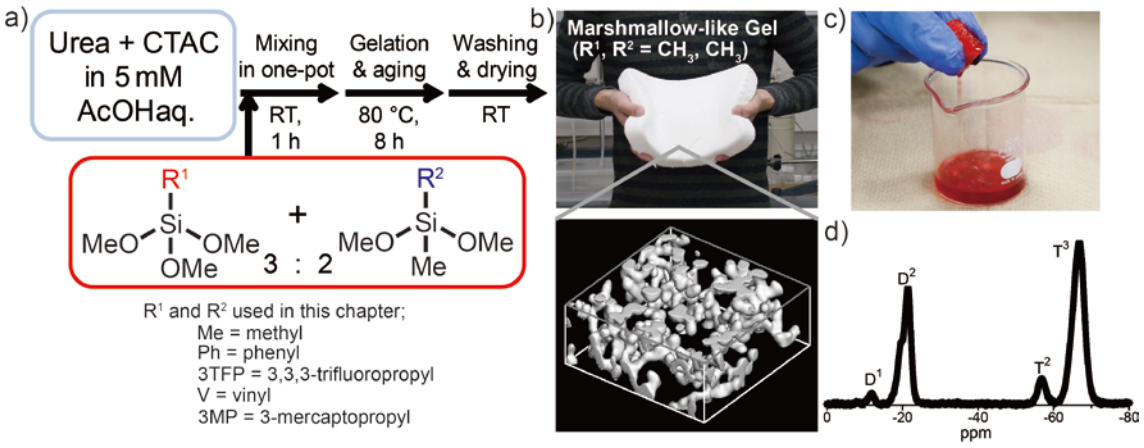

Figure 5.1 a) Facile synthesis of marshmallow-like gels derived from di- and tri-functional alkoxysilanes as co-precursors. b) The shape of the MTMS–DMDMS (R^1,R^2=Me) gel produced on a 2.5 L scale, and its 3D microstructure (73.1×73.1×30.8 μm). c) The gel can be used to absorb organic liquids and then be squeezed out by hand. d) ^{29}Si solid-state NMR spectrum of the MTMS–DMDMS gel.

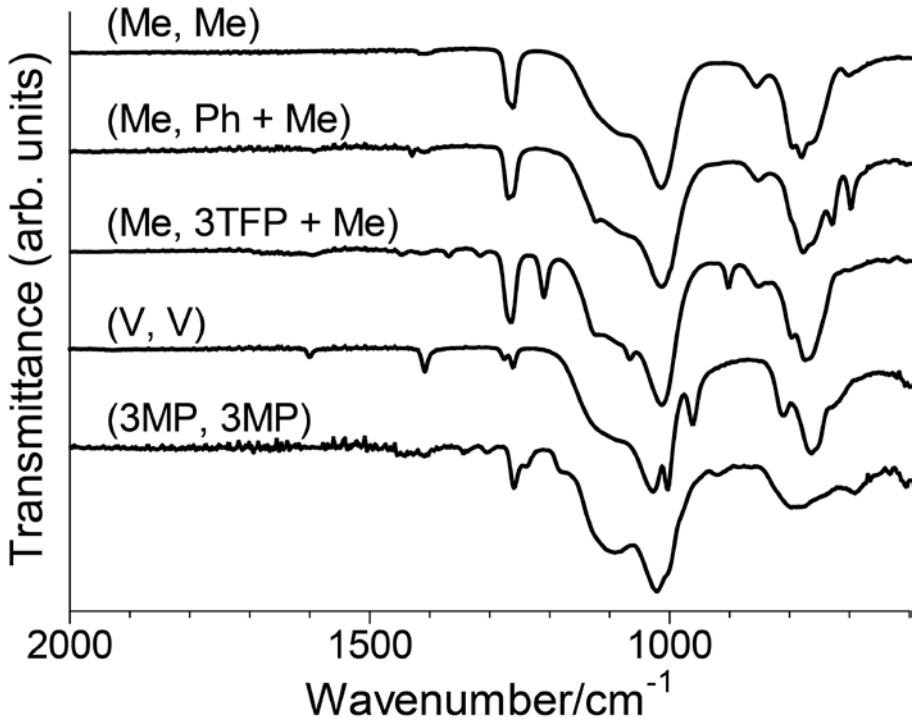

Figure 5.2 IR spectra of the marshmallow-like gels derived from di- and tri-functional alkoxysilane (R^1, R^2). All samples contain Si–O–Si asymmetric stretching at 1025 cm^{-1} (linear and branch) and 1100 cm^{-1} (polycyclic oligomers) as well as C-H (methyl groups) asymmetric deformations at 1280 and 1400 cm^{-1}. For (Me, Me), multiple peaks at 750-870 cm^{-1} are combinations of –CH3 rocking in Si–CH3 and Si–$(CH_3)_2$, and C–Si asymmetric stretching in C–Si–O units. For (Me, Ph+Me), out-of-plane vibration and bending of H–C in phenyl groups are observed at 720 cm^{-1}, and planar ring vibration is at 1120 cm^{-1}. For (Me, 3TFP+Me), symmetric and asymmetric stretching modes characteristic for C–F are observed at 1220 and 1315 cm^{-1}. For (V, V), =CH2 wagging at 970 cm^{-1}, C=C twist at 1000 cm^{-1}, =CH2 scissor at 1400 cm^{-1} and C=C stretching at 1600 cm^{-1} are recognized. For (3MP, 3MP), although absorptions related to –SH (such as stretching at 2600 cm^{-1}) cannot be observed because of the weak intensity, adsorption of gold ions indicates the presence of thiol groups on the surface (Figure 5.10).

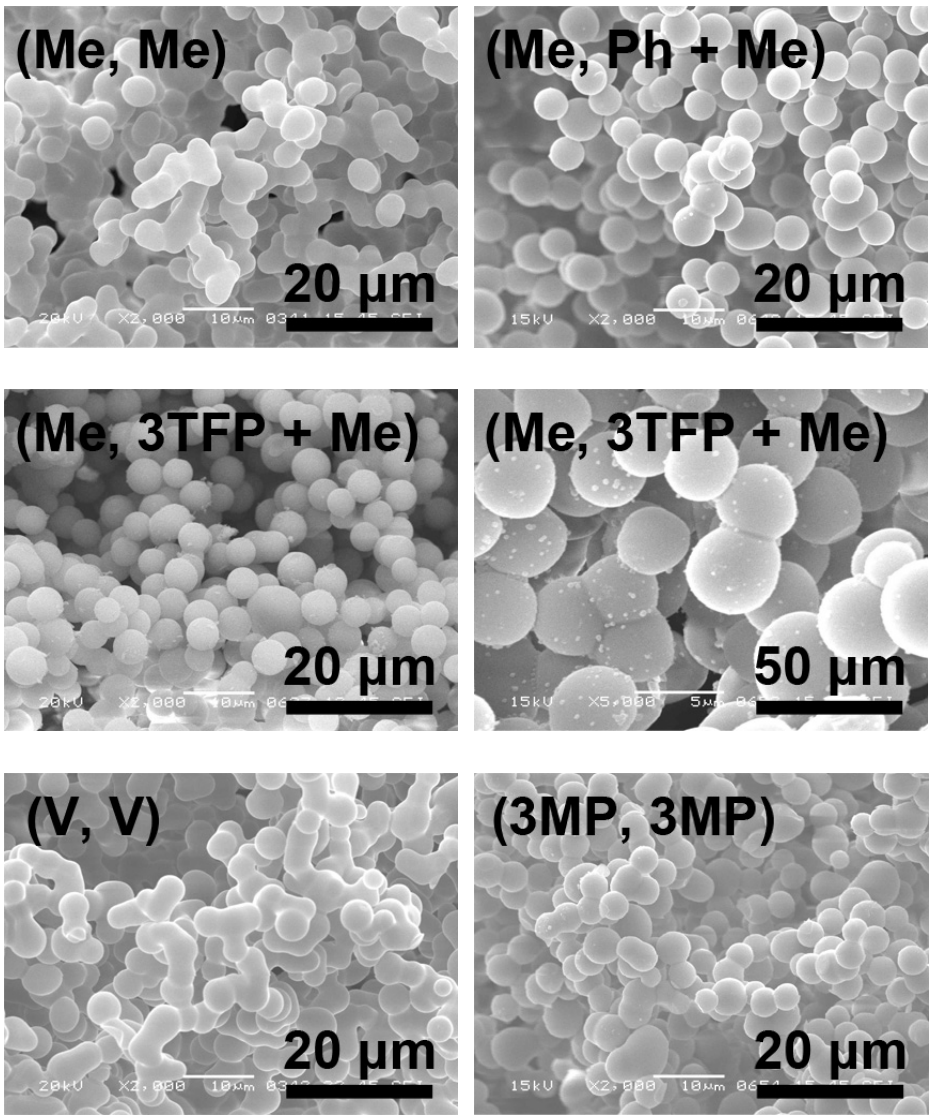

Figure 5.3 SEM images of the marshmallow-like gels derived from di- and tri-functional alkoxysilane (R^1, R^2).

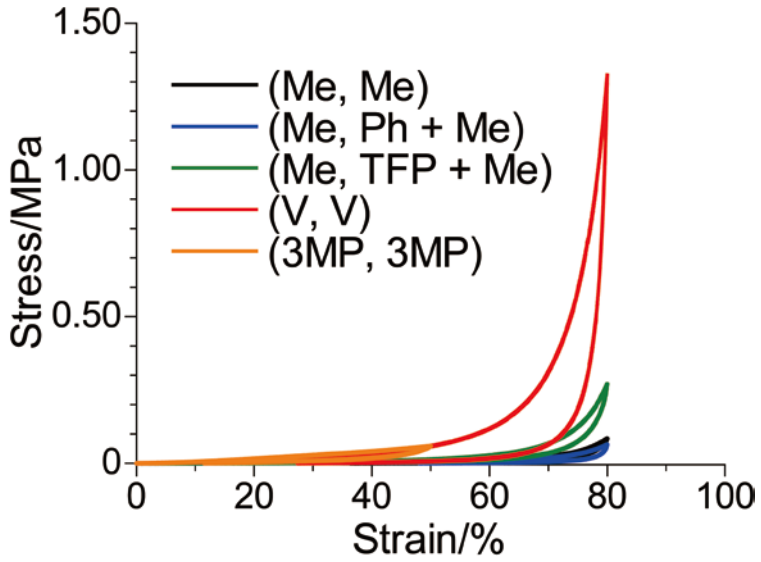

Figure 5.4 Stress–strain curves of the marshmallow-like gels derived from di- and trifunctional alkoxysilane for 80 % uniaxial compression (R^1, R^2). Only (3-mercaptpropyl)trimethoxysilane–(3-mercaptpropyl)methyldimethoxysilane (3MP, 3MP) gel was tested for 50 % compression due to corruption of bulk body for the 80 % test. All gels returned to their original shape after removal of stress.

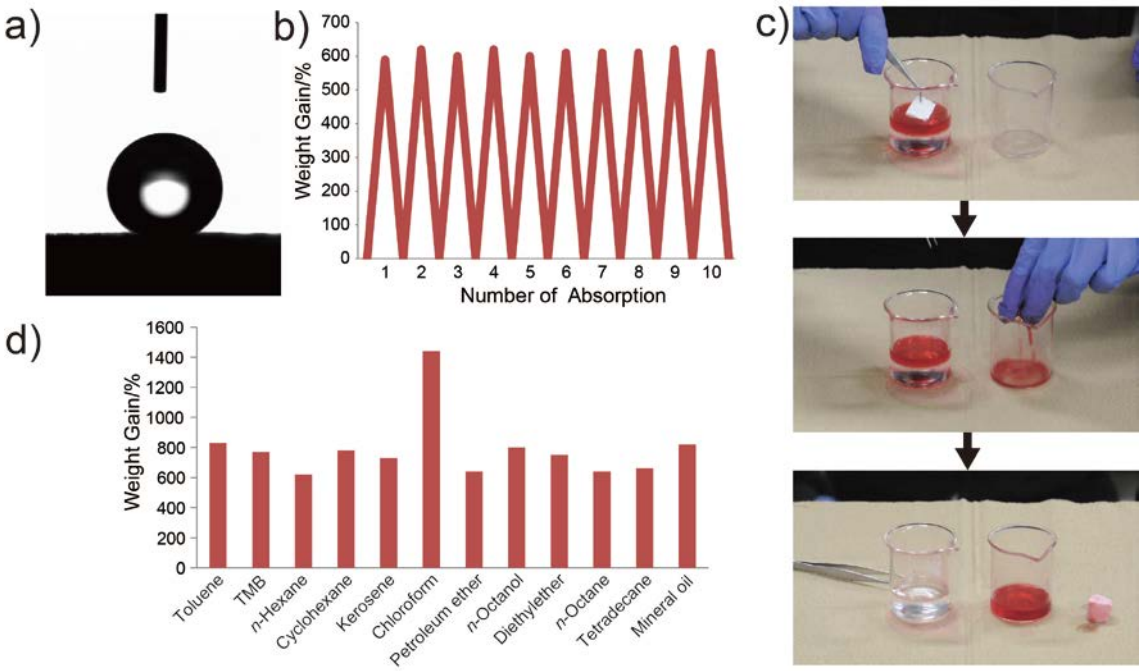

Figure 5.5 a) Superhydrophobic surface of the MTMS–DMDMS marshmallow-like gel. Contact angle is 153 °. b) Weight gain during *n*-hexane absorption/drying cycles. c) The marshmallow-like gel can separate *n*-hexane from water. d) Absorption capacities of the MTMS–DMDMS gel for various organic solvents and oils, as indicated by weight gain.

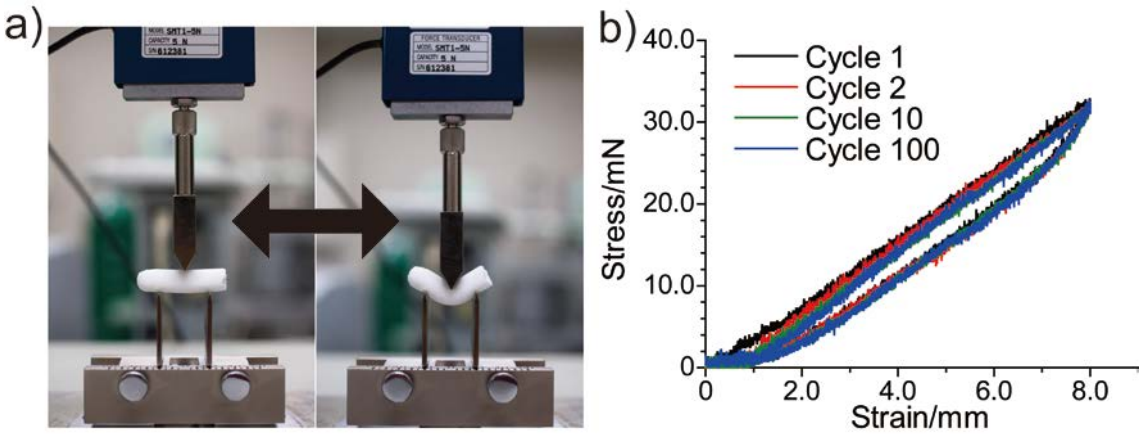

Figure 5.6 a) Photograph and b) stress–strain curves of a 3-point bending test on the MTMS–DMDMS gel.

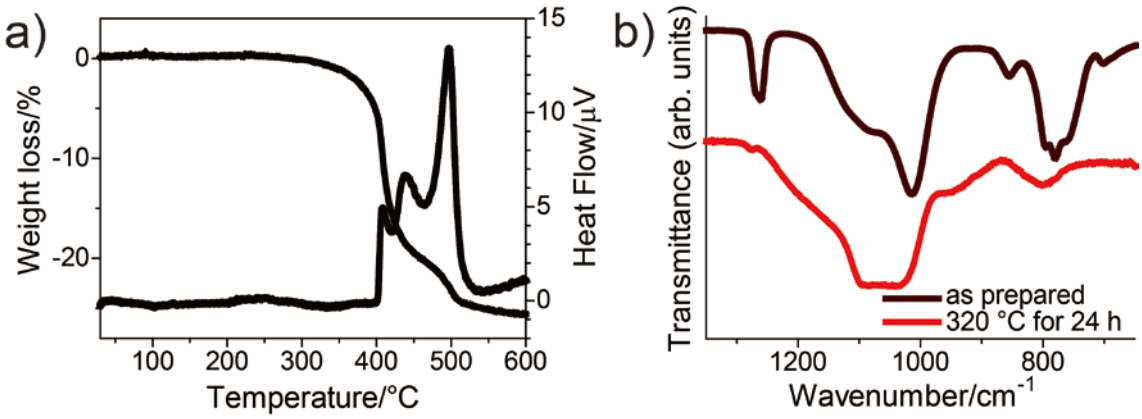

Figure 5.7 a) TG–DTA curves of the MTMS–DMDMS (Me, Me) marshmallow-like gel and b) IR spectra before and after heat-treated at 320 ° C for 24 h.

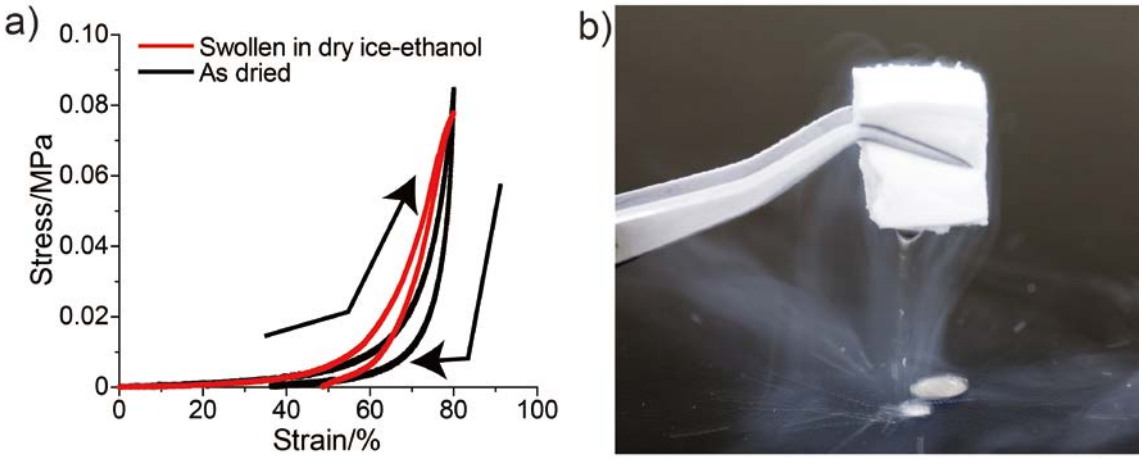

Figure 5.8 a) Stress–strain curves of the MTMS–DMDMS gel, both dried (black) and swollen with a dry ice–ethanol mixture (red). b) Squeezing out LN_2.

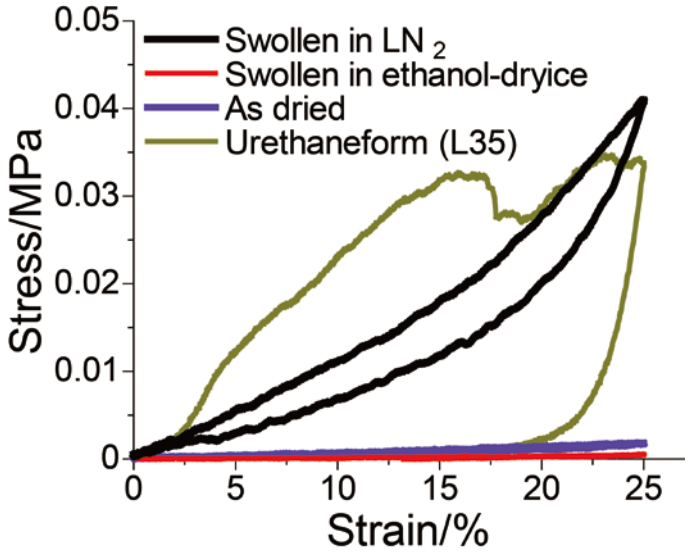

Figure 5.9 Stress–strain curves of the MTMS–DMDMS (Me, Me) marshmallow-like gel and a common polyurethane form ("L35" according to JIS A 1419-2: 2000 and ISO 717-2: 1996 for impact sound insulation). The marshmallow-like gel maintains the flexibility even when swollen with liquid nitrogen whereas the polyurethane form collapses.

Figure 5.10 The (3-mercaptopropyl)trimethoxysilane–(3-mercaptopropyl)methyldimethoxysilane (3MP, 3MP) marshmallow-like gel adsorbed gold ions on the surface by soaking in an aqueous tetrachloroauric acid solution.

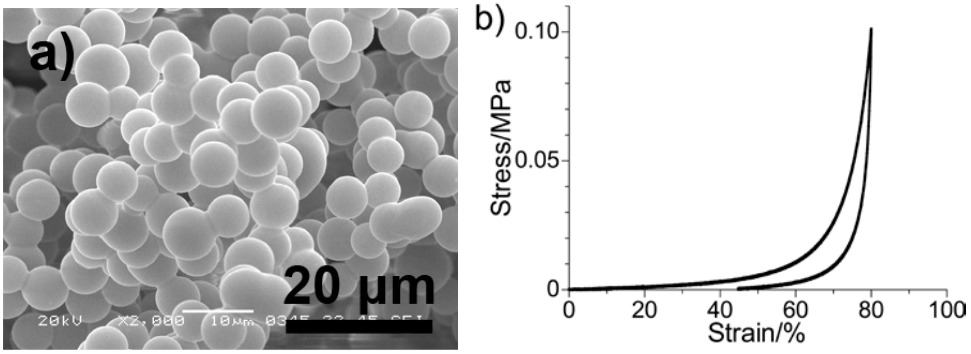

Figure 5.11 a) SEM image and b) a stress–strain curve of uniaxial compression test (strain completely recovered after measurement) on the bis(methyldiethoxysilyl)ethane–DMDMS gel.

5.4 Conclusion

A new kind of superhydrophobic medium for the separation of oil and water is developed. Marshmallow-like gels, which are based on polyorganosiloxane networks, are synthesized from various alkoxysilanes, such as tri-, di-functional, and bridged alkoxysilanes, as co-precursors by a facile process and without special conditions. Copolymerization with various types of alkoxysilanes adds functionality to the gels, which allows for the flexible design of surface chemical properties. The obtained MTMS–DMDMS gels display superhydrophobicity and can act as a sponge, removing organic compounds from water by absorbing them and then releasing them upon being squeezed out. The elastic properties are maintained over a wide temperature range, from LN_2 temperatures up to ca. 320 °C, which extends their possible applications to use in harsh environments. The introduction of different functional groups allows for changing of the adsorption/absorption properties, which is advantageous in their use as separation media for different target compounds. Together with high sound absorption properties,[17] these unique multifunctional gels are expected to further extend the practical applications of this class of compounds.

References in Chapter 5

[1] Z. Xue, S.Wang, L. Lin, L. Chen, M. Liu, L. Feng, L. Jiang, *Adv. Mater.* **2011**, *23*, 4270.

[2] a) M. Inagaki, A. Kawahara, Y. Nishi, N. Iwashita, *Carbon* **2002**, *40*, 1487; b) H.-W. Liang, Q.-F. Guan, L.-F. Chen, Z. Zhu, W.-J. Zhang, S.-H. Yu, *Angew. Chem. Int. Ed.* **2012**, *51*, 5101.

[3] a) J. Lahann, *Nat. Nanotechnol.* **2008**, *3*, 320; b) J. Yuan, X. Liu, O. Akbulut, J. Hu, S. L. Suib, J. Kong, F. Stellacci, *Nat. Nanotechnol.* **2008**, *3*, 332.

[4] a) A. Tuteja, W. Choi, M. Ma, J. M. Mabry, S. A. Mazzella, G. C. Rutledge, G. H. McKinley, R. E. Cohen, *Science* **2007**, *318*, 1618; b) J. T. Korhonen, M. Kettunen, R. H. A. Ras, O. Ikkala, *ACS Appl. Mater. Interfaces* **2011**, *3*, 1813.

[5] J. Zhang, S. Seeger, *Adv. Funct. Mater.* **2011**, *21*, 4699.

[6] M. Nicolas, F. Guittard, S. Geribaldi, *Angew. Chem. Int. Ed.* **2006**, *45*, 2251.

[7] a) J. G. Reynolds, P. R. Coronado, L.W. Hrubesh, *Energy Sources* **2001**, *23*, 831; b) M. Ma, R. M. Hill, Curr. Opin, *Colloid Interface Sci.* **2006**, *11*, 193; c) A. V. Rao, N. D. Hegde, H. Hirashima, *J. Colloid Interface Sci.* **2007**, *305*, 124.

[8] a) K. Tsujii, T. Yamamoto, T. Onda, S. Shibuichi, *Angew. Chem. Int. Ed. Engl.* **1997**, *36*, 1011; b) M. Jin, J. Wang, X. Yao, M. Liao, Y. Zhao, L. Jiang, *Adv. Mater.* **2011**, *23*, 2861.

[9] a) K. Liu, X. Yao, L. Jiang, *Chem. Soc. Rev.* **2010**, *39*, 3240; b) X. Yao, Y. Song, L. Jiang, *Adv. Mater.* **2011**, *23*, 719.

[10] H. Jinnai, Y. Nishikawa, H. Morimoto, T. Koga, T. Hashimoto, *Langmuir* **2000**, *16*, 4380.

[11] a) W. R. Thompson, M. Cai, M. K. Ho, J. E. Pemberton, *Langmuir* **1997**, *13*, 2291; b) R. Al-Oweini, H. Ei-Rassy, *J. Mol. Struct.* **2009**, *919*, 140; c) Y.-S. Li, Y. Wang, S. Ceesay, *Spectrochim. Acta Part A* **2009**, *71*, 1819.

[12] Z. Olejniczak, M. Leczka, K. Cholewa-Kowalska, K. Wojtach, M. Rokita, W. Mozgawa, *J. Mol. Struct.* **2005**, *744*, 465.

[13] K. Nakanishi, *J. Porous Mater.* **1997**, *4*, 67.

[14] J. M. Al-Besharah, O. A. Salman, S. A. Akashar, *Ind. Eng. Chem. Res.* **1987**,

26, 2445.

[15] M. Xu, D. N. Futaba, T. Yamada, M. Yumura, K. Hata, *Science* **2010**, *330*, 1364.

[16] a) D. Louch, S. Motlagh, J. Pawliszyn, *Anal. Chem.* **1992**, *64*, 1187; b) M. C. Hennion, *J. Chromatogr. A* **1999**, *856*, 3.

[17] G. Hayase, K. Kanamori, K. Nakanishi, *J. Mater. Chem.* **2011**, *21*, 17077.

Chapter 6

A Superamphiphobic Marshmallow-like Macroporous Gel by Using Thiol–ene Click Reaction on Surface

6.1 Introduction

As discussed in chapter 5, marshmallow-like gels can be obtained from many combinations of tri- and difunctional organoalkoxysilanes as co-precursors. For the next step, a synthesis of new functionalized marshmallow-like flexible materials by utilizing surface reactions on the surface of microstructures is attempted.

A number of research groups have been studying hydrophobic and oleophobic surfaces, both for pure scientific interest and industrial applications. These studies are drawing increasing attention because of the growing demands for applications such as anti-fingerprint touch panels on electronic devices and solar panels that can prevent output fall from dust and smears on the surface by the self-cleaning effect.[1] In nature, many examples of superhydrophobic surface exist with a water contact angle of more than 150 °, such as eyes of mosquitos and lotus leaves,[1d, 2] and these are important for their survival. Their non-wetting surfaces possess a combination of nano- or micro-scaled roughness[3] and low surface energy, which are known for the key of creating artificial superhydrophobic surfaces.[1d] However, most of the superhydrophobic materials can easily be wetted by organic liquids because of the lower surface tension of the liquids. In recent years, techniques for creating oleophobic surfaces have been vigorously investigated. A promising way to obtain a surface with a contact angle of more than 150 ° for organic liquids is to make rough microstructures covered with perfluoroalkyl groups, which are bound on some kinds of polyhedral oligomeric silsesquioxanes (POSS),[4] monomeric silanes,[5] and polymers.[6] However, the reported technologies to achieve superamphiphobicity are limited in the forms of films and fibres. As far as the author knows, there have been no reports on monolithic superamphiphobic

materials that can be prepared in a wide range of thickness and in any shapes.

Marshmallow-like gels can be obtained through a facile one-pot sol–gel reaction, as discussed in chapters 4 and 5.[7] By changing the combination of the alkoxysilanes, various kinds of marshmallow-like gels with different functional groups can be obtained. For example, in the case of (3-mercaptopropyl)trimethoxysilane–(3-mercaptopropyl)methyldimethoxysilane copolymer system, gold ions can be adsorbed on the pore surface by the mercapto groups. Marshmallow-like gels derived from MTMS–DMDMS shows the ability for using oil–water separation media. These flexible gels can quickly remove organic liquids/oils from oil–water mixtures. This means that the surface of these macroposous gels have only hydrophobicity but no oleophobicity.

The marshmallow-like gels derived from VTMS and VMDMS as co-precursor can also be used as oil–water separation media. In the case of this co-precursors system, the surface of the microstructure has reactivility with organic molecules such as vinyl-functionalized reagents and thiols. In this chapter, the auther employs a VTMS–VMDMS co-precursors system to prepare the new functionalized flexible monolith which has both hydrophobicity and oleophobicity.

6.2 Experimental

6.2.1 Chemicals

Acetic acid, distilled water, and urea were purchased from Hayashi Pure Chemical Industry, Ltd. (Japan). Surfactant CTAC was obtained from Tokyo Chemical Industry, Ltd. (Japan). Precursors VTMS and VMDMS were purchased from Shin-Etsu Chemical Co., Ltd. (Japan) and Tokyo Chemical Industry, Ltd. (Japan), respectively. All of the chemical reagents were used as received.

6.2.2 Synthesis procedures

First, 1.0 g of CTAC, 5.0 g of urea, and 15 mL of 5 mM aqueous acetic acid were mixed in a glass sample tube. Then 0.025 mol (3.71 g) of VTMS and 0.010 mol (1.32 g) of VMDMS were added at the same time under vigorous stirring at ambient temperature, and stirring was continued for 60 min until the solution became homogeneous. The obtained sol was transferred into a tightly-sealed container, which was then placed in a forced convection oven at 80 °C for 9 h to complete gelation and aging. The obtained gels were washed with methanol by soaking/squeezing by hand for several times to remove the residual surfactant and other unreacted chemicals. The washed samples were dried under an ambient condition to obtain xerogels (MG1). To obtain the superamphiphobic marshmallow-like gel MG2, 0.5 g (6.2 mmol) of MG1 was soaked into 50 mL of a 2-propanol solution containing 10 v/v % 1*H*,1*H*,2*H*,2*H*-perfluorodecanethiol (18 mmol) with a catalytic amount of azobisisobutyronitrile as an initiator at 60 °C for 10 h to attach perfluoroalkyl groups on the pore surface by the thiol–ene click reaction. Then, the wet gel was washed with 2-propanol for several times and dried under an ambient condition.

6.2.3 Measurements

A scanning electron microscope (JSM-6060S, JEOL, Japan) was employed to observe the microstructure. Mechanical properties of aerogels were measured by a material tester (EZGraph, Shimadzu Corp., Japan). For uniaxial compression tests, a carved gel (typical length × width × height was 15 × 15 × 10

mm^3) was compressed–decompressed using a load cell of 5 kN with a rate of 0.5 mm min^{-1}. For three-point bending tests, a cylindrical sample with 8 mm diameter and 40 mm length was put on a fixture with a 30 mm span and applied loading-unloading for 100 times by a wedge-shaped crosshead with 60 ° and 0.3 mm diameter at the point with using a load cell of 5 N at a rate of 5 mm min^{-1}. To assess molecular-level structure of the obtained siloxane networks, Fourier transform infrared spectroscopy (FTIR), ^{29}Si solid-state cross polarization/magic angle spinning (CP/MAS) NMR measurements and ^{13}C solid-state dipolar decoupling/magic angle spinning (DD/MAS) NMR measurements were performed. The FTIR spectra were recorded with IRAffinity-1 (Shimadzu Corp., Japan) using an attenuated total reflection (ATR) attachment. A total of 100 scans were recorded with a resolution of 4 cm^{-1} on the samples dried in vacuum at 80 °C for 1 d in advance. An NMR spectrometer Avance III 800 (Bruker Corp.,Germany) has been operated under a static magnetic field of 18.8 T. For ^{29}Si solid-state CP/MAS measurements, the contact time for the cross polarization was fixed at 5.5 ms and the rate of sample spinning was set to 15 kHz. The ^{29}Si chemical shifts were expressed as values relative to tetramethylsilane (Me_4Si) by using the resonance line at −9.66 ppm for hexamethylcyclotrisiloxane crystals as an external reference. For ^{13}C solid-state DD/MAS measurements, the recycle delay was fixed at 25 s and the rate of sample spinning was set to 15 kHz. The ^{13}C chemical shifts were expressed as values relative to tetramethylsilane (Me_4Si) by using the resonance line at 176.46 ppm for glycine as an external reference. Elemental analysis (C, H, F) was performed at Center for Organic Elemental Microanalysis in Kyoto University using YANACO MT-3 and MT-6 analyzers. Contact angles were measured with Drop Master DM-561Hi (Kyowa Interface Science Co., Ltd., Japan). Volume of water and organic liquids droplet was fixed at 3 μL and a contact angle was determined at 2 s after the attachment to gel surface. The elemental analysis of the samples was carried out by X-ray photoelectron spectroscopy (XPS) (MT-5500, ULVAC-PHI, Inc., Japan). The monochromatized X-ray Mg Kα radiation (1253.6 eV) was used. The core levels were calibrated by reference to the first component of the C_{1s} core level peak (unfunctionalized hydrocarbons) set at 284.6 eV.

Thermogravimetric-differential thermal analysis (TG–DTA) was performed with a Thermo plus TG 8120 (Rigaku Corp., Japan) instrument at a heating rate of 5 °C min^{-1} while continuously supplying air at a rate of 100 mL min^{-1}.

6.3 Result and Discussion

The VTMS–VMDMS marshmallow-like gel can be obtained by four simple, routine steps within half a day: 1) mixing VTMS, VMDMS, urea, and surfactant CTAC in a dilute aqueous acetic acid solution, and stirring for 60 min at room temperature for acid-catalyzed hydrolysis of alkoxysilanes; 2) transferring the resulting transparent sol to an oven for gelation and aging at 80 °C over several hours to promote the siloxane network formation under basic conditions, which is brought up by the hydrolysis of urea into ammonia; 3) washing with alcohol by hand; and 4) evaporative drying under ambient conditions (Figure 6.1a). The obtained gel (MG1) shows enough marshmallow-like flexibility to recover their original shape from 80 % uniaxial compression and 3-point bending (Figures 6.2 and S1). This material has a superhydrophobic surface with a water contact angle of 153 °, which is due to the negligible amount of residual hydrophilic silanol groups, as characterized by ^{29}Si solid-state CP/MAS NMR spectroscopy (Figure 6.3).[8] However, MG1 does not show oleophobicity, but absorbs organic liquids quickly like a sponge (Figure 6.4a. See also Figure 5.5.)

To transform the superhydrophobic gel into the superamphiphobic one, the thiol–ene click reaction, which is wellknown as a facile and reliable method to bind molecules for the purpose of surface modification as well as in organic synthesis,[9] has been used. The author attached perfluoroalkyl groups to the rich vinyl groups on the pore surface of MG1 (0.5 g, 6.2 mmol) by soaking in 50 mL of a 2-propanol solution containing 10 v/v % 1*H*,1*H*,2*H*,2*H*-perfluorodecanethiol (18 mmol, excess) with a catalytic amount of *N*,*N*'-azobisisobutyronitrile (AIBN, a radical initiator) for 10 h, and characterized surface and microstructure of the obtained gel (MG2; Figure 6.1b). By an XPS survey spectra, the presence of the elements F (F_{1s} at 688.6 eV) and S (S_{2p} at 163.8 eV)[10] is detected on MG2 (Figure 6.5a). Consistent with the elemental analysis (C, H, F) results, the fluoride content on the surface of MG2 is around 50 atom%, which indicates that 1*H*,1*H*,2*H*,2*H*-perfluorodecanethiol is well-attached to the vinyl groups, covering the most part of the macropores of MG1.

Unreacted vinyl groups are also detected from FTIR spectroscopy (=CH_2 wagging at 970 cm^{-1}, C=C twist at 1000 cm^{-1}, =CH_2 scissor at 1400 cm^{-1}, and C=C stretching at 1600 cm^{-1})[11] and ^{13}C solid-state DD/MAS NMR spectra (Figure 6.5b,c). The percentage of reacted vinyl groups is only 3–5% by estimating from the density change of MG1 and MG2 (0.122 g cm^{-3} and 0.157 g cm^{-3}, respectively), ^{13}C NMR spectra, and elemental analysis, simply because the perfluoroalkyl groups are attached only onto the vinyl groups on the macropore surface. The rather large perfluorododecanethiol molecules could not permeate into the core of the nonporous micrometer-sized skeletons. During this surface reaction, there is no change in the microstructure, which possesses enough roughness to have a high water contact angle (Figure 6.1b). After the treatment, MG2 acquired superoleophobicity (Figure 6.4a). The contact angles of water and *n*-hexadecane are 160 ° and 151 °, respectively (Figure 6.4b,c). Likewise, the surface of monolithic MG2 shows superoleophobicity for ethylene glycol, formamide, diiodomethane, and 1-bromonaphthalene (Figure 6.4c). From these results, it can be concluded that the hydrophobic monolithic macroporous silicone gels bearing vinyl groups on the surface is imparted with oleophobicity by a facile process.

Significant features of the marshmallow-like gel including MG1 are not only the flexibility but also the wide controllability in size and shape of the monolith. In fact, the author obtained MG1 as flexible sheets as well as bulky monoliths, which can be carved into desired shape and size. These features are maintained in MG2 because MG2 can be obtained from MG1 only by the surface modification without changing the original siloxane network and microstructure. The most important feature of MG2 is superamphiphobicity on any cutting surface. This can be explainedby the microstructure of marshmallow-like gels. Marshmallow-like gels have co-continuous structure derived from the transient structure of spinodal decomposition.[7,12] On cutting any face, the fraction of the unmodified cores of intricate micrometer-sized skeletons on the new surface plane is appreciably low and the modified pore surfaces of the skeletons largely contribute to the oleophobicity. In fact, it is hard to recognize the cross-section of cut skeletons in the SEM image (Figure 6.6). Thus, nonoleophobized core

parts of the cutting surfaces of MG2 can be ignored and this material keeps superamphiphobicity on any surfaces after cutting into desired shape. Although marshmallow-like gels are rather brittle against tensile stress and friction owing to their thin skeletons, their superamphiphobicity is perfectly maintained. By this feature together with low density, the machined MG2 can float on organic liquids such as 1,3,5-trimethylbenzene and *n*-hexadecane by surface tension for at least over a week without any change (Figure 6.4a). These features have not been reported on other materials to date. Thermogravimetry–differential thermal analysis (TG–DTA) result shows that MG2 is stable up to about 170 °C (Figure 6.7). At higher temperatures, the macroporous structure was gradually collapsed by oxidation and degradation of vinyl groups.

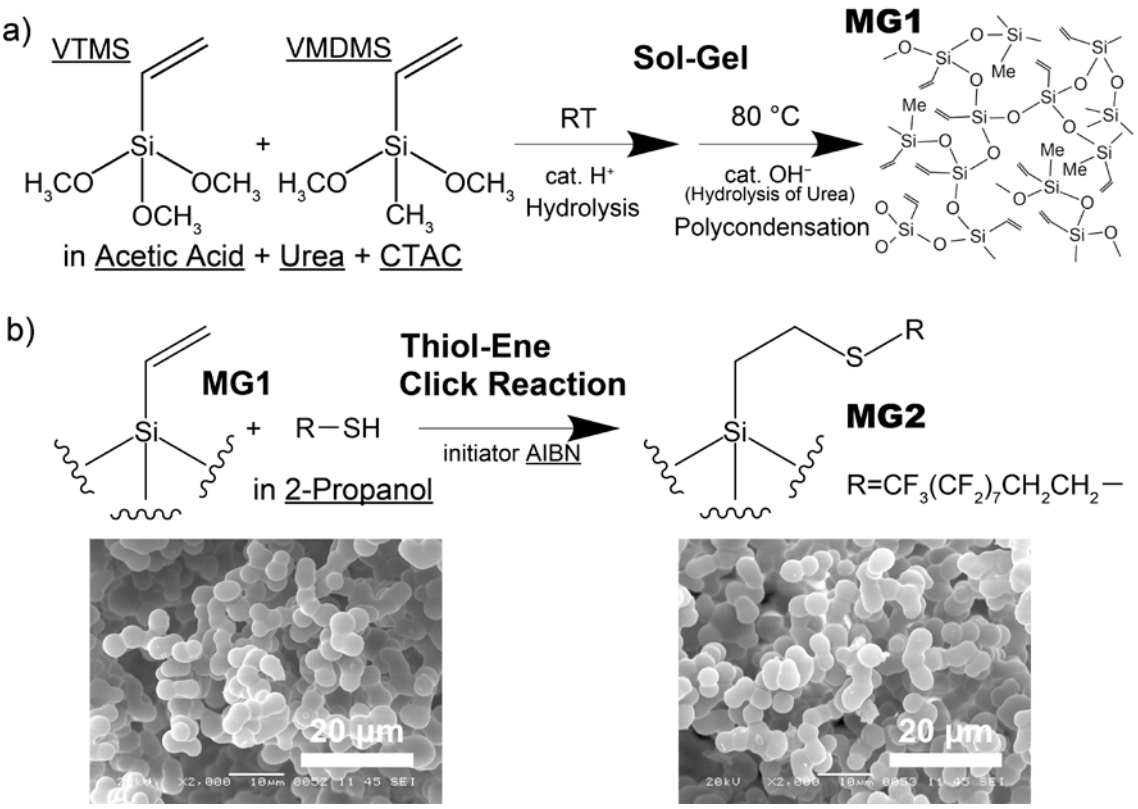

Figure 6.1 a) One-pot acid-base sol–gel synthesis scheme for the VTMS–VMDMS marshmallow-like gel (MG1). b) Synthetic approach for the oleophobic MG2 by attachment of perfluoroalkyl groups onto the rich vinyl groups on MG1 pore surface by the thiol–ene click reaction. From SEM observations, no changes are found in the macroporous morphology by the reaction.

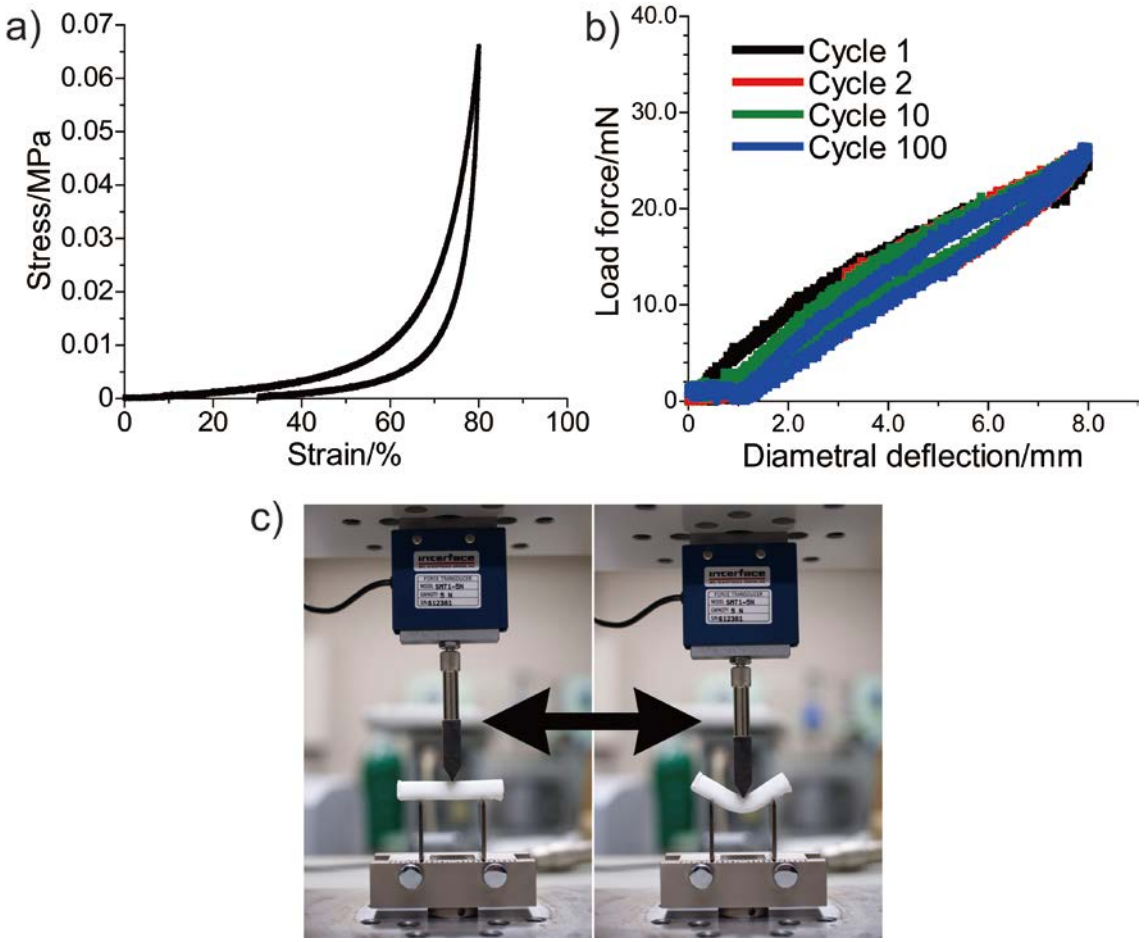

Figure 6.2 Stress–strain curves of a) uniaxial compression test and b) 100 cycles of 3-point bending test on the sample MG1. In both cases, VTMS–VMDMS marshmallow-like gels perfectly recover their original shape. c) Photographs of a 3-point bending test on the VTMS–VMDMS marshmallow-like gel (MG1). The sample returned to its original shape after removal of stress during 100 cycles.

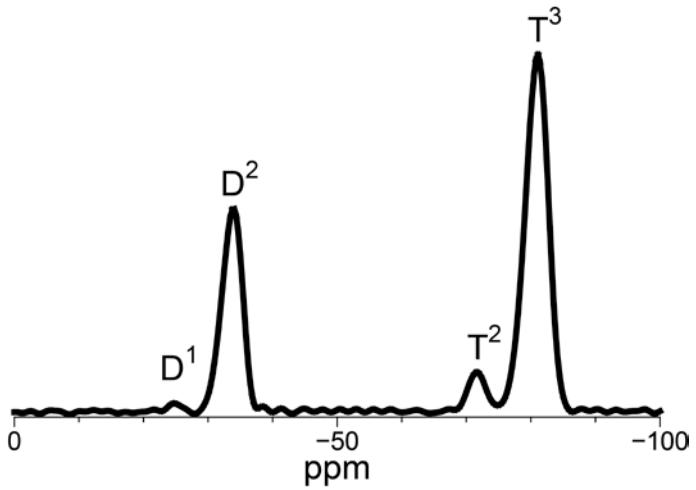

Figure 6.3 ^{29}Si solid-state CP/MAS NMR spectrum of MG1. Only negligible amounts of D^1, T^1 and T^2 species are found, which shows that well-developed polysiloxane network was successfully formed by the facile one-pot process.

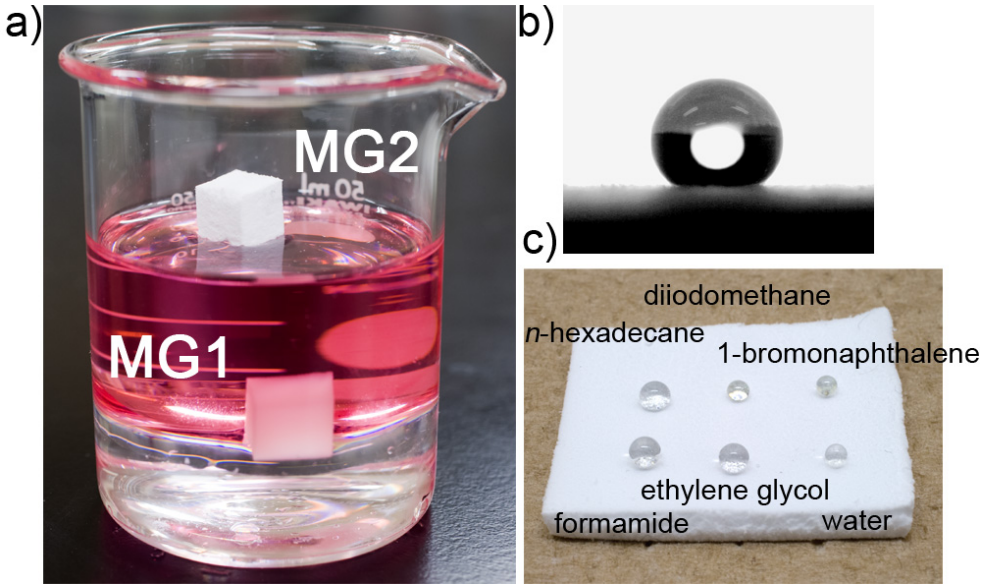

Figure 6.4 a) The superhydrophobic marshmallow-like gel (MG1) and the superamphiphobic marshmallow-like gel (MG2). MG2 floats on 1,3,5-trimethylbenzene (colored by Oil Red O) by its surface tension, while MG1 absorbs it. The colorless liquid at the bottom is water. b) The contact angle of *n*-hexadecane is 151 °. c) MG2 with droplets of water, ethylene glycol, formamide, 1-bromonaphthalene, diiodomethane and *n*-hexadecane.

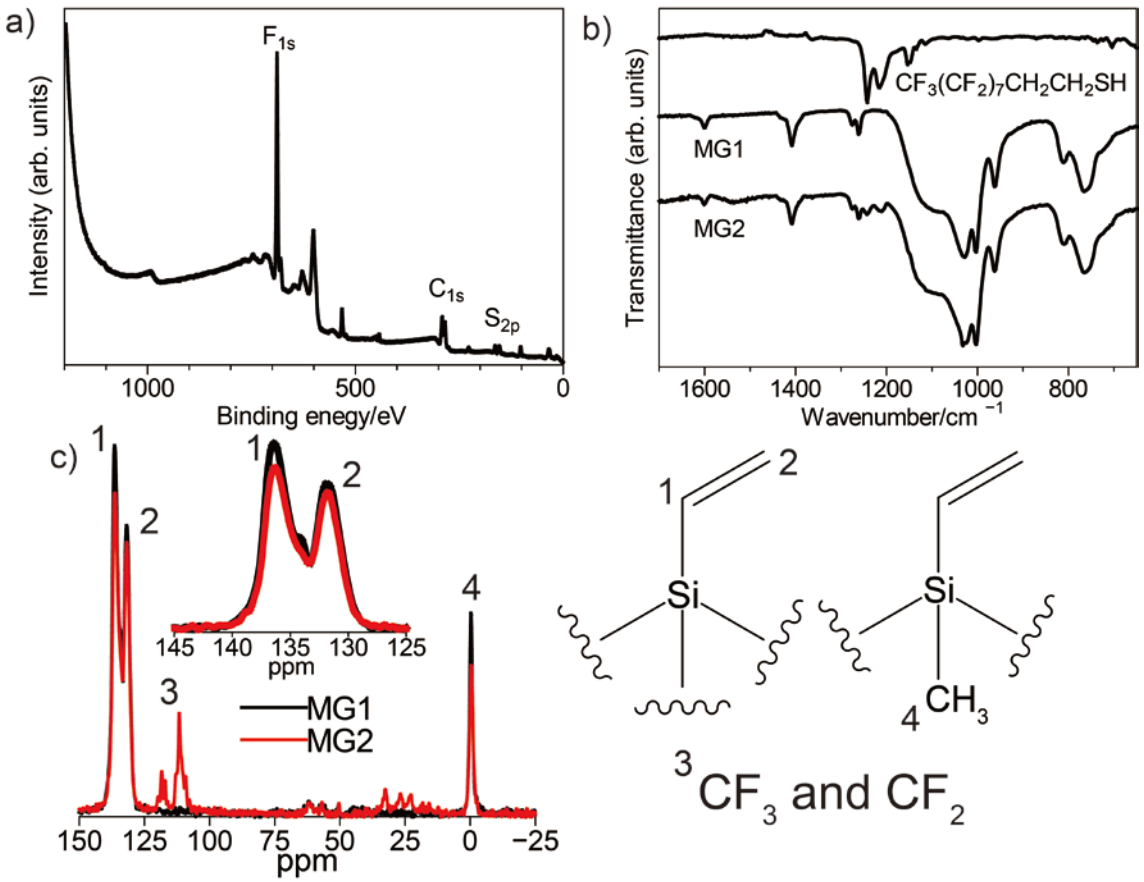

Figure 6.5 a) XPS survey spectrum of MG2, revealing the presence of F. b) FTIR spectra of 1*H*,1*H*,2*H*,2*H*-perfluorodecanethiol, MG1 and MG2. c) ^{13}C solid-state DD/MAS spectra of MG1 and MG2. Four percent of vinyl groups are reacted by the thiol–ene click reaction. For MG2; ^{13}C NMR δ = 0.38 (s, Si–$\underline{C}H_3$, overlapped with Si–$\underline{C}H_2$), 22.77−32.57 (t, CF_2–$\underline{C}H_2$), 50.41 (s, O$\underline{C}H_3$), 109.17−118.33 (m, other carbons in $\underline{C}F_3$ and $\underline{C}F_2$), 131.76 (s, CH=$\underline{C}H_2$), 136.31 (s, $\underline{C}$H=CH_2).[13] Two peaks at *ca.* 60 ppm are spinning sidebands.

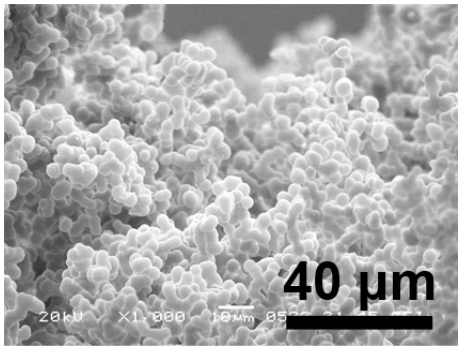

Figure 6.6 SEM image of a cutting surface of MG2. Since the unmodified cross-section can be hardly recognized on the surface, MG2 shows superamphiphobicity on any cutting surfaces.

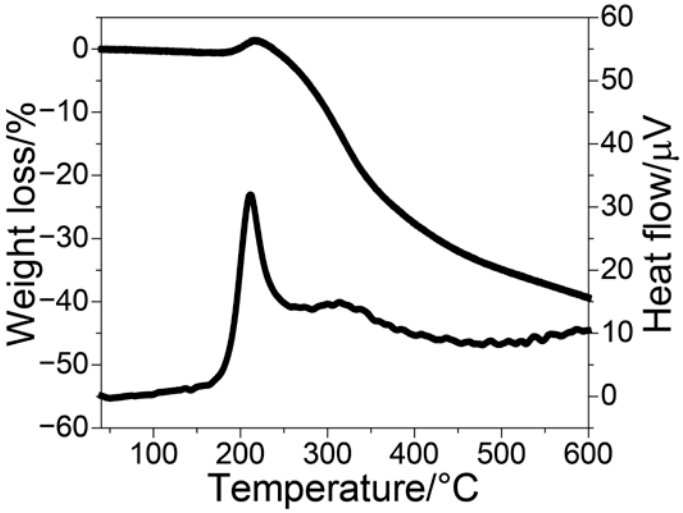

Figure 6.7 TG–DTA curves of MG2. This superamphiphobic material is stable up to ~170 °C where vinyl groups are oxidized.

6.4 Conclusion

In summary, the author has successfully obtained the first superamphiphobic monolith with contact angle greater than 150 ° for both water and organic liquids, such as ethylene glycol, formamide, diiodomethane, 1-bromonaphthalene, and *n*-hexadecane. This material can be obtained in a facile manner by a combination of the simple one-pot sol–gel process and the thiol-ene click reaction. Co-continuous macroporous structure covered with perfluoro-alkyl groups supplies roughness and low surface energy, resulting in superamphiphobicity on any cutting surfaces of the monolith. The superamphiphobic marshmallow-like gel floats on the surface of water and oils for long by surface tension. This unique and outstanding monolithic material is expected to pioneer the scientific and technological interests of three-dimensional superamphiphobic materials. Furthermore, novel applications to new self-cleaning and antifouling surfaces, gas-permeable separators, medical/biomedical materials, and selective separation media for organic liquid would be developed by carefully tuning the surface energy and roughness of the monolith.[7a, 14] Formability of the material in such as monoliths and sheets/membranes, as well as developing coating films and particles, would allow extended applications in various fields.

References in Chapter 6

[1] a) R. Blossey, *Nat. Mater.* **2003**, *2*, 301; b) M. Ma, R. M. Hill, *Curr. Opin. Colloid Interface Sci.* **2006**, *11*, 193; c) J. A. Howarter, J. P. Youngblood, *Adv. Mater.* **2007**, *19*, 3838; d) W.-L. Min, B. Jiang, P. Jiang, *Adv. Mater.* **2008**, *20*, 3914; e) K. Liu, X. Yao, L. Jiang, *Chem. Soc. Rev.* **2010**, *39*, 3240.

[2] a) W. Barthlott, C. Neinhuis, *Planta* **1997**, *202*, 1; b) K. Koch, B. Bhushan, W. Barthlott, *Soft Matter* **2008**, *4*, 1943; c) B. Bhushan, *Philos. Trans. R. Soc., A* **2009**, *367*, 1445.

[3] a) R. N. Wenzel, *Ind. Eng. Chem.* **1936**, *28*, 988; b) A. B. D. Cassie, S. Baxter, *Trans. Faraday Soc.* **1944**, *40*, 546.

[4] a) A. Tuteja, W. Choi, M. Ma, J. M. Mabry, S. A. Mazzella, G. C. Rutledge, G. H. McKinley, R. E. Cohen, *Science* **2007**, *318*, 1618; b) W. Choi, A. Tuteja, S. Chhatre, J. M. Mabry, R. E. Cohen, G. H. McKinley, *Adv. Mater.* **2009**, *21*, 2190; c) H. Wang, Y. Xue, J. Ding, L. Feng, X. Wang, T. Lin, *Angew. Chem. Int. Ed.* **2011**, *50*, 11433.

[5] a) B. Leng, Z. Shao, G. de With, W. Ming, *Langmuir* **2009**, *25*, 2456; b) C. Aulin, J. Netrval, L. Wagberg, T. Lindstrom, *Soft Matter* **2010**, *6*, 3298; c) J. Zhang, S. Seeger, *Angew. Chem. Int. Ed.* **2011**, *50*, 6652; d) X. Deng, L. Mammen, H.-J. Butt, D. Vollmer, *Science* **2012**, *335*, 67.

[6] a) S. R. Coulson, I. S. Woodward, J. P. S. Badyal, S. A. Brewer, C. Willis, *Chem. Mater.* **2000**, *12*, 2031; b) Q. D. Xie, J. Xu, L. Feng, L. Jiang, W. H. Tang, X. D. Luo, C. C. Han, *Adv. Mater.* **2004**, *16*, 302; c) A. Steele, I. Bayer, E. Loth, *Nano Lett.* **2009**, *9*, 501; d) J. Yang, Z. Zhang, X. Xu, X. Zhu, X. Men, X. Zhou, *J. Mater. Chem.* **2012**, *22*, 2834.

[7] a) G. Hayase, K. Kanamori, K. Nakanishi, *J. Mater. Chem.* **2011**, *21*, 17077; b) G. Hayase, K. Kanamori, M. Fukuchi, H. Kaji, K. Nakanishi, *Angew. Chem. Int. Ed.* **2013**, *52*, 1986.

[8] Z. Olejniczak, M. Leczka, K. Cholewa-Kowalska, K. Wojtach, M. Rokita, W. Mozgawa, *J. Mol. Struct.* **2005**, *744*, 465.

[9] a) H. C. Kolb, M. G. Finn, K. B. Sharpless, *Angew. Chem. Int. Ed.* **2001**, *40*, 2004; b) J. E. Moses, A. D. Moorhouse, *Chem. Soc. Rev.* **2007**, *36*, 1249; c) C.

E. Hoyle, C. N. Bowman, *Angew. Chem. Int. Ed.* **2010**, *49*, 1540; d) A. K. Tucker-Schwartz, R. A. Farrell, R. L. Garrell, *J. Am. Chem. Soc.* **2011**, *133*, 11026.

[10] a) X. Yao, J. Gao, Y. Song, L. Jiang, *Adv. Funct. Mater.* **2011**, *21*, 4270; b) S. P. R. Kobaku, A. K. Kota, D. H. Lee, J. M. Mabry, A. Tuteja, *Angew. Chem. Int. Ed.* **2012**, *51*, 10109.

[11] R. Al-Oweini, H. Ei-Rassy, *J. Mol. Struct.* **2009**, *919*, 140.

[12] K. Nakanishi, *J. Porous Mater.* **1997**, *4*, 67.

[13] a) A. L. Smith Ed., in *The Analytical Chemistry of Silicones*, John Wiley & Sons, Inc., New York, NY, **1991**, pp. 364; b) N. Yoshino, Y. Yamamoto, K. Hamano, T. Kawase, *Bull. Chem. Soc. Jpn.* **1993**, *66*, 1754.

[14] a) A. Tuteja, W. Choi, G. H. McKinley, R. E. Cohen, M. F. Rubner, *MRS Bull.* **2008**, *33*, 752; b) L. Joly, T. Biben, *Soft Matter* **2009**, *5*, 2549; c) A. K. Kota, G. Kwon, W. Choi, J. M. Mabry, A. Tuteja, *Nat. Commun.* **2012**, *3*, 1025; d) S. M. Kang, S. M. Kim, H. N. Kim, M. K. Kwak, D. H. Tahk, K. Y. Suh, *Soft Matter* **2012**, *8*, 8563.

Summary

The present thesis deals with the studies on polyorganosiloxane porous materials derived from alkoxysilanes as (co-)precursors via the sol–gel process with controlled phase separation. The contents of the respective chapters are summarized as follows:

In chapter 1, the relationship between the starting compositions and the properties of the PMSQ aerogels by employing cationic CTAC as a surfactant to suppress phase separation is reported. Visible-light transmittance, density and mechanical properties were systematically investigated with varied starting compositions. Since the surfactant predominantly controls the phase separation tendency in the system, the porous texture of the aerogels is changed with the varied amount of CTAC. To successfully obtain monolithic PMSQ aerogels by sufficiently suppressing macroscopic phase separation, a small amount of CTAC (at least [CTAC]/[MTMS] = 0.009) should be included in the solution. At [CTAC]/[MTMS] = 0.036, the obtained gel exhibits the highest light transmittance (89 % through 10 mm thickness at 550 nm). Density and Young's modulus are strongly correlated, because both of these properties depend on the structure and bonding properties of the gel networks. Concentrations of acid and base catalysts affect the molecular-level network and porous texture of the gels, as is well known in the sol–gel chemistry. With diluted acetic acid and increased amount of urea as the acid and base catalysts, respectively, aerogels with high light transmittance and low density are obtained. With increasing the volume ratio of solvent to MTMS, density monotonously decreased and the lowest density of PMSQ aerogels obtained without cracks is 0.045 g cm^{-3}.

In chapter 2, aerogels with varied pore size were prepared using nonionic surfactant F127, instead of CTAC, to investigate the relationships between thermal conductivity, gas pressure and pore size. A change in the concentration of F127 leads to aerogels with pore size from ~50 nm to 3 μm. Thermal conductivity of each aerogel sample varies depending on the gas pressure, and shows good agreement with the theoretical values. An aerogel-like xerogel panel with sufficiently low thermal conductivity (15 mW m^{-1} K^{-1}) with

visible-light transmittance (29 % through 10 mm thickness at 550 nm) was also successfully prepared. The low thermal conductivity can be even lower under a light evacuation like 10^4 Pa. These results show the possibility of practical applications of PMSQ aerogels to highly insulating and daylighting materials under ambient pressure or light evacuation.

In chapter 3, improvement of mechanical properties of PMSQ aerogels by compositing with cellulose nanofibers (CNFs) is reported. By adding only a small amount of CNFs in the same starting solution examined in chapter 1, bending flexibility has been introduced in the obtained low-density aerogels, which had not been observed in any monolithic aerogels including the pristine PMSQ aerogels. The CNFs are homogeneously fused with the PMSQ networks through a moderate interaction, which gives a favorable effect on the physical properties of PMSQ aerogels. A bendable PMSQ aerogel with low density (0.020 g cm^{-3}), which is below the minimum value of the pure PMSQ aerogels, was successfully obtained. Also, these composites show high hydrophobicity without any hydrophobizing treatments. With the stability of the PMSQ and CNFs under ambient emvironment, PMSQ–CNF composite aerogels will extend the usability of excellent thermal insulation of aerogels.

In chapter 4, the synthesis of marshmallow-like flexible macroporous gels is described using MTMS and DMDMS as the co-precursors. The synthesis process is almost the same as that of PMSQ aerogels (chapter 1). The fundamental properties of the marshmallow-like gels have been systematically investigated by changing the synthetic parameters. By increasing only the ratio of DMDMS to MTMS, the microstructure is coarsened and Young's modulus of the gels is dramatically decreased while the high porosity is maintained. Because of the highly flexible nature, the marshmallow-like gels can be obtained by a more facile manner without supercritical drying. The result shows the availability of these unique materials for extended applications such as sound absorbing materials.

In chapter 5, detailed properties and multi-functionality of the marshmallow-like gels are shown. The flexible macroporous materials show stable structure and properties in the wide temperature range (−130 to 315 °C)

similarly to a typical silicone polymer, PDMS. The marshmallow-like gels even show flexibility at the liquid nitrogen temperature, which extends their usability to harsh environments. Absorption and squeezing-out of liquid nitrogen have been successfully demonstrated like a sponge without any physical damages. The external surfaces of marshmallow-like gels show superhydrophobicity due to the low surface energy of PDMS-like polymethylsiloxane and geometrical roughness. Utilizing their hydrophobic surfaces and wettability of oil/organic liquids, it is possible to quickly separate biphasic oil–water mixtures. Alteration of the surface property of the marshmallow-like gels is investigated by employing different combinations of alkoxysilanes instead of MTMS and DMDMS. The marshmallow-like gels prepared from the (3-mercaptopropyl)trimethoxysilane–(3-mercaptopropyl)methyldimethoxysilane co-precursor can adsorb gold ions on the surface when soaked in an aqueous tetrachloroauric acid solution. These results show the possibilities as new separation media by utilizing the surface functionalities of organic groups attached to the precursors.

In chapter 6, surface modification of the marshmallow-like gels is examined. The surface on the microstructure of marshmallow-like gels derived from a co-precursor system of VTMS and VMDMS has been reacted with perfluoroalkyl thiol by the thiol–ene click reaction. The resultant marshmallow-like gel attained superoleophobicity. The contact angles on the surface of the resultant material after the surface modification are greater than 150 ° for both water and organic liquids such as ethylene glycol, formamide, diiodomethane, 1-bromonaphthalene, and *n*-hexadecane. The superoleophobicity is maintained on any cut surfaces of the monoliths, and these monoliths can float on the surface of water and oils for long by surface tension. This result shows the possibility of designing new self-cleaning and antifouling surfaces, gas-permeable separators, medical/biomedical materials, and selective separation media with desired shapes.

The present study has revealed the practical sol–gel pathways to design flexible and functional organosiloxane porous gels from organoalkoxysilane precursors by controlling phase separation in aqueous media. Through the structural controls over multiple length scales such as molecular-level networks and porous microstructures of nano- to micrometer scales, these porous materials

represent remarkable properties such as low thermal conductivity, sound absorption and superamphiphobicity. As discussed with the polymethylsilsesquioxane (PMSQ) aerogels and xerogels and polyorganosiloxane marshmallow-like gels for examples, flexibility and elasticity against compression and bending stresses are the progeny of successful multiple structural controls in the network and porous structures. Unlike inorganic materials, sol–gel-derived inorganic–organic hybrid materials with well-defined porosity and properties have not been reported much. Because of the fine controls by the simple processes and availability of functionalities, the present studies on porous organosiloxane materials are expected to further develop to change our life in the near future.

List of Publications

Chapter 1

"Structure and properties of polymethylsilsesquioxane aerogels synthesized with surfactant *n*-hexadecyltrimethylammonium chloride"
Gen Hayase, Kazuyoshi Kanamori and Kazuki Nakanishi
Microporous & Mesoporous Materials **2012**, *158*, 247-252.

Chapter 2

"Transition from transparent aerogels to hierarchically porous monoliths in polymethylsilsesquioxane sol–gel system"
Kazuyoshi Kanamori, Yasunori Kodera, Gen Hayase, Kazuki Nakanishi and Teiichi Hanada
Journal of Colloid and Interface Science **2011**, *357*, 2, 336-344.

"Thermal conductivity of polymethylsilsesquioxane aerogels and xerogels with varied pore size for practical application to thermal superinsulators"
Gen Hayase, Kazuma Kugimiya, Mitsue Ogawa, Yasunori Kodera, Kazuyoshi Kanamori and Kazuki Nakanishi
Journal of Materials Chemistry A, accepted. (DOI: 10.1039/C3TA15094A)

Chapter 3

"Polymethylsilsesquioxane–cellulose nanofiber biocomposite aerogels with high thermal insulation, bendability and superhydrophobicity"
Gen Hayase, Kazuyoshi Kanamori, Kentaro Abe, Hiroyuki Yano, Ayaka Maeno, Hironori Kaji and Kazuki Nakanishi
submitted.

Chapter 4

"New flexible aerogels and xerogels derived from methyltrimethoxysilane/dimethyldimethoxysilane co-precursors"
Gen Hayase, Kazuyoshi. Kanamori and Kazuki Nakanishi

Journal of Materials Chemistry **2011**, *21*, 43, 17077-17079.

Chapter 5

"Facile Synthesis of Marshmallow-like Macroporous Gels Usable under Harsh Conditions for the Separation of Oil and Water"

Gen Hayase, Kazuyoshi Kanamori, Masashi Fukuchi, Hironori Kaji and Kazuki Nakanishi

Angewandte Chemie International Edition **2013**, *52*, 7, 1986-1989.

Chapter 6

"A Superamphiphobic Macroporous Silicone Monolith with Marshmallow-like Flexibility"

Gen Hayase, Kazuyoshi Kanamori, George Hasegawa, Ayaka Maeno, Hironori Kaji, Kazuki Nakanishi

Angewandte Chemie International Edition **2013,** *52*, 41, 10788-10791.

Acknowledgement

The present thesis has been carried out at Graduate School of Science, Kyoto University, under the direction of Professor Kazuki Nakanishi.

First of all, the author wishes to express his sincere gratitude to Professor Kazuki Nakanishi for continuous encouragement and valuable advices all thorough the graduation of the present works. The author is also greatly indebted to Dr. Kazuyoshi Kanamori for his discussions, experimental directions, and sincere supports in proceeding with the present studies. The author is also grateful to Professor Teiichi Hanada, Dr. George Hasegawa, Dr. Kei Morisato, Dr. Riichi Miyamoto, Dr. Yasuaki Tokudome and Yasunori Kodera for the useful advices and discussions on experiments and writing research papers. Hearty thanks are made to all students of Nakanishi Group for everyday activities.

The author would like to thank Professor Hironori Kaji, Dr. Masashi Fukuchi and Ayaka Maeno (Institute Chemical Research, Kyoto University) for NMR measurement, Professor Keisuke Yamada and Tomoya Nakazawa (Graduate School of Engineering, Kyoto University), for sound absorption analysis, Dr. Kazuma Kugimiya and Mitsue Ogawa, (Japan Fine Ceramics Center), for thermal conductivity analysis, and Dr. Kentaro Abe and Professor Hiroyuki Yano (Research Institute for Sustainable Humanosphere, Kyoto University) for providing bionanofibers and advices. Suggestion for applications of materials and advices about research life from Professor Shin-ichiro M. Nomura (Graduate School of Engineering, Tohoku University), Professor Hirohide Saito and Dr. Shunichi Kashida (Center for iPS Cell Research and Application, Kyoto University) and Dr. Masahiro Takinoue (Interdisciplinary Graduate School of Science and Engineering, Tokyo Institute of Technology) are gratefully acknowledged. The collaboration research with Nobuyuki Matsumoto (Graduate School of Science, The University of Tokyo) and Dr. Takehiro Ando (School of Engineering, The University of Tokyo) brought a fresh perspective to science.

Finally, the author expresses his sincere gratitude to his parents, Yutaka Hayase and Takako Hayase, for their all-time support.

Kyoto, winter 2013 Gen Hayase